Topical Report No. UN-TR-08-001(NP)

Spent and New Fuel Storage Analyses for U.S. EPR

Topical Report

(Non-proprietary Version)

March 2008

HOLTEC
INTERNATIONAL

Holtec Center, 555 Lincoln Drive West, Marlton, NJ 08053
Telephone (856) 797- 0900
Fax (856) 797 - 0909

NEW AND SPENT FUEL STORAGE RACKS FOR CALVERT CLIFFS UNIT 3 U.S. EPR TOPICAL REPORT

FOR

UNISTAR

Holtec Report No: HI-2083956

Holtec Project No: 1721

Report Class : SAFETY RELATED

HOLTEC INTERNATIONAL

DOCUMENT NUMBER: __HI-2083956___ PROJECT NUMBER: 1721__

DOCUMENT ISSUANCE AND REVISION STATUS

DOCUMENT NAME: New and Spent Fuel Storage Racks for Calvert Cliffs Unit 3 U.S. EPR Topical Report

DOCUMENT CATEGORY: ☐ GENERIC ☒ PROJECT SPECIFIC

No.	Document Portion††	REVISION No. __0_____			REVISION No. _____			REVISION No. _____		
		Author's Initials	Date Approved	VIR #	Author's Initials	Date Approved	VIR #	Author's Initials	Date Approved	VIR #
1.	Chap 1	ER	03/13/08	453061						
2.	Chap 2	ER	03/13/08	594197						
3.	Chap 3	ER	03/13/08	243458						
4.	Chap 4	KC	03/14/08	825438						
5.	Chap 5	CWB	03/14/08	504095						
6.	Chap 6	ER	03/13/05	927913						
7.	Chap 7	CWB	03/14/08	617763						
8.	Chap 8	ER	03/14/08	99115						
9.										
10.										
11.										
12.										

†† Chapter or section number.

HOLTEC INTERNATIONAL

DOCUMENT NUMBER: HI-2083956 PROJECT NUMBER: 1721

DOCUMENT CATEGORIZATION

In accordance with the Holtec Quality Assurance Manual and associated Holtec Quality Procedures (HQPs), this document is categorized as a:

- ☐ Calculation Package[3] (Per HQP 3.2)
- ☒ Technical Report (Per HQP 3.2)(Such as a Licensing Report)
- ☐ Design Criterion Document (Per HQP 3.4)
- ☐ Design Specification (Per HQP 3.4)
- ☐ Other (Specify):

DOCUMENT FORMATTING

The formatting of the contents of this document is in accordance with the instructions of HQP 3.2 or 3.4 except as noted below:

DECLARATION OF PROPRIETARY STATUS

☒ Nonproprietary ☐ Holtec Proprietary ☐ Privileged Intellectual Property (PIP)

Documents labeled Privileged Intellectual Property contain extremely valuable intellectual/commercial property of Holtec International. They cannot be released to external organizations or entities without explicit approval of a company corporate officer. The recipient of Holtec's proprietary or Top Secret document bears full and undivided responsibility to safeguard it against loss or duplication.

Notes:

1. This document has been subjected to review, verification and approval process set forth in the Holtec Quality Assurance Procedures Manual. Password controlled signatures of Holtec personnel who participated in the preparation, review, and QA validation of this document are saved in the N-drive of the company's network. The Validation Identifier Record (VIR) number is a random number that is generated by the computer after the specific revision of this document has undergone the required review and approval process, and the appropriate Holtec personnel have recorded their password-controlled electronic concurrence to the document.

2. A revision to this document will be ordered by the Project Manager and carried out if any of its contents is materially affected during evolution of this project. The determination as to the need for revision will be made by the Project Manager with input from others, as deemed necessary by him.

3. Revisions to this document may be made by adding supplements to the document and replacing the "Table of Contents", this page and the "Revision Log".

SUMMARY OF REVISIONS

Revision 0 – Original Revision.

TABLE OF CONTENTS

TABLE OF CONTENTS (continued)

1.0 INTRODUCTION

The Calvert Cliffs Nuclear Power Plant (CCNPP) Unit 3 U.S. Evolutionary Pressurized Water Reactor (EPR) is a next-generation nuclear power plant designed by Areva NP. The CCNPP Unit 3 U.S. EPR reactor is sized to hold 241 fuel assemblies, with each assembly consisting of 265 fuel rods and 24 guide tubes in a 17x17 array, and has a rated thermal capacity of about 4612 MW. The CCNPP Unit 3 U.S. EPR is equipped with storage facilities for both new and spent fuel assemblies. This topical report provides descriptions of the new fuel storage and the spent fuel storage equipment, and the operational and performance criteria that must be satisfied by the equipment. In addition, this topical report addresses the following Combined License (COL) items included in the U.S. EPR Final Safety Analysis Report (FSAR) dated December 11, 2007:

- From U. S. EPR FSAR Section 9.1.1.3, "A COL applicant that references the U.S. EPR design certification will demonstrate that the design satisfies the criticality analysis requirements for the new and spent fuel storage racks, and describe the results of the analyses for normal and credible abnormal conditions, including a description of the methods used, approximations and assumptions made, and handling of design tolerances and uncertainties."

- From U. S. EPR FSAR Section 9.1.2.2.1, "A COL applicant that references the U.S. EPR design certification will describe the new fuel storage racks, including a description of confirmatory structural dynamic and stress analyses."

- From U. S. EPR FSAR Section 9.1.2.2.2, "A COL applicant that references the U.S. EPR design certification will describe the spent fuel storage racks, including a description of confirmatory structural dynamic and stress analyses and thermal-hydraulic cooling analyses."

The new fuel storage facility will consist of two vaults holding 3 racks with locations to hold 168 un-irradiated fuel assemblies in the vertical orientation. All new fuel storage racks will be flux trap racks, where a gap bounded by neutron absorber panels separates adjacent fuel storage locations. Figure 1.1 shows the proposed configuration of the new fuel storage racks in the new fuel storage vaults. The new fuel storage vaults will be a normally dry facility, and the fuel assemblies stored therein will not be submerged in water. New fuel assemblies received at the

plant will be stored in the new fuel storage vaults until a refueling occurs, at which time they will be transferred into the spent fuel storage facility for loading into the reactor.

The spent fuel storage facility will consist of a steel-lined concrete spent fuel pool (SFP) holding 14 racks with locations to store 1360 fuel assemblies in the vertical orientation. There will be two types of racks in the SFP. The first type of racks, called Region 1 racks, will be flux trap racks suitable for storing both irradiated and/or un-irradiated fuel assemblies. There will be 4 of these racks each capable of holding 90 fuel assemblies, for a total Region 1 capacity of 360 assemblies. The second type of racks, called Region 2 racks, will be non-flux-trap racks with a single neutron absorber panel separating adjacent fuel storage locations and will be suitable for storing only fuel assemblies with prescribed enrichment and exposure characteristics. There will be 10 of these racks each capable of holding 100 fuel assemblies, for a total Region 2 capacity of 1000 assemblies. Figure 1.2 shows the proposed configuration of the spent fuel storage racks in the SFP. The spent fuel pool will be a wet facility, and the fuel assemblies stored therein will be kept submerged in borated water. Used fuel assemblies removed from the reactor will be stored in the SFP until they are removed for onsite dry storage or shipment to an offsite facility.

All new and spent fuel storage racks will be freestanding and self-supporting. The principal construction materials for the racks will be SA240-304 or -304L stainless steel sheet and plate stock, and SA564-630 precipitation hardened stainless steel bar for the adjustable support spindles. The only non-stainless material utilized in the rack will be the neutron absorber material, which is a boron carbide and aluminum metal matrix composite available under the patented product name Metamic™.

The new and spent fuel storage racks have been designed to meet the stress limits of, and be analyzed in accordance with, Section III, Division 1, Subsection NF of the ASME Boiler and Pressure Vessel (B&PV) Code [1-1]. The structural materials of the racks will be procured in accordance with the specifications of Section II of the ASME B&PV Code [1-2]. All applicable structural welds will be performed using procedures developed and qualified in accordance with Section IX of the ASME B&PV Code [1-3], and will be inspected in accordance with Section V

of the B&PV Code [1-4]. The material procurement, analysis, and fabrication of the rack modules will conform to USNRC 10CFR50 Appendix B requirements.

The rack designs described herein are direct evolutions of previous license applications. The operational and performance criteria specified for the racks are intended to ensure that the racks will meet all governing requirements of the applicable codes and standards and, in particular, the "OT Position for Review and Acceptance of Spent Fuel Storage and Handling Applications," USNRC (1978) and 1979 Addendum thereto [1-5].

This topical report was prepared to support the COL Application for the Calvert Cliffs Nuclear Power Plant (CCNPP) Unit 3. The CCNPP Unit 3 COL Application is the "Reference COL Application" (R-COLA) for the U.S. EPR Design-Centered Working Group (DCWG). This topical report is also applicable to each of the "Subsequent COL Applications" (S-COLAs) of the U.S. EPR DCWG. The individual chapters of this report present the following information:

- Chapters 2 and 3 of this report provide an abstract of the racks design and information about the materials that will be used for construction of the racks, respectively.
- Chapter 4 provides a summary of the criticality-related operational and performance criteria that must be satisfied by the new and spent fuel storage racks.
- Chapter 5 provides a summary of the seismic/structural operational and performance criteria that must be satisfied by the new and spent fuel storage racks.
- Chapter 6 provides a summary of the thermal-hydraulic operational and performance criteria that must be satisfied by the spent fuel storage racks (new fuel storage racks do not contain any heat).
- Chapter 7 provides a summary of the mechanical accident-related operational and performance criteria that must be satisfied by the spent fuel storage racks (new fuel storage racks do not contain any radioactive materials).
- Chapter 8 provides a summary of the radiological-related operational and performance criteria that must be satisfied by the spent fuel storage racks (new fuel storage racks do not contain any radioactive materials).

Chapters 4 through 8 also provide descriptions of any preliminary analyses performed to demonstrate that the associated operational and performance criteria will be satisfied.

1.1 References

[1-1] American Society of Mechanical Engineers (ASME), Boiler & Pressure Vessel Code, Section III, Subsection NF, 2004 Edition.

[1-2] American Society of Mechanical Engineers (ASME), Boiler & Pressure Vessel Code, Section II, 2004 Edition.

[1-3] American Society of Mechanical Engineers (ASME), Boiler & Pressure Vessel Code, Section IX, 2004 Edition.

[1-4] American Society of Mechanical Engineers (ASME), Boiler & Pressure Vessel Code, Section V, 2004 Edition.

[1-5] USNRC, "OT Position for Review and Acceptance of Spent Fuel Storage and Handling Applications," April 14, 1978, and Addendum dated January 18, 1979.

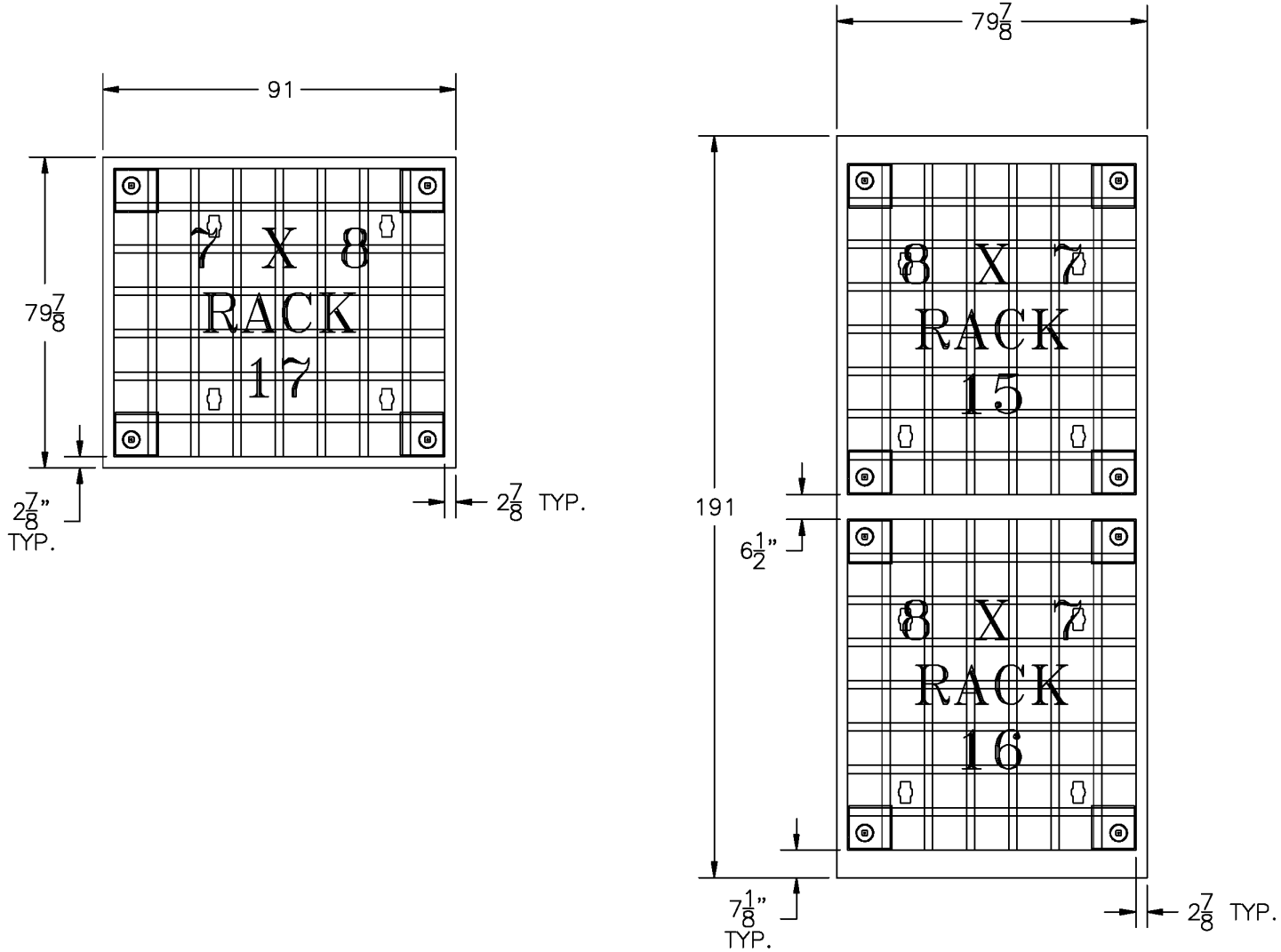

FIGURE 1.1 – PROPOSED NEW FUEL STORAGE RACKS LAYOUT FOR CALVERT CLIFFS EPR
(For Reference Only – All Dimensions Approximate)

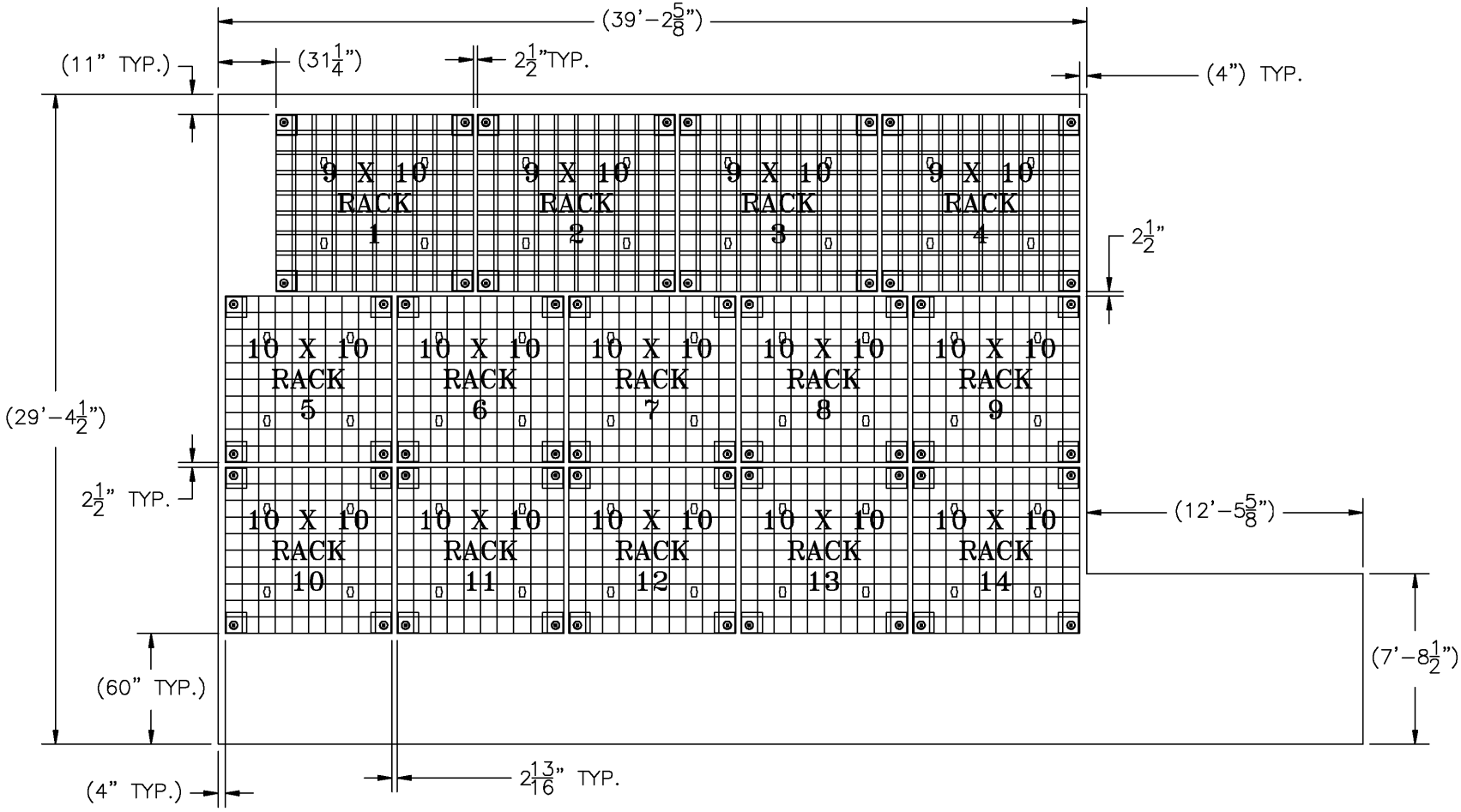

FIGURE 1.2 – PROPOSED SPENT FUEL STORAGE RACKS LAYOUT FOR CALVERT CLIFFS EPR
(For Reference Only – All Dimensions Approximate)

2.0 FUEL STORAGE RACKS

2.1 Introduction

The new fuel storage vaults will contain 3 safety-related, Seismic Category I, fuel storage racks with a total storage capacity of 168 new fuel assemblies. All new fuel storage racks will be of freestanding modules, made primarily from Type 304 or 304L austenitic stainless steel, containing honeycomb storage cells [redacted]
As described in Chapter 1, a flux trap bounded by two panels of Metamic metal matrix composite containing a high areal loading of enriched Boron-10 (B-10) isotope provides appropriate neutron attenuation between adjacent storage cells. Figure 2.1.1 provides an isometric schematic of a typical flux trap design storage rack module. Data on the cross sectional dimensions, weight and cell count for each rack module is presented in Table 2.1.1.

The SFP will contain 14 safety-related, Seismic Category I, fuel storage racks with a total storage capacity of 1360 new and/or spent fuel assemblies. All spent fuel storage racks will be freestanding modules, made primarily from Type 304 or 304L austenitic stainless steel, containing honeycomb storage cells [redacted]
As described in Chapter 1, Region 1 racks have a flux trap bounded by two panels of Metamic metal matrix composite containing a high areal loading of enriched Boron-10 (B-10) isotope to provide appropriate neutron attenuation between adjacent storage cells. Also as described in Chapter 1, Region 2 racks do not have a flux trap but do have a single panel of Metamic metal matrix composite between adjacent storage cells. Figure 2.1.1 provides an isometric schematic of a typical flux trap design storage rack module. Figure 2.1.2 provides an isometric schematic of a typical non-flux trap design storage rack module. Data on the cross sectional dimensions, weight and cell count for each rack module is presented in Table 2.1.1.

The baseplates on all new and spent fuel storage rack modules [redacted]. Each new and spent fuel rack module is supported by four pedestals, which are remotely adjustable. The rack module support

pedestals length adjustment is primarily provided to accommodate minor level variations in the pool floor flatness. Thus, the racks can be made vertical and the top of adjacent racks can easily be made co-planar with each other. Between the rack module pedestals and the supporting floor liner is a bearing pad, which serves to diffuse the dead load of the loaded racks into the reinforced concrete structure of the floor.

The overall design of the rack modules is similar to those presently in service in the spent fuel pools at many other nuclear plants. Altogether, Holtec has provided over 50 thousand storage cells of these designs to various nuclear plants around the world.

2.2 Summary of Principal Design Criteria

The key design criteria for the new and spent fuel storage racks are set forth in the USNRC memorandum entitled "OT Position for Review and Acceptance of Spent Fuel Storage and Handling Applications," dated 14 April 1978, as modified by amendment dated 18 January 1979. The individual sections of this report expound on the specific design bases derived from the above-mentioned "OT Position Paper". A brief summary of the design bases for the racks is presented in the following:

a. Disposition: All rack modules are required to be freestanding.

b. Kinematic Stability: All freestanding modules must be kinematically stable (against tipping or overturning) if a seismic event is imposed on any module.

c. Structural Compliance: All primary stresses in the rack modules must satisfy the limits postulated in Section III, Subsection NF, of the ASME B&PV Code.

d. Thermal-Hydraulic Compliance: The integrated average (i.e., bulk) pool temperature is required to remain below 140ºF in the wake of a bounding partial offload with the only one SFP cooling system train in operation. The bulk pool temperature is required to remain below 140ºF subsequent to a full core offload with the entire SFP cooling system in operation.

e. Criticality Compliance: The fuel storage racks must be able to store Zircaloy clad fuel of 5.0 weight percent (wt%) maximum enrichment while maintaining the

reactivity (K_{eff}) less than 0.95. This requirement must be applied to advanced, zirconium-based alloys such as Zirlo™ and M5™ as well as the Zircaloy.

f. Bearing Pads: The bearing pad size and thickness must ensure that the pressure on the concrete satisfies the American Concrete Institute (ACI) limits during and after a seismic event.

g. Accident Events: In the event of postulated drop events (uncontrolled lowering of a fuel assembly, for instance), it is necessary to demonstrate that the subcritical geometry of the rack structure is not compromised.

The foregoing design bases are further articulated in Chapters 4 through 8 of this report.

2.3 Applicable Codes and Standards

The following codes, standards and practices are used as applicable for the design, construction, and assembly of the fuel storage racks. Additional specific references related to detailed analyses are given in each section.

a. Design Codes

(1) American National Standards Institute/ American Nuclear Society ANSI/ANS 57.1, "Design Requirements for Light Water Reactor Fuel Handling Systems."

(2) American National Standards Institute/ American Nuclear Society ANSI/ANS 57.2, "Design Requirements for Light Water Reactor Spent Fuel Storage Facilities at Nuclear Power Plants".

(3) American National Standards Institute/ American Nuclear Society ANSI/ANS 57.3, "Design Requirements for New Fuel Storage Facilities at Light Water Reactor Plants."

(4) ASME B&PV Code Section III, 2004 Edition.

(5) American Society for Nondestructive Testing SNT-TC-1A, "Recommended Practice for Personnel Qualifications and Certification in Nondestructive Testing".

(6) ASME B&PV Code, Section II-Parts A and C, 2004 Edition.

b. Standards of American Society for Testing and Materials (ASTM)

(1) ASTM A262 - Standard Practices for Detecting Susceptibility to Intergranular Attack in Austenitic Stainless Steel.

(2) ASTM C750 - Standard Specification for Nuclear-Grade Boron Carbide Powder.

(3) ASTM E3 - Standard Practice for Preparation of Metallographic Specimens.

c. Welding Codes

(1) ASME B&PV Code, Section IX - Welding and Brazing Qualifications, 2004 Edition.

d. Quality Assurance, Cleanliness, Packaging, Shipping, Receiving, Storage, and Handling

(1) ASME B&PV Code, Section V, Nondestructive Examination, 2004 Edition.

(2) ASME NQA-1 – Quality Assurance Program Requirements for Nuclear Facilities.

e. USNRC Standard Review Documents

(1) "OT Position for Review and Acceptance of Spent Fuel Storage and Handling Applications," dated April 14, 1978, and the modifications to this document of January 18, 1979.

(2) Standard Review Plan (SRP) Section 3.7, Seismic Design.

(3) Standard Review Plan (SRP) Section 3.8.4, Other Seismic Category I Structures, Appendix D, Technical Position on Spent Fuel Racks.

(4) Standard Review Plan (SRP) Section 3.8.5, Foundations.

(5) Standard Review Plan (SRP) Section 9.1.1, New Fuel Storage.

(6) Standard Review Plan (SRP) Section 9.1.2, Spent Fuel Storage.

(7) Standard Review Plan (SRP) Section 9.1.3, Spent Fuel Pool Cooling and Cleanup System.

(9) Standard Review Plan (SRP) Section 15.4.7, Radiological Consequences of Fuel Handling Accidents.

f. ANSI Standards

(1) ANSI/ANS 8.1 - Nuclear Criticality Safety in Operations with Fissionable Materials Outside Reactors.

(2) ANSI/ANS 8.17 - Criticality Safety Criteria for the Handling, Storage, and Transportation of LWR Fuel Outside Reactors.

g. Code-of-Federal Regulations (CFR)

(1) 10CFR20 - Standards for Protection Against Radiation.

(2) 10CFR21 - Reporting of Defects and Non-compliance.

(3) 10CFR50 Appendix A - General Design Criteria for Nuclear Power Plants, General Design Criteria 2, 61 and 62.

(4) 10CFR50 Appendix B - Quality Assurance Criteria for Nuclear Power Plants and Fuel Reprocessing Plants.

h. USNRC Regulatory Guides (RG)

(1) RG 1.13 - Spent Fuel Storage Facility Design Basis.

(2) RG 1.25 - Assumptions Used for Evaluating the Potential Radiological Consequences of a Fuel Handling Accident in the Fuel Handling and Storage Facility for Boiling and Pressurized Water Reactors.

(3) RG 1.28 - Quality Assurance Program Requirements - Design and Construction.

(4) RG 1.33 – Quality Assurance Program Requirements.

(5) RG 1.29 - Seismic Design Classification.

(6) RG 1.31 - Control of Ferrite Content in Stainless Steel Weld Metal.

(7) RG 1.44 - Control of the Use of Sensitized Stainless Steel.

(8) RG 1.60 – Design Response Spectra for Seismic Design of Nuclear Power Plants.

(9) RG 1.61 - Damping Values for Seismic Design of Nuclear Power Plants.

(10) RG 1.92 - Combining Modal Responses and Spatial Components in Seismic Response Analysis.

(11) RG 1.124 - Service Limits and Loading Combinations for Class 1 Linear-Type Component Supports.

(12) RG 3.4 - Nuclear Criticality Safety in Operations with Fissionable Materials at Fuels and Materials Facilities.

i. American Welding Society (AWS) Standards

(1) AWS D1.1 - Structural Welding Code - Steel.

(2) AWS A2.4 - Standard Symbols for Welding, Brazing and Nondestructive Examination.

(3) AWS A3.0 - Standard Welding Terms and Definitions.

(4) AWS A5.12 Specification for Tungsten and Tungsten Alloy Electrodes for Arc-Welding and Cutting

(5) AWS QC1 - Standard for AWS Certification of Welding Inspectors.

(6) AWS 5.4 – Specification for Stainless Steel Electrodes for Shielded Metal Arc Welding.

(7) AWS 5.9 – Specification for Bare Stainless Steel Welding Electrodes and Rods.

2.4 Quality Assurance Program

The governing quality assurance requirements for design and fabrication of the new and spent fuel racks are stated in 10CFR50 Appendix B. Holtec's Nuclear Quality Assurance program complies with this regulation and is designed to provide a flexible but highly controlled system for the design, analysis and licensing of customized components in accordance with various codes, specifications, and regulatory requirements.

2.5 Mechanical Design

The rack modules are designed as cellular structures such that each fuel assembly has a square opening with conforming lateral support and a flat horizontal-bearing surface. All of the spent fuel storage locations are constructed with multiple cooling flow holes to ensure that redundant

flow paths for the coolant are available. The basic characteristics of the new and spent fuel racks are summarized in Tables 2.5.1 and 2.5.2.

A central objective in the design of the new rack modules is to maximize structural strength while minimizing inertial mass and dynamic response. Accordingly, the rack modules have been designed to simulate multi-flange beam structures resulting in excellent de-tuning characteristics with respect to the applicable seismic events. The next section presents an item-by-item description of the rack modules in the context of the fabrication methodology.

2.6 Rack Fabrication

The object of this section is to provide a brief description of the rack module construction activities, which enable an independent appraisal of the adequacy of design. The pertinent methods used in manufacturing the new and spent fuel storage racks may be stated as follows:

1. The rack modules will be fabricated in such a manner that the storage cell surfaces, which would come in contact with the fuel assembly, will be free of harmful chemicals and projections (e.g., weld splatter).

2. The component connection sequence and welding processes will be selected to reduce fabrication distortions.

3. The fabrication process will involve operational sequences that permit immediate accessibility for verification by the inspection staff.

4. The racks will be fabricated per the Holtec Appendix B Quality Assurance program, which ensures, and documents, that the fabricated rack modules will meet all of the requirements of the design and fabrication documents.

2.6.1 Flux Trap Rack Module Description

This section describes the constituent elements of the flux trap rack module in the fabrication sequence. Figure 2.1.1 provides a schematic view of a typical flux trap rack. The rack is constructed with water flux traps located between adjacent panels of neutron absorbing material.

The rack module manufacturing begins with fabrication of the "box". The boxes are fabricated . Figure 2.6.1 shows the box.

A die is used to flare out one end of the box to provide the tapered lead-in (Figure 2.6.2). are made on all four sides near the other end of the box to provide the requisite auxiliary flow holes.

Each box constitutes a storage location. Each external box side for the flux trap rack is equipped with a stainless steel sheathing, which holds one integral Metamic sheet (neutron absorber material). The design objective calls for attaching Metamic tightly on the box surface. This is accomplished by , as shown in Figure 2.6.1. The flanges of the sheathing are attached to the box using skip welds and spot welds. The sheathings serve to locate and position the neutron absorber sheet accurately, and to preclude its movement under seismic conditions.

Having fabricated the required number of composite box assemblies, they are joined together in a fixture using in the manner shown in Figure 2.6.3. Figure 2.6.4 shows an elevation view of two storage cells of the flux trap rack module. A representative is also shown in the figure. Joining the cells results in a well-defined shear flow path, and essentially makes the box assemblage into a multi-flanged beam-type structure. The "baseplate" is attached to the bottom edge of the boxes. The baseplate is an austenitic stainless steel plate stock that has large diameter holes (

) cut out in a pitch identical to the box pitch. The baseplate is attached to the cell assemblage by fillet welding the box edge to the plate.

In the final step, adjustable leg supports (shown in Figure 2.6.5) are welded to the underside of the baseplate. The adjustable legs provide for vertical height adjustment at each leg location.

Appropriate NDE (nondestructive examination) occurs on all welds including visual examination of sheathing welds, box longitudinal seam welds, box-to-baseplate welds, and box-to-box connection welds, as well as liquid penetrant examination of support leg welds, in accordance with the design drawings.

2.6.2 Non-Flux Trap Rack Module

Non-flux trap storage cell locations have a single neutron absorber panel between adjacent cell boxes on the wall surfaces separating them. The significant components (discussed below) of the non-flux trap rack are: (1) the storage box subassembly (2) the baseplate, (3) the neutron absorber material, (4) the sheathing, and (5) the support legs.

1. Storage cell box subassembly: As described for the flux trap rack, the boxes are fabricated from . Figure 2.6.1 shows a typical box subassembly.

   Each box has four lateral holes near its bottom edge to provide auxiliary flow holes. As shown in Figure 2.6.1, sheathing is attached to each side of the box with the neutron absorber material installed in the sheathing cavity. The edges of the sheathing and the box are welded together to form a smooth edge. The box, with integrally connected sheathing, is referred to as the "composite box".

   The composite boxes are arranged in a checkerboard array to form an assemblage of storage cell locations (Figure 2.6.6). Filler panels and corner angles are welded to the edges of boxes at the outside boundary of the rack to make the peripheral formed cells. The inter-box welding and pitch adjustment are accomplished by . This assemblage of box assemblies is welded as shown in Figure 2.6.6, resulting in a honeycomb structure with axial, flexural and torsional rigidity depending on the extent of inter-cell welding provided. It can be seen from Figure 2.6.6

that two edges of each interior box are connected to the contiguous boxes resulting in a well-defined path for "shear flow".

2. Baseplate: The baseplate provides a continuous horizontal surface for supporting the fuel assemblies. The baseplate is an austenitic stainless steel plate, which has a large diameter hole in each cell location ( ) as described in the preceding section. The baseplate is attached to the cell assemblage by fillet welds.

3. Neutron Absorber Material: As mentioned in the preceding section, Metamic is used as the neutron absorber material.

4. Sheathing: As described earlier, the sheathing serves as the locator and retainer of the neutron absorber material.

5. Support legs: As stated earlier, all support legs are the adjustable type (Figure 2.6.5). The top (female threaded) portion is made of austenitic steel material. The bottom (male) part is made of 17-4 Ph series stainless steel to avoid galling problems.

   Each support leg is equipped with a to enable remote leveling of the rack after its placement in the pool.

An elevation view of three contiguous Region 2 cells is shown in Figure 2.6.7.

TABLE 2.1.1: GEOMETRIC AND PHYSICAL DATA FOR THE NEW FUEL RACKS							
RACK I.D.	RACK TYPE	NO. OF CELLS		MODULE ENVELOPE SIZE		WEIGHT (Lbs)	NO. OF CELLS PER RACK
		N-S Dir.	E-W Dir.	N-S	E-W		
FUEL STORAGE RACKS IN SPENT FUEL POOL							
1	Flux Trap	9	10	96.5	107.4	30,000	90
2	Flux Trap	9	10	96.5	107.4	30,000	90
3	Flux Trap	9	10	96.5	107.4	30,000	90
4	Flux Trap	9	10	96.5	107.4	30,000	90
5	Non-Flux Trap	10	10	90.7	90.7	19,000	100
6	Non-Flux Trap	10	10	90.7	90.7	19,000	100
7	Non-Flux Trap	10	10	90.7	90.7	19,000	100
8	Non-Flux Trap	10	10	90.7	90.7	19,000	100
9	Non-Flux Trap	10	10	90.7	90.7	19,000	100
10	Non-Flux Trap	10	10	90.7	90.7	19,000	100
11	Non-Flux Trap	10	10	90.7	90.7	19,000	100
12	Non-Flux Trap	10	10	90.7	90.7	19,000	100
13	Non-Flux Trap	10	10	90.7	90.7	19,000	100
14	Non-Flux Trap	10	10	90.7	90.7	19,000	100
FUEL STORAGE RACKS IN NEW FUEL STORAGE VAULTS							
15	Flux Trap	8	7	85.6	74.7	19,000	56
16	Flux Trap	8	7	85.6	74.7	19,000	56
17	Flux Trap	7	8	74.7	85.6	19,000	56

Note: All dimensions and weights in this table are approximate.

Table 2.5.1 MODULE DATA FOR FLUX TRAP (NEW FUEL STORAGE AND REGION 1 SPENT FUEL STORAGE) RACKS[1]	
Storage Cell Inside Dimension	8.8 in.
Cell Pitch	10.9 in.
Storage Cell Height (above baseplate)	197 in.
Baseplate Hole Size ( )	5 in.
Baseplate Thickness	3/4 in.
Support Pedestal Height (including bearing pad)	
Support Pedestal Type	Remotely adjustable pedestals
Number Of Support Pedestals Per Rack	4
Number Of Cell Walls Containing Auxiliary Flow Holes At Base Of Cell Wall	4
Remote Lifting And Handling Provisions	Yes
Neutron Absorber Material	Metamic
Neutron Absorber Length	
Neutron Absorber Width	

1 All dimensions indicate nominal values.

Table 2.5.2 MODULE DATA FOR NON-FLUX TRAP (REGION 2) SPENT FUEL STORAGE RACKS[1]	
Storage Cell Inside Dimension	8.8 in.
Cell Pitch	9.03 in.
Storage Cell Height (above baseplate)	197 in.
Baseplate Hole Size ( )	5 in.
Baseplate Thickness	3/4 in.
Support Pedestal Height (including bearing pad)	
Support Pedestal Type	Remotely adjustable pedestals
Number Of Support Pedestals Per Rack	4
Number Of Cell Walls Containing Auxiliary Flow Holes At Base Of Cell Wall	4
Remote Lifting And Handling Provisions	Yes
Neutron Absorber Material	Metamic
Neutron Absorber Length	
Neutron Absorber Width	

1 All dimensions indicate nominal values.

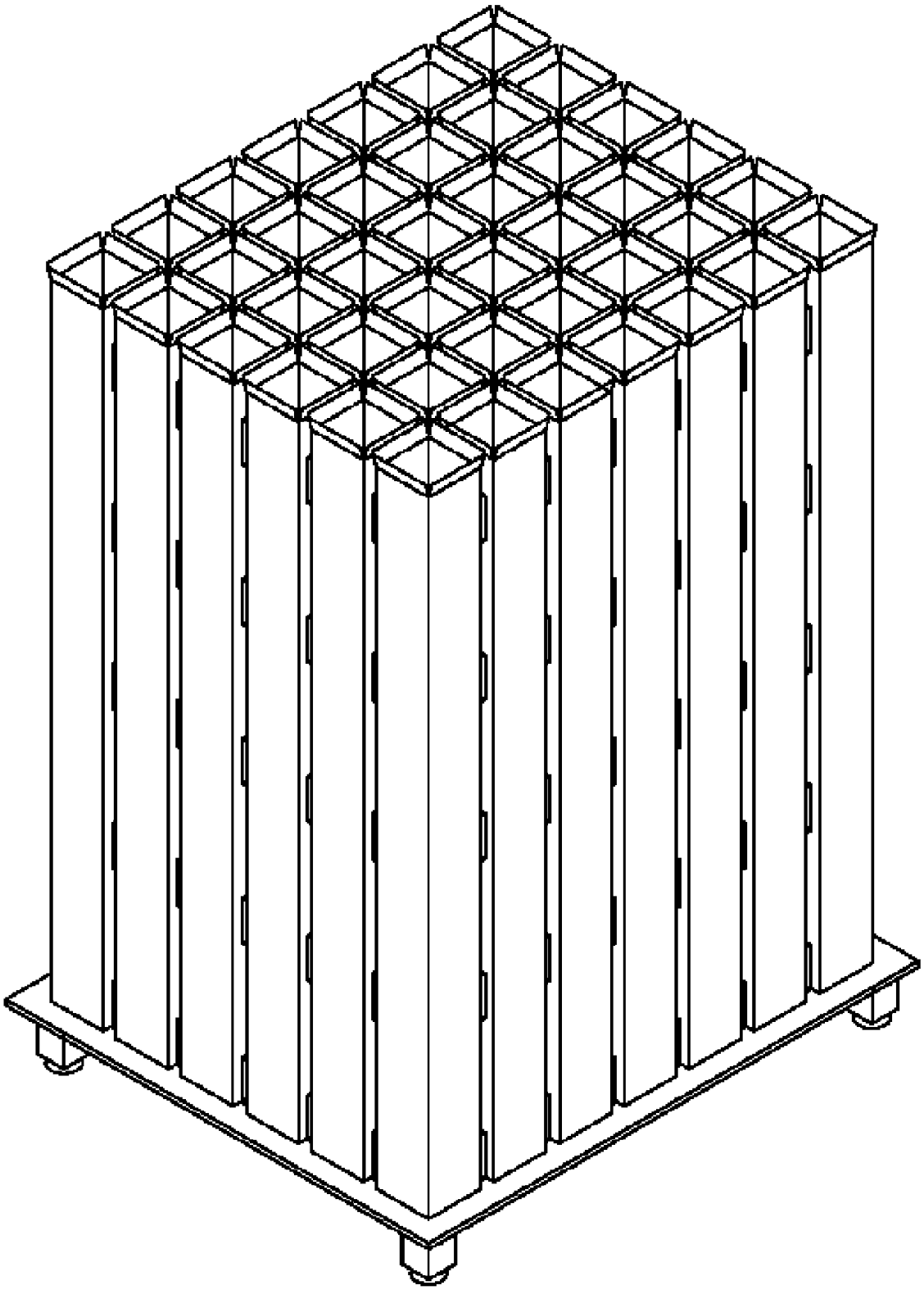

FIGURE 2.1.1 – ISOMETRIC VIEW OF A GENERIC FLUX TRAP RACK

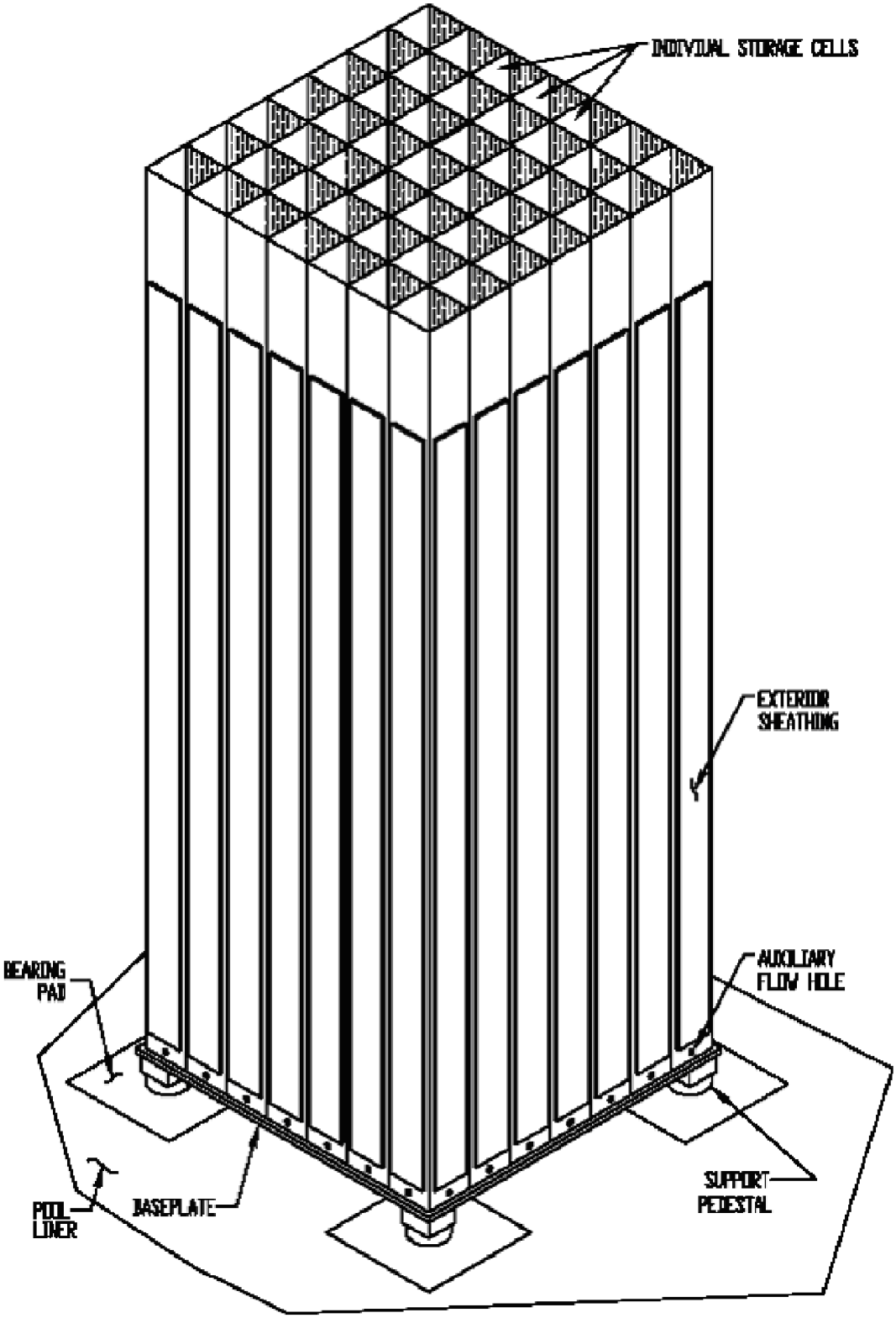

FIGURE 2.1.2 – ISOMETRIC VIEW OF GENERIC NON-FLUX TRAP RACK

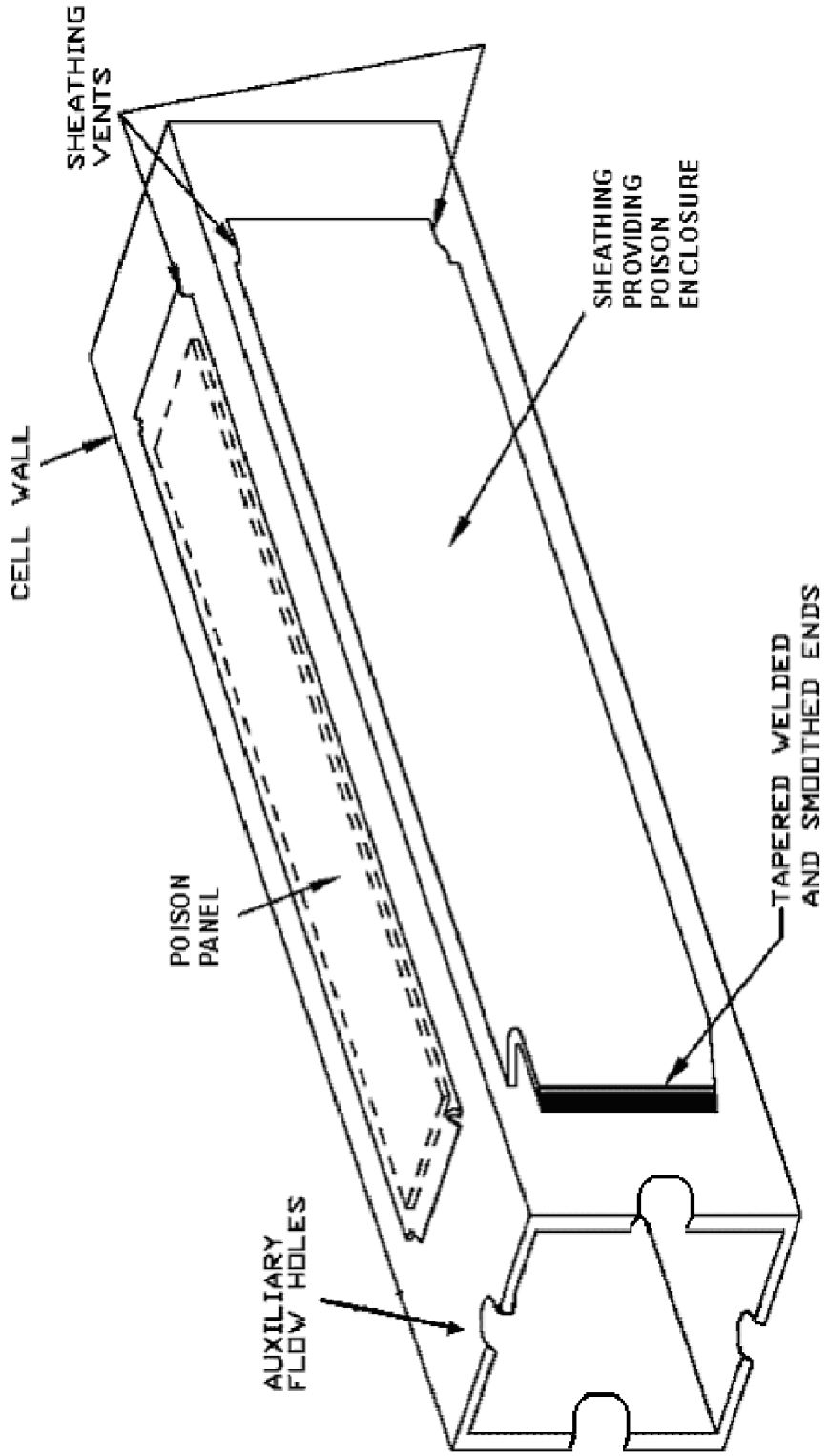

FIGURE 2.6.1 – ISOMETRIC VIEW OF COMPOSITE BOX ASSEMBLY

(Flared Top End for Flux Trap Boxes Not Shown)

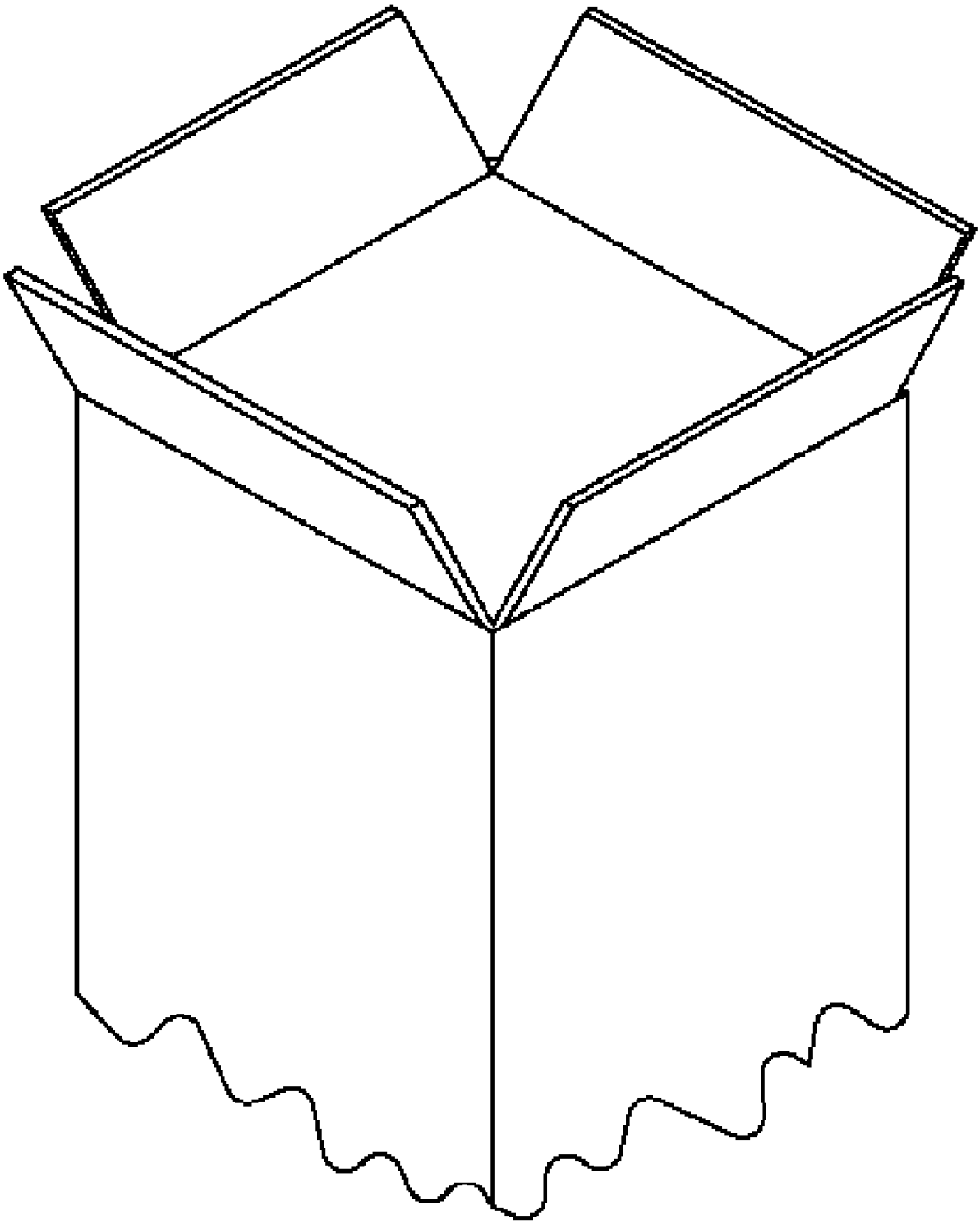

FIGURE 2.6.2 – ISOMETRIC VIEW OF FLUX TRAP RACK CELL LEAD-IN

PROPRIETARY FIGURE REDACTED

FIGURE 2.6.3 – ASSEMBLAGE OF FLUX TRAP RACK CELLS

PROPRIETARY FIGURE REDACTED

FIGURE 2.6.4 – FLUX TRAP RACK CELLS ELEVATION VIEW

PROPRIETARY FIGURE REDACTED

FIGURE 2.6.5 – ADJUSTABLE PEDESTAL DESIGN

PROPRIETARY FIGURE REDACTED

FIGURE 2.6.6 – PLAN VIEW OF GENERIC NON-FLUX TRAP RACK ARRAY

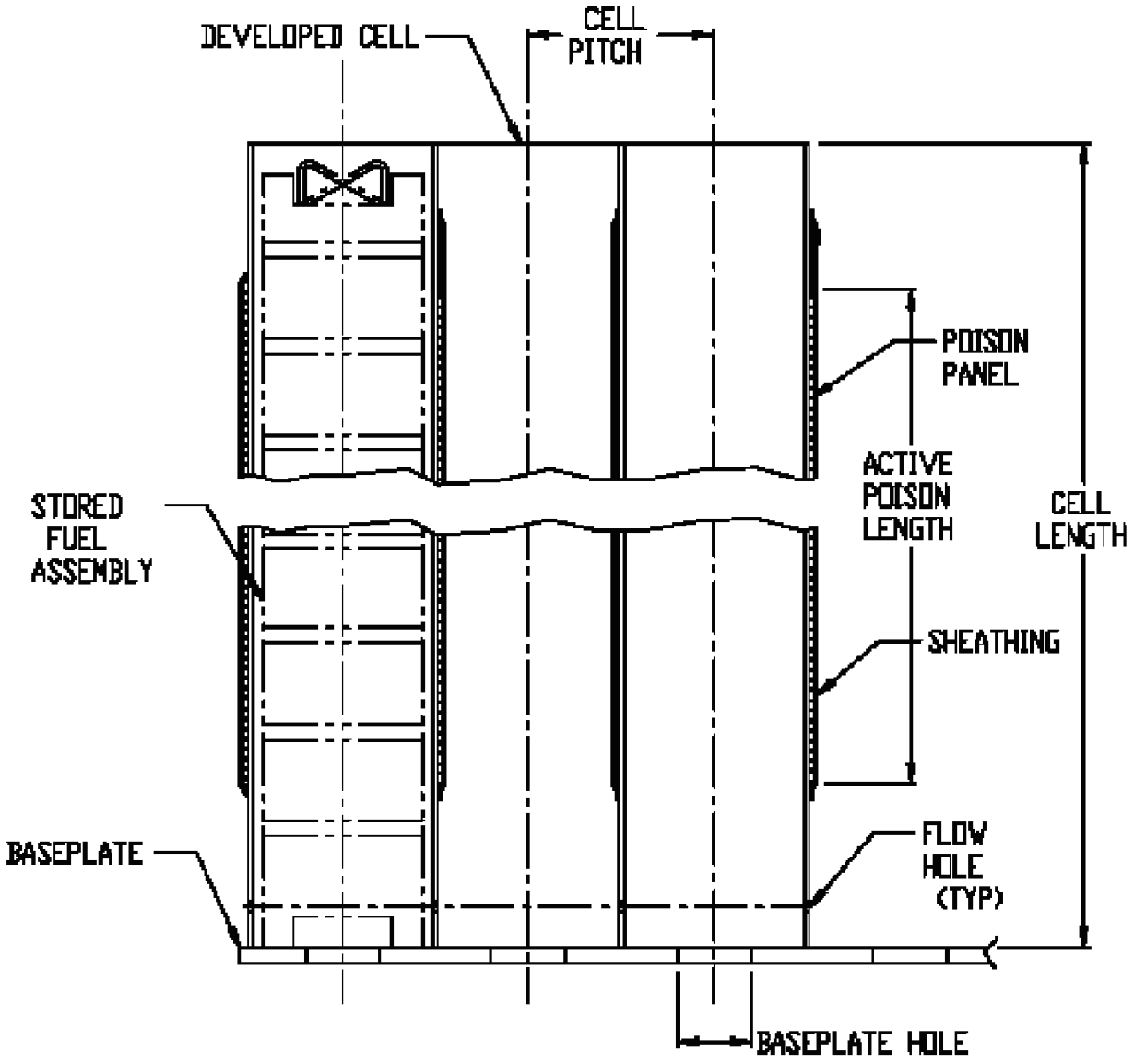

FIGURE 2.6.7 – NON-FLUX TRAP RACK CELLS ELEVATION VIEW

3.0 MATERIAL CONSIDERATIONS

3.1 Introduction

Safe storage of nuclear fuel in the new and spent fuel storage facilities requires that the materials utilized in the rack fabrication be of proven durability and compatible with the environments to which they will be exposed. This section provides a synopsis of the considerations with regard to long-term service life.

3.2 Structural Materials

The following structural materials will be utilized in the fabrication of the fuel storage racks:

a. Sheet Stock (cells and sheathing): ASME SA240-304 or -304L
b. Plate Stock (baseplates and female pedestals): ASME SA240-304 or -304L
c. Bar Stock (male pedestals): ASME SA564-630 (heat treated to 1100°F)
d. Weld Material: ASME Type 308 or 308L

The capacity for being passivated is the strength of stainless steels. Steels with chromium content greater than 12% are easily passivated. The addition of nickel markedly facilitates passivation and molybdenum will further facilitate passivation. AISI Type 304 and 304L stainless steels contain a minimum of 16% chromium and 8% nickel, and at least traces of molybdenum. The passive films of stainless steels range between 10 to 50 angstroms (0.04 to 0.2 microinches) thick [3.2.11].

For PWRs, the soluble boron levels are typically maintained at or below 2500 ppm (0.25% boric acid solution). Experimental corrosion data for AISI Type 304 stainless steels (Swedish Designation SIS-14-2333) is available from the Swedish Avesta Jernverk laboratory [3.2.11]. Corrosive media evaluated in these tests include 4% (40,000 ppm) and 20% (200,000 ppm) boric acid solutions and water, all at boiling. Under the evaluated conditions, the tested steel is identified as “fully resistant”. An even more extensive set of experimental corrosion data is

available from ASM International [3.2.12]. For test conditions without rapid agitation, similar to conditions that would exist in a spent fuel pool, all AISI Type 304 stainless steel is resistant to corrosion in boric acid and water.

Various NRC Information Notices, Bulletins, Generic Letters, and Circulars [3.2.13] have been reviewed in an effort to gain additional industry experience on corrosion of stainless steels. It is recognized that stainless steels in borated water and treated water (demineralized water) environments are susceptible to loss of material due to pitting corrosion and cracking due to stress corrosion and intergranular attack (IGSCC) but these mechanisms depend greatly on presence of halogens and oxygen or the presence of sulfates and oxygen. Spent fuel pool and treated water chemistry programs normally keep the concentrations of halogens and sulfates at very low levels for the very same reason of avoiding corrosion problems not only with spent fuel assemblies but with other systems such as those that are relied upon for the operation of the spent fuel pool. In addition, stringent controls on conductivity, which is essentially a measure of impurities, further limits corrosion in treated and borated water environments. The fuel storage racks temperature during normal operation is below the 200°F temperature threshold for cracking from dissolved oxygen.

3.3 Neutron Absorbing Material

The Metamic® neutron absorber material, proposed for use in the fuel storage racks, is manufactured by Metamic, LLC of Lakeland, Florida (www.metamic.com). As discussed below, Metamic has been subjected to rigorous tests by various organizations including Holtec International, and has been approved by the USNRC in recent dry as well as wet storage applications.

Metamic was developed in the mid-1990s by the Reynolds Metals Company [3.2.9] with the technical support of the Electric Power Research Institute (EPRI) for spent fuel reactivity control in dry and wet storage applications with the explicit objective to eliminate the performance frailties of aluminum cermet type of absorbers reported in the industry. Metallurgically, Metamic™ is a metal matrix composite (MMC) consisting of a matrix of aluminum reinforced

with [redacted] boron carbide. Metamic is characterized by extremely fine aluminum ([redacted]) and boron carbide (B_4C) powder. Typically, the average B_4C particle size is between [redacted]. The high performance and reliability of Metamic derives from the fineness of the B_4C particle size and uniformity of its distribution, which is solidified into a metal matrix composite structure by the powder metallurgy process. This yields excellent homogeneity and a porosity-free material.

In Metamic's manufacturing process, the aluminum and boron carbide powders [redacted] An array of U.S. patents discloses the unique technologies that underlie the Metamic neutron absorber [3.2.1-3.2.4].

In recognition of the central role of the neutron absorber in maintaining the subcriticality, Holtec International utilizes appropriately rigorous technical and quality assurance criteria and acceptance protocols to ensure satisfactory neutron absorber performance over the service life of the fuel racks. Holtec International's Quality Assurance program ensures that Metamic will be manufactured under the control and surveillance of a Quality Assurance/Quality Control Program that conforms to the requirements of 10CFR50 Appendix B, "Quality Assurance Criteria for Nuclear Power Plants." Consistent with its role in reactivity control, all neutron absorbing material procured for use in the Holtec racks is categorized as Safety Related (SR). SR manufactured items, as required by Holtec's NRC-approved Quality Assurance program, must be produced to essentially preclude, to the extent possible, the potential of an error in the procurement of constituent materials and the manufacturing processes.

Accordingly, material and manufacturing control processes must be established to eliminate the incidence of errors, and inspection steps are implemented to serve as an independent set of barriers to ensure that all critical characteristics defined for the material by Holtec's design team are met in the manufactured product.

3.3.1 Characteristics of Metamic

Because Metamic is a [redacted]

To determine its physical stability and performance characteristics, Metamic was subjected to an extensive array of tests sponsored by EPRI that evaluated the functional performance of the material at elevated temperatures (up to 900ºF) and radiation levels (1E+11 rads gamma). The results of the tests documented in an EPRI report [3.2.5] indicate that Metamic maintains its physical and neutron absorption properties with little variation in its properties from the unirradiated state. The main conclusions provided in the above-referenced EPRI report, which endorsed Metamic for dry and wet storage applications on a generic basis, are summarized below:

- The metal matrix configuration produced by the powder metallurgy process with almost a complete absence of open porosity in Metamic ensures that its density is essentially equal to the theoretical density.
- The physical and neutronic properties of Metamic are essentially unaltered under exposure to elevated temperatures (750°F - 900°F).
- No detectable change in the neutron attenuation characteristics under accelerated corrosion test conditions has been observed.

Additional technical information on Metamic in the literature includes independent measurements of boron carbide particle distribution in Metamic panels, which showed extremely small particle-to-particle distance [3.2.6]. *The USNRC has previously approved Metamic for use in both wet storage [3.2.7] and dry storage [3.2.8] applications.*

Metamic has also been subjected to independent performance assessment tests by Holtec International in the company's Florida laboratories since 2001 [3.2.9, 3.2.10]. These independent Holtec tests essentially confirmed earlier EPRI and other industry reports cited in the foregoing with regard to Metamic™'s suitability as a neutron absorber in fuel storage applications.

3.4 In-Service Surveillance of the Neutron Absorber

3.4.1 Purpose

Metamic, the neutron absorbing material incorporated in the fuel storage rack design to assist in controlling system reactivity, consists of finely divided particles of boron carbide (B_4C) uniformly distributed in Type 6061 aluminum powder. Tests simulating the radiation, thermal and chemical environment of the spent fuel pool have demonstrated the stability and chemical inertness of Metamic.

Based upon the accelerated test programs, Metamic is considered a satisfactory material for reactivity control in fuel storage racks and is fully expected to fulfill its design function over the lifetime of the racks. Nevertheless, as a defense-in-depth measure, a Metamic surveillance program has been developed and will be implemented for the SFP in order to monitor the integrity and performance of Metamic.

The purpose of the surveillance program is to characterize certain properties of the Metamic with the objective of providing data necessary to assess the capability of the Metamic panels in the racks to continue to perform their intended function. The surveillance program is also capable of detecting the onset of any significant degradation with ample time to take such corrective action as may be necessary.

The Metamic surveillance program depends primarily on representative coupon samples to monitor performance of the absorber material without disrupting the integrity of the storage

system. The principal parameters to be measured are the thickness (to monitor for swelling) and B-10 loading (to monitor for the continued presence of boron in the Metamic).

3.4.2 Coupon Surveillance Program

3.4.2.1 Coupon Description

The coupon measurement program includes coupons suspended on a mounting (called a tree), placed in a designated cell, and surrounded by spent fuel. Coupons are removed from the array on a prescribed schedule and certain physical measured from which the stability and integrity of the Metamic in the storage cells may be inferred.

The coupon surveillance program uses two trees (one tree each for Region 1 and Region 2), with a total of 8 to10 test coupons per tree. In mounting the coupons on the tree, the coupons are positioned axially within the central eight feet (approximate) of the active fuel zone where the gamma flux is expected to be reasonably uniform.

The coupons will be taken from the same lot as that used for construction of the racks. Each coupon will be carefully pre-characterized prior to insertion in the pool to provide reference initial values for comparison with measurements made after irradiation. As a minimum, the surveillance coupons will be pre-characterized for weight, dimensions (especially thickness) and B-10 loading.

3.4.2.2 Surveillance Coupon Testing Schedule

To assure that the coupons will have experienced a slightly higher radiation dose than the Metamic in the racks, the Region 1 coupon tree will be surrounded by freshly-discharged fuel assemblies after each refueling. At the time of the first fuel offload, the four storage cells surrounding the Region 1 tree shall be loaded with freshly-discharged fuel assemblies from among those which are not scheduled to be returned to the core. At the scheduled test date, the coupon tree will be removed and a coupon removed for evaluation. Effort will be made to

surround the coupon tree with freshly discharged fuel during each refueling discharge. The fuel assemblies initially placed in the four cells surrounding the tree will be removed and replaced with freshly discharged assemblies and the tree will remain in place. The recommended coupon measurement schedule is shown in Table 3.4.1.

Evaluation of the coupons removed will provide information of the effects of the radiation, thermal and chemical environment of the pool and by inference, comparable information on the Metamic panels in the racks. Over the duration of the coupon testing program, the coupons will have accumulated more radiation dose than the expected lifetime dose for normal storage cells. Coupons, which have not been destructively analyzed by wet-chemical processes, may optionally be returned to the storage pool and remounted on the tree. They will then be available for subsequent investigation of defects, should any be found.

3.4.2.3 Measurement Program

The coupon measurement program is intended to monitor changes in physical properties of the Metamic absorber material by performing the following measurements on the preplanned schedule:

- Visual Observation and Photography
- Neutron Attenuation
- Dimensional Measurements (length, width and thickness)
- Weight and Specific Gravity

3.4.2.4 Surveillance Coupon Acceptance Criteria

Of the measurements to be performed on the Metamic surveillance coupons, the most important are (1) the neutron attenuation[1] measurements (to verify the continued presence of the boron) and (2) the thickness measurement (as a monitor of potential swelling). Acceptance criteria for these measurements are as follows:

1 Neutron attenuation measurements are a precise instrumental method of chemical analysis for Boron-10 content using a nondestructive technique in which the percentage of thermal neutrons transmitted through the panel is measured and compared with predetermined calibration data. Boron-10 is the nuclide of principal interest since it is the isotope responsible for neutron absorption in the Metamic panel.

- A decrease of no more than 5% in Boron-10 content, as determined by neutron attenuation, is acceptable. This is tantamount to a requirement for no loss in boron within the accuracy of the measurement.

- An increase in thickness at any point should not exceed 10% of the initial thickness at that point.

Changes in excess of either of these two criteria requires investigation and engineering evaluation, which may include early retrieval and measurement of one or more of the remaining coupons to provide corroborative evidence that the indicated changes are real. If the deviation is determined to be real, an engineering evaluation shall be performed to identify further testing or any corrective action that may be necessary.

The remaining measurement parameters serve a supporting role and should be examined for early indications of the potential onset of Metamic degradation that would suggest a need for further attention and possibly a change in measurement schedule. These include (1) visual or photographic evidence of unusual surface pitting, corrosion or edge deterioration, or (2) unaccountable weight loss in excess of the measurement accuracy.

3.5 References

[3.2.1] U.S. Patent # 6,332,906 entitled "Aluminum-Silicon Alloy formed by Powder", Thomas G. Haynes III and Dr. Kevin Anderson, issued December 25, 2001.

[3.2.2] U.S. Patent # 5,965,829 entitled "Radiation Absorbing Refractory Composition and Method of Manufacture", Dr. Kevin Anderson, Thomas G. Haynes III, and Edward Oschmann, issued October 12, 1999.

[3.2.3] U.S. Patent # 6,042,779 entitled "Extrusion Fabrication Process for Discontinuous Carbide Particulate Metal and Super Hypereutectic Al/Si Alloys", Thomas G. Haynes III and Edward Oschmann, issued March 28, 2000.

[3.2.4] U.S. Patent Application 09/433773 entitled "High Surface Area Metal Matrix Composite Radiation Absorbing Product", Thomas G. Haynes III and Goldie Oliver, filed May 1, 2002.

[3.2.5] "Qualification of METAMIC® for Spent Fuel Storage Application," EPRI, 1003137, Final Report, October 2001.

[3.2.6] "METAMIC Neutron Shielding", by K. Anderson, T. Haynes, and R. Kazmier, EPRI Boraflex Conference, November 19-20 (1998).

[3.2.7] "Safety Evaluation by the Office of Nuclear Reactor Regulation Related to Holtec International Report HI-2022871 Regarding Use of Metamic in Fuel Pool Applications," Facility Operating License Nos. DPR-51 and NPF-6, Entergy Operations, Inc., Docket No. 50-313 and 50-368, USNRC, June 2003.

[3.2.8] USNRC Docket No. 72-1004, NRC's Safety Evaluation Report on NUHOMS 61BT (2002).

[3.2.9] "Use of METAMIC® in Fuel Pool Applications," Holtec Information Report No. HI-2022871, Revision 1 (2002).

[3.2.10] "Sourcebook for Metamic™ Performance Assessment" by Dr. Stanley Turner, Holtec Report No. HI-2043215, Revision 2 (2006).

[3.2.11] Peckner and Bernstein, "Handbook of Stainless Steels," First Edition, 1977.

[3.2.12] Craig and Anderson, "Handbook of Corrosion Data," ASM International, First Edition, 1995.

[3.2.13] NRC Generic Communications (Information Notices IN80027, IN82006, IN84041, IN86108s2, IN90066, IN90068s1, IN93020, IN95038, IN97013, IN97010 and IN03002; Bulletins BL-96-04 and BL-76-04; Generic Letters GL88001, GL88005 and GL91017; Circular CR76006).

Table 3.4.1 RECOMMENDED COUPON MEASUREMENT SCHEDULE	
Coupon	Years[1]
1	2
2	4
3	6
4	8
5	10
6	15
7	20
8	25
9	30
10	40

1 The years pertain to those after the installation of the spent fuel storage racks.

4.0 CRITICALITY EVALUATION

4.1 Introduction

This topical report provides information on the new and spent fuel storage racks to support a COLA for the Calvert Cliffs Nuclear Power Plant (CCNPP) Unit 3 U.S. EPR. This chapter, specifically, provides information on the required criticality control performance characteristics of the fuel storage racks.

The objective of the requirements in this chapter is to ensure that the effective neutron multiplication factor (k_{eff}) is less than or equal to 0.95 with the storage racks fully loaded with fuel of the highest anticipated reactivity and the pool flooded with un-borated water at a temperature corresponding to the highest reactivity. The maximum calculated reactivity includes a margin for uncertainty in reactivity calculations including manufacturing tolerances and is shown to be less than 0.95 with a 95% probability at a 95% confidence level. Reactivity effects of abnormal and accident conditions have also been evaluated to assure that under all credible abnormal and accident conditions, the reactivity will not exceed the regulatory limit of 0.95. The purpose of the present analysis is to confirm the acceptability of the storage rack designs.

The Region 1 and Region 2 style high-density spent fuel storage racks at the CCNPP Unit 3 U.S. EPR nuclear power plant will be designed and analyzed for the following:

- Region 1 racks can be loaded with fresh fuel of up to 5.0 wt% ^{235}U enrichment.
- For Region 2 racks a minimum burnup is required as a function of the initial enrichment. These minimum burnups are listed in Table 4.8.4.
- Under normal conditions, no soluble boron is required in the spent fuel pool
- Under accident conditions, a minimum soluble boron level of 276 ppm in the pool is required, with a B-10 enrichment of 37%. [4-12]

4.2 Methodology

The principal method for the criticality analysis of the high-density storage racks is the use of the MCNP4a code [4-2]. MCNP4a is a continuous energy three-dimensional Monte Carlo code developed at the Los Alamos National Laboratory. MCNP4a was selected because it has been used previously and verified for criticality analyses and has all of the necessary features for this analysis. MCNP4a calculations use continuous energy cross-section data predominantly based on ENDF/B-V and ENDF/B-VI. Exceptions are two lumped fission products calculated by the CASMO-4 depletion code, which do not have corresponding cross sections in MCNP4a. For these isotopes, the CASMO-4 cross sections are used in MCNP4a. This approach has been validated in [4-3] by showing that the cross sections result in the same reactivity effect in both CASMO-4 and MCNP4a.

Benchmark calculations indicate a bias of 0.0009 with an uncertainty of ± 0.0011 for MCNP4a, evaluated with a 95% probability at the 95% confidence level. The calculations for this analysis will utilize the same computer platform and cross-section libraries used for the benchmark calculations.

The convergence of a Monte Carlo criticality problem is sensitive to the following parameters: (1) number of histories per cycle, (2) the number of cycles skipped before averaging, (3) the total number of cycles and (4) the initial source distribution. The MCNP4a criticality output contains a great deal of useful information that may be used to determine the acceptability of the problem convergence. This information has been used in parametric studies to develop appropriate values for the aforementioned criticality parameters to be used in storage rack criticality calculations. Based on these studies, a minimum of 10,000 histories will be simulated per cycle, a minimum of 50 cycles will be skipped before averaging, a minimum of 100 cycles will be accumulated, and the initial source will be specified as uniform over the fueled regions (assemblies). Further, the output will be reviewed to ensure that each calculation achieved acceptable convergence. These parameters represent an acceptable compromise between calculational precision and computational time.

Fuel depletion analyses during core operation will be performed with CASMO-4 (using the 70-group cross-section library), a two-dimensional multigroup transport theory code based on capture probabilities [4-4 - 4-6]. CASMO-4 will be used to determine the isotopic composition of the spent fuel. In addition, the CASMO-4 calculations will be restarted in the storage rack geometry, yielding the two-dimensional infinite multiplication factor (k_{inf}) for the storage rack to determine the reactivity effect of fuel and rack tolerances, temperature variation, and to perform various studies. For all calculations in the spent fuel pool racks, the Xe-135 concentration in the fuel will be conservatively set to zero.

The maximum k_{eff} will be determined from the MCNP4a calculated k_{eff}, the calculational bias, the temperature bias, and the applicable uncertainties and tolerances (bias uncertainty, calculational uncertainty, rack tolerances, fuel tolerances, depletion uncertainty) using the following formula:

$$\text{Max } k_{eff} = \text{Calculated } k_{eff} + \text{biases} + [\textstyle\sum_i (\text{Uncertainty})^2]^{1/2}$$

In the geometric models used for the calculations, each fuel rod and its cladding will be described explicitly and reflecting or periodic boundary conditions will be used in the radial direction which has the effect of creating an infinite radial array of storage cells, except for the assessment of certain accident conditions.

4.3 Acceptance Criteria

The high-density spent fuel PWR storage racks for the CCNPP Unit 3 U.S. EPR are designed in accordance with the applicable codes and standards listed below. The objective of evaluations performed as described in this chapter is to show that the effective neutron multiplication factor, k_{eff}, is equal to or less than 0.95 with the racks fully loaded with fuel of the highest anticipated reactivity, and flooded with un-borated water at a temperature corresponding to the highest reactivity. Reactivity effects of abnormal and accident conditions have also been evaluated to assure that under all credible abnormal and accident conditions, the reactivity will not exceed the regulatory limit of 0.95 under borated conditions.

Applicable codes, standard, and regulations or pertinent sections thereof, include the following:

- Code of Federal Regulations, Title 10, Part 50, Appendix A, General Design Criterion 62, "Prevention of Criticality in Fuel Storage and Handling."
- USNRC Standard Review Plan, NUREG-0800, Section 9.1.1, Criticality Safety of Fresh and Spent Fuel Storage and Handling, Rev. 3 – March 2007.
- USNRC letter of April 14, 1978, to all Power Reactor Licensees - OT Position for Review and Acceptance of Spent Fuel Storage and Handling Applications (GL-78-011), including modification letter dated January 18, 1979 (GL-79-004).
- L. Kopp, "Guidance on the Regulatory Requirements for Criticality Analysis of Fuel Storage at Light-Water Reactor Power Plants," NRC Memorandum from L. Kopp to T. Collins, August 19, 1998 [4-10].
- ANSI ANS-8.17, Criticality Safety Criteria for the Handling, Storage and Transportation of LWR Fuel Outside Reactors.
- Code of Federal Regulations, Title 10, Part 50, Section 68, "Criticality Accident Requirements", as referenced in Title 10, Part 52, Section 47.

4.4 Preliminary Analyses

To provide a demonstration that the proposed rack layouts and rack designs (see Chapters 1 and 2) will appropriately satisfy the requirements discussed in the preceding sections of this chapter, a series of preliminary criticality evaluations have been performed and are described in the remaining sections of this chapter. These preliminary evaluations are not intended as final qualifications, which will be performed in the future in accordance with the preceding sections of this chapter, but rather to give confidence that the proposed racks are suitably designed.

4.5 Assumptions

To assure the true reactivity will always be less than the calculated reactivity, the following conservative design criteria and assumptions were employed:

1) Moderator is borated or un-borated water at a temperature in the operating range that results in the highest reactivity, as determined by the analysis.

2) Neutron absorption in minor structural members is neglected, i.e., spacer grids are replaced by water.

3) The effective multiplication factor of an infinite radial array of fuel assemblies was used in the analyses, except for the assessment of certain abnormal/accident conditions and conditions where leakage is inherent.

4) The neutron absorber length is modeled to be the same length as the active region of the fuel.

5) No cooling time is credited in rack calculations.

6) The presence of burnable absorbers in the fuel is neglected. This is conservative as burnable absorbers would reduce the reactivity of the fuel assembly.

4.6 Input Data

4.6.1 Fuel Assembly Specification

The spent fuel storage racks are designed to accommodate the 17x17 fuel assembly used at the CCNPP Unit 3 U.S. EPR. The design parameters for this fuel assembly type that are used in the analyses are given in Table 4.6.1.

4.6.2 Core Operating Parameters

Core operating parameters are necessary for fuel depletion calculations performed with CASMO-4. The core parameters used for the depletion calculations are presented in Table 4.6.2. Temperature and soluble boron values are taken as the conservatively high values. The neutron spectrum is hardened by each of these parameters, leading to a greater production of plutonium during depletion. Using a high value therefore results in conservative reactivity values.

4.6.3 Axial Burnup Distribution

The analyses use axial burnup profiles specified at node centers for 36 equally-spaced axial sections for several assembly-average burnups. The profiles are presented in Table 4.6.3.

4.6.4 Burnable Absorbers

Some fuel assemblies at the CCNPP Unit 3 U.S. EPR use fuel rods with gadolinia for reactivity control. A study presented in reference [4-10] demonstrates that for both fresh and burned fuel, the reactivity of an assembly containing rods with gadolinia is bounded by the reactivity of an assembly without gadolinia, given all other parameters (enrichment, burnup etc.) are the same. Therefore, as a bounding approach, all calculations in this report are performed for assemblies that do not contain gadolinia.

4.6.5 Storage Rack Specification

The storage rack characteristics used in the criticality evaluations are summarized in Table 4.6.4. The composition of the neutron absorber is calculated from the B_4C content listed in Table 4.6.4 and information from [4-11].

4.6.5.1 Region 1 Style Storage Racks

The Region 1 storage cells are composed of stainless steel boxes separated by a water gap, with fixed neutron absorber panels centered on each side. The steel walls define the storage cells, and stainless steel sheathing supports the neutron absorber panel and defines the boundary of the flux-trap water-gaps used to augment reactivity control. Stainless steel channels connect the storage cells in a rigid structure and define the flux-trap between the neutron absorber panels. Neutron absorber panels are installed on all exterior walls.

4.6.5.2 Region 2 Style Storage Racks

The Region 2 storage cells are composed of stainless steel boxes with a single fixed neutron absorber panel centered on each side, attached by stainless steel sheathing. The stainless steel boxes are arranged in an alternating pattern such that the connection of the box corners form storage cells between those of the stainless steel boxes. Neutron absorber panels are installed on all exterior walls.

4.6.5.3 Rack Interfaces

Minimum distances between racks are maintained by the extensions of the base plates of each rack.

4.7 Computer Codes

The following computer codes were used during this analysis.

- MCNP4a [4-2] is a three-dimensional continuous energy Monte Carlo code developed at Los Alamos National Laboratory. This code offers the capability of performing full three-dimensional calculations for the loaded storage racks. MCNP4a was run on the PCs at Holtec.

- CASMO-4, Version 2.05.14 [4-4 - 4-6] is a two-dimensional multigroup transport theory code developed by Studsvik of Sweden. CASMO-4 performs cell criticality calculations and burnup. CASMO-4 has the capability of analytically restarting burned fuel assemblies in the rack configuration. This code was used to determine the reactivity effects of tolerances and fuel depletion.

4.8 Calculations

This section describes the calculations that were used to determine the acceptable storage criteria for the Region 1 and Region 2 style racks. In addition, this section discusses the possible abnormal and accident conditions.

Figures 4.6.1 and 4.6.2 are pictures of the basic calculational models used in MCNP4a. These pictures were created with the two-dimensional plotter in MCNP and clearly indicate the explicit modeling of fuel rods in each fuel assembly. The calculational model for the Region 1 racks (see Figure 4.6.1) consist of a single cell with reflective boundary conditions through the centerline of the water gaps, thus simulating an infinite array of Region 1 storage cells. The calculational model for the Region 2 racks (see Figure 4.6.2) consists of a group of four identical cells surrounded by reflective boundary conditions through the centerline of the composite of materials between the cells, thus simulating an infinite array of Region 2 storage cells. Additional models with more storage cells were generated with MCNP4a to investigate the effect of abnormal and accident conditions. These models are discussed in the appropriate section.

The three-dimensional MCNP4a models included axial leakage by assuming approximately 30 cm of water above and below the active fuel length. In CASMO-4, a single cell is modeled, and since CASMO-4 is a two-dimensional code, the sections above and below the active fuel length are not represented.

Unless otherwise stated, all calculations assumed nominal characteristics for the fuel and the fuel storage cells. The effect of the manufacturing tolerances is accounted for with a reactivity adjustment as discussed below.

4.8.1 Region 1

The goal of the criticality calculations for the Region 1 style racks is to qualify the racks for storage of fuel assemblies with design specifications as shown in Table 4.6.1 and a maximum nominal initial enrichment of 5.0 wt% ^{235}U.

4.8.1.1 Eccentric Fuel Assembly Positioning

The fuel assemblies are normally assumed to be located in the center of the storage rack cell. To investigate the potential reactivity effect of eccentric positioning of assemblies in the cells,

MCNP4a calculations were performed with the fuel assemblies assumed to be in the corner of the storage rack cell (four-assembly cluster at closest approach). The calculations indicate that eccentric fuel positioning results in a negative reactivity effect. The highest reactivity, therefore, corresponds to the reference design with the fuel assemblies positioned in the center of the storage cells.

4.8.1.2 Uncertainties Due to Manufacturing Tolerances

In the calculation of the final k_{eff}, the effect of manufacturing tolerances on reactivity must be included. CASMO-4 was used to perform these calculations. As allowed in [4-7], the methodology employed to calculate the tolerance effects combine both the worst-case bounding value and sensitivity study approaches. The evaluations include tolerances of the rack dimensions and tolerances of the fuel dimensions listed in Tables 4.6.1 and 4.6.4. The reference condition is the condition with nominal dimensions and properties. To determine the Δk associated with a specific manufacturing tolerance, the k_{inf} calculated for the reference condition is compared to the k_{inf} from a calculation with the tolerance included. Note that for the individual parameters associated with a tolerance, no statistical approach is utilized. Instead, the full tolerance value is utilized to determine the maximum reactivity effect. All of the Δk values from the various tolerances are statistically combined (square root of the sum of the squares) to determine the final reactivity allowance for manufacturing tolerances. In some cases it is not obvious whether an increase or decrease of the parameter will lead to an increase in reactivity. In these cases, the reactivity effect of both the increase and the decrease of the parameter are calculated, and the positive reactivity effect is used when calculating the statistical combination.

Note that the tolerance in the flux trap is conservatively captured in the tolerances of the cell ID and cell pitch, since variations of the cell ID are evaluated for a constant cell pitch and vice versa. Therefore, no separate variation of the flux trap width is performed.

4.8.1.3 Temperature and Water Density Effects

Pool water temperature effects on reactivity in the Region 1 racks have been evaluated. The results show that the spent fuel pool temperature coefficient of reactivity is negative, i.e. a lower temperature results in a higher reactivity. Consequently, the design basis calculations are evaluated at 4 °C (39 °F) for normal conditions.

In MCNP4a, the Doppler treatment and cross-sections are valid only at 300K (80.33 °F). Therefore, a Δk is determined from 39 °F to 80.33 °F, and is included in the final k_{eff} calculation as a bias.

4.8.1.4 Calculation of Maximum k_{eff}

Using the calculational model shown in Figure 4.6.1, the k_{eff} in the Region 1 storage racks has been calculated. The calculation of the maximum k_{eff} value, based on the formula in Section 4.2, is shown in Table 4.6.1. In summary, the results show that the maximum k_{eff} of the Region 1 racks is less than 0.95 at a 95% probability at a 95% confidence level with no credit for soluble boron.

4.8.1.5 Abnormal and Accident Conditions

The effects on reactivity of credible abnormal and accident conditions are examined in this section. This section identifies which of the credible abnormal or accident conditions will result in exceeding the limiting reactivity ($k_{eff} \leq 0.95$). For those accident or abnormal conditions that result in exceeding the limiting reactivity, a minimum soluble boron concentration is determined to ensure that $k_{eff} \leq 0.95$. The double contingency principal of ANS-8.1/N16.1 [4-8] (and the USNRC letter of April 1978) specifies that it shall require at least two unlikely independent and concurrent events to produce a criticality accident. This principle precludes the necessity of considering the simultaneous occurrence of multiple accident conditions. As specified in [4-12], a B-10 enrichment of 37% is assumed for the soluble boron.

4.8.1.5.1 Abnormal Temperature

All calculations for Region 1 are performed at a pool temperature of 39°F. As discussed in Section 4.8.1.3 above, the temperature coefficient of reactivity is negative, therefore any increase in temperature above 39°F would cause a reduction in the reactivity. Therefore, no further evaluations of abnormal temperatures are performed.

4.8.1.5.2 Dropped Assembly - Horizontal

For the case in which a fuel assembly is assumed to be dropped on top of a rack, the fuel assembly will come to rest horizontally on top of the rack with a minimum separation distance from the active fuel region of more than 12 inches, which is sufficient to preclude neutron coupling (i.e., an effectively infinite separation). Consequently, the horizontal fuel assembly drop accident will not result in a significant increase in reactivity. Furthermore, the soluble boron in the spent fuel pool water assures that the true reactivity is always less than the limiting value for this dropped fuel accident.

4.8.1.5.3 Dropped Assembly – Vertical Into Fuel Cell

It is also possible to vertically drop an assembly into a location that might be occupied by another assembly or that might be empty. Such a vertical impact onto another assembly would at most cause a small compression of the stored assembly, reducing the water-to-fuel ratio and thereby reducing reactivity. A vertical drop into an empty storage cell could result in a small deformation of the baseplate. The resultant effect would be the lowering of a single fuel assembly by the amount of the deformation. This could potentially result in a misalignment between the active fuel region and the neutron absorber. However, the amount of deformation for this drop would be small and restricted to a localized area of the rack around the storage cell where the drop occurs. Furthermore, the soluble boron in the spent fuel pool water assures that the true reactivity is always less than the limiting value for this dropped fuel accident.

4.8.1.5.4 Misloaded Fresh Fuel Assembly

The Region 1 racks are qualified for the storage of fresh unburned fuel assemblies with the maximum permissible enrichment (5.0 wt% ^{235}U). Therefore the abnormal location of a fuel assembly within normal Region 1 cells is of no concern.

4.8.1.5.5 Mislocated Fresh Fuel Assembly

The mislocation of a fresh unburned fuel assembly could, in the absence of soluble poison, result in exceeding the regulatory limit (k_{eff} of 0.95). This could possibly occur if a fresh fuel assembly of the highest permissible enrichment (5.0 wt% ^{235}U) were to be accidentally mislocated outside of a storage rack adjacent to other fuel assemblies. An analysis was performed that considers this condition, conservatively analyzing a mislocated assembly facing fresh assemblies in rack cells on two sides. The results of the analysis are used to determine the soluble boron level that is required to ensure that the maximum k_{eff} value for this condition remains at or below 0.95.

4.8.2 Region 2

The goal of the criticality calculations for the Region 2 style racks is to qualify the racks for storage of fuel assemblies with design specifications as shown in Table 4.6.1 and a maximum nominal initial enrichment of 5.0 wt% ^{235}U. The purpose of the criticality calculations is to determine the initial enrichment and burnup combinations required for the uniform storage of spent fuel assemblies

4.8.2.1 Axial Burnup and Enrichment Distributions

Initially, fuel loaded into the reactor will burn with a slightly skewed cosine power distribution. As burnup progresses, the burnup distribution will tend to flatten, becoming more highly burned in the central regions than in the upper and lower ends.

Regarding the enrichment, the CCNPP Unit 3 U.S. EPR assemblies contain axial blankets, with a length of 8 inches at the top and 6 inches at the bottom of the active region. The enrichment of the blankets is lower than that of the central region of the fuel, with a maximum value of 3 wt% U-235.

The axial burnup and enrichment distributions are accounted for in the analysis as follows:

- For each burnup and enrichment combination analysed, calculations are performed with an axial burnup distribution and with an axial constant burnup, and the higher of the two resulting reactivities is used.
- For the axial constant burnup, an axially constant enrichment is used, equal to the enrichment in the center part of the assembly.
- For calculations with a burnup profile, the axial blankets are assumed to have an enrichment of 3 wt%, but not to exceed the enrichment in the center part of the axial region. This is conservative, since the enrichment of the axial blankets have a maximum value of only 2.3 wt%.
- The axial blanket is assumed to be only as long as the first and last of the 36 axial sections, i.e. about 4.6 inches, instead of the actual value of 6 or 8 inches. This means that the second-to last axial section is assumed to contain fuel with the full enrichment, while in reality part of this section is still part of the axial blanket with the reduced enrichment. The enrichment in this second section is therefore overestimated, resulting in an increased reactivity effect of this section. This assumption is therefore conservative.

4.8.2.2 Isotopic Compositions

To perform the criticality evaluation for spent fuel in MCNP4a, the isotopic composition of the fuel is calculated with the depletion code CASMO-4 and then specified as input data in the MCNP4a run. The CASMO-4 calculations to obtain the isotopic compositions for MCNP4a were performed generically, with one calculation for each enrichment, and burnups in increments of 2.5 GWD/MTU or less. The isotopic composition for any given burnup is then determined by linear interpolation.

4.8.2.3 Uncertainty in Depletion Calculations

Since critical experiment data with spent fuel is not available for determining the uncertainty in burnup-dependent reactivity calculations, an allowance for uncertainty in reactivity was assigned based upon other considerations. Based on the recommendation in [4-7], a burnup dependent uncertainty in reactivity for burnup calculations of 5% of the reactivity decrement is used. This allowance is statistically combined with the other reactivity allowances in the determination of the maximum k_{eff} for normal conditions where assembly burnup is credited.

4.8.2.4 Eccentric Fuel Assembly Positioning

The fuel assemblies are normally assumed to be located in the center of the storage rack cell. To investigate the potential reactivity effect of eccentric positioning of assemblies in the cells, MCNP4a calculations were performed with the fuel assemblies assumed to be in the corner of the storage rack cell (four-assembly cluster at closest approach). The calculations indicate that eccentric fuel positioning results in a negative reactivity effect. The highest reactivity, therefore, corresponds to the reference design with the fuel assemblies positioned in the center of the storage cells.

4.8.2.5 Uncertainties Due to Manufacturing Tolerances

In the calculation of the final k_{eff}, the effect of manufacturing tolerances on reactivity must be included. CASMO-4 was used to perform these calculations. As allowed in [4-7], the methodology employed to calculate the tolerance effects combine both the worst-case bounding value and sensitivity study approaches. The evaluations include tolerances of the rack dimensions and the fuel dimensions in Tables 4.6.1 and 4.6.4. Calculations are performed for different enrichments and burnups. The reference condition is the condition with nominal dimensions and properties. To determine the Δk associated with a specific manufacturing tolerance, the k_{inf} calculated for the reference condition is compared to the k_{inf} from a calculation with the tolerance included. Note that for the individual parameters associated with a tolerance, no statistical approach is utilized. Instead, the full tolerance value is utilized to determine the

maximum reactivity effect. All of the Δk values from the various tolerances are statistically combined (square root of the sum of the squares) to determine the final reactivity allowance for manufacturing tolerances. Only the Δk values in the positive direction (increasing reactivity) were used in the statistical combination.

4.8.2.6 Temperature and Water Density Effects

Pool water temperature effects on reactivity in the Region 2 racks have been calculated with CASMO-4 for various enrichments with a maximum value of 5.0 wt% ^{235}U. The results show that the spent fuel pool temperature coefficient of reactivity is negative, i.e. a higher temperature results in a lower reactivity. Consequently, all CASMO-4 calculations are evaluated at 39 °F.

In MCNP4a, the Doppler treatment and cross-sections are valid only at 300K (80.33 °F). Therefore, a Δk is determined in CASMO-4 from 39 °F to 80.33 °F, and is included in the final k_{eff} calculation as a bias.

4.8.2.7 Calculation of Maximum k_{eff}

Using the calculational model shown in Figure 4.6.2, the k_{eff} in the Region 2 storage racks has been calculated with MCNP4a. The maximum k_{eff} value, based on the formula in Section 4.2, is determined for initial enrichments between 2.0 wt% ^{235}U and 5.0 wt% ^{235}U. A summary of the calculations of the maximum k_{eff} for spent fuel of maximum nominal enrichment of 5.0 wt% ^{235}U is shown in Table 4.8.3. The resulting loading curve, i.e. the minimum burnup as a function of enrichment, is shown in Table 4.8.4 and Figure 4.8.1. The results show that for this loading curve, the maximum k_{eff} of the Region 2 racks is less than 0.95 at a 95% probability and at a 95% confidence level, without credit for soluble boron in the pool.

4.8.2.8 Abnormal and Accident Conditions

The effects on reactivity of credible abnormal and accident conditions are examined in this section. This section identifies which of the credible abnormal or accident conditions will result

in exceeding the limiting reactivity ($k_{eff} \leq 0.95$). For those accident or abnormal conditions that result in exceeding the limiting reactivity, a minimum soluble boron concentration is determined to ensure that $k_{eff} \leq 0.95$. The double contingency principal of ANS-8.1/N16.1 [4-8] (and the USNRC letter of April 1978) specifies that it shall require at least two unlikely independent and concurrent events to produce a criticality accident. This principle precludes the necessity of considering the simultaneous occurrence of multiple accident conditions. As specified in [4-12], a B-10 enrichment of 37% is assumed for the soluble boron.

4.8.2.8.1 Abnormal Temperature

All calculations for Region 2 are performed at a pool temperature of 39 °F. As shown in Section 4.8.2.6 above, the temperature coefficient of reactivity is negative, therefore no additional calculations are required.

4.8.2.8.2 Dropped Assembly - Horizontal

For the case in which a fuel assembly is assumed to be dropped on top of a rack, the fuel assembly will come to rest horizontally on top of the rack with a minimum separation distance from the active fuel region of more than 12 inches, which is sufficient to preclude neutron coupling (i.e., an effectively infinite separation). Consequently, the horizontal fuel assembly drop accident will not result in a significant increase in reactivity. Furthermore, the soluble boron in the spent fuel pool water assures that the true reactivity is always less than the limiting value for this dropped fuel accident.

4.8.2.8.3 Dropped Assembly - Vertical

It is also possible to vertically drop an assembly into a location that might be occupied by another assembly or that might be empty. Such a vertical impact would at most cause a small compression of the stored assembly, if present, or result in a small deformation of the baseplate for an empty cell. These deformations could potentially increase reactivity. However, the reactivity increase would be small compared to the reactivity increase created by the misloading

of a fresh assembly discussed in the following section. The vertical drop is therefore bounded by this misloading accident and no separate calculation is performed for the drop accident.

4.8.2.8.4 Misloaded Fresh Fuel Assembly

The misloading of a fresh unburned fuel assembly could, in the absence of soluble poison, result in exceeding the regulatory limit (k_{eff} of 0.95). This could possibly occur if a fresh fuel assembly of the highest permissible enrichment (5.0 wt% ^{235}U) were to be inadvertently misloaded into a storage cell intended to be used for spent fuel. The reactivity consequence of this situation was investigated. The soluble boron level that is required to ensure that the maximum k_{eff} value for this condition remains below 0.95 is listed in Table 4.8.5.

4.8.2.8.5 Mislocated Fresh Fuel Assembly

The mislocation of a fresh unburned fuel assembly could, in the absence of soluble poison, result in exceeding the regulatory limit (k_{eff} of 0.95). This could possibly occur if a fresh fuel assembly of the highest permissible enrichment (5.0 wt% ^{235}U) were to be accidentally mislocated outside of a Region 2 storage rack adjacent to other fuel assemblies. This condition is bounded by the mislocation analysis for the Region 1 racks, where the mislocated assembly is next to a fresh assembly. Therefore, no further analyses need to be performed.

4.8.3 Interfaces Between Racks

All interfaces between racks are bounded by the calculations for infinite arrays of Region 1 and Region 2 cells, due to the following conditions:

- All racks have poison panels on all exterior surfaces. The number of poison panels between assemblies across a rack-to-rack gap is therefore identical or larger than the one analyzed in the infinite arrays
- The base plate extensions on the racks ensure that the assembly distance across a rack-to-rack gap between racks of the same type is not less than the corresponding distance between the assemblies within a rack.

- The base plate extensions on the racks ensure that the assembly distance across a rack-to-rack gap between Region 1 (fresh fuel) and Region 2 (spent fuel) racks is not less than the distance between the assemblies within a Region 1 (fresh fuel) rack.

4.9 Summary

Calculations have been performed to qualify the Region 1 racks for storage of fuel assemblies with a maximum nominal initial enrichment of 5.0 wt% ^{235}U. The results of these calculations are summarized in Table 4.8.1 and Table 4.8.2. The calculations demonstrate that maximum k_{eff} is less than 0.95 without credit for soluble. Furthermore, all reactivity effects of abnormal and accident conditions have also been evaluated to assure that under all credible abnormal and accident conditions, the reactivity will not exceed the regulatory limit of 0.95.

Calculations have been performed to qualify the Region 2 racks for storage of fuel assemblies with a nominal initial enrichment of up to 5.0 wt% ^{235}U for both normal and abnormal conditions. The calculations demonstrate that for the loading curve shown in Figure 4.8.1, the maximum k_{eff} is less than 0.95. Under normal conditions, no credit for soluble boron is taken. Credible accidents conditions require soluble boron as listed in Table 4.8.5.

In all pertinent cases for all rack designs, the maximum k_{eff} values are below the regulatory limits.

4.10 References

4-1. M.G. Natrella, Experimental Statistics, National Bureau of Standards, Handbook 91, August 1963.

4-2. J.F. Briesmeister, Editor, "MCNP - A General Monte Carlo N-Particle Transport Code, Version 4A," LA-12625, Los Alamos National Laboratory (1993).

4-3. "Lumped Fission Product and Pm148m Cross Sections for MCNP," Holtec Report HI-2033031, Rev 0, September 2003.

4-4. M. Edenius, K. Ekberg, B.H. Forssén, and D. Knott, "CASMO-4 A Fuel Assembly Burnup Program User's Manual," Studsvik/SOA-95/1, Studsvik of America, Inc. and Studsvik Core Analysis AB (proprietary).

4-5. D. Knott, “CASMO-4 Benchmark Against Critical Experiments”, SOA-94/13, Studsvik of America, Inc., (proprietary).

4-6. D. Knott, “CASMO-4 Benchmark Against MCNP,” SOA-94/12, Studsvik of America, Inc., (proprietary).

4-7. L.I. Kopp, “Guidance on the Regulatory Requirements for Criticality Analysis of Fuel Storage at Light-Water Reactor Power Plants,” NRC Memorandum from L. Kopp to T. Collins, August 19, 1998.

4-8. ANS-8.1/N16.1, “American National Standard for Nuclear Criticality Safety in Operations with Fissionable Materials Outside Reactors,”

4-9. S.E. Turner, "Uncertainty Analysis - Burnup Distributions", presented at the DOE/SANDIA Technical Meeting on Fuel Burnup Credit, Special Session, ANS/ENS Conference, Washington, D.C., November 2, 1988.

4-10. “Study of the Effect of Integral Burnable Absorbers for PWR Burnup Credit,” NUREG/CR-6760, ORNL/TM-2000-321, March 2002.

4-11. Nuclides and Isotopes, 15th Edition, GE Co. and KAPL Inc, 1996

4-12. U.S. EPR Technical Specifications

Table 4.6.1

FUEL ASSEMBLY SPECIFICATION

Parameter	Value
Rod Array	17x17
Stack Density, % of theoretical value of 10.96 g/cm^3	96 ± 1.5
Fuel Rod Pitch, in	0.496
Number of Fuel Rods	265
Number of Guide Tubes	24
Fuel Rod Clad OD, in	0.3740 ± 0.0016
Fuel Rod Clad ID, in	0.3291
Active Length, mm	4200
Fuel Pellet Diameter, in	0.3225 ± 0.0005
Guide Tube OD, in	0.49
Guide Tube ID, in	0.451
Length of Axial Blankets, in (bottom and top)	6 and 8
Maximum Enrichment, wt% U-235	5.0
Maximum Enrichment of Axial Blankets, wt% U-235	2.3

Table 4.6.2

CORE OPERATING PARAMETERS FOR DEPLETION ANALYSES

Parameter	**Value**
Soluble Boron Concentration, ppm (natural boron)	1000
Reactor Specific Power, MW/MTU	34.1
Fuel Temperature, K	934
Core Average Moderator Temperature at the Top of the Active Region, K	602.6
In-Core Assembly Pitch, Inches	8.426

Table 4.6.3
AXIAL BURNUP PROFILES

Axial Height (cm)	Average Assembly Burnup (GWd/MTU)			
	25	30	40	50
5.83 (bottom)	9.40	9.48	13.18	17.60
17.50	15.59	18.88	25.62	33.11
29.17	20.72	26.40	35.49	45.22
40.83	23.76	29.83	39.93	50.27
52.50	26.05	32.07	42.50	53.27
64.17	27.18	33.10	43.82	54.62
75.83	27.86	33.65	44.53	55.32
87.50	28.24	33.92	44.90	55.67
99.17	28.46	34.05	45.07	55.85
110.83	28.57	34.10	45.14	55.92
122.50	28.61	34.11	45.15	55.95
134.17	28.62	34.10	45.12	55.94
145.83	28.62	34.07	45.09	55.93
157.50	28.60	34.05	45.04	55.90
169.17	28.58	34.01	44.98	55.87
180.83	28.57	33.98	44.92	55.83
192.50	28.55	33.95	44.86	55.79
204.17	28.53	33.91	44.80	55.76
215.83	29.05	34.33	45.25	55.92
227.50	29.02	34.29	45.21	55.85
239.17	29.00	34.26	45.17	55.77
250.83	28.97	34.23	45.12	55.69
262.50	28.93	34.19	45.06	55.60
274.17	28.87	34.13	44.98	55.51
285.83	28.78	34.05	44.86	55.39
297.50	28.64	33.92	44.69	55.24
309.17	28.41	33.71	44.43	55.01
320.83	28.05	33.38	44.02	54.66
332.50	27.50	32.84	43.39	54.11
344.17	26.66	32.01	42.40	53.20
355.83	25.40	30.71	40.85	51.69
367.50	23.49	28.67	38.40	49.18
379.17	20.10	25.00	34.27	44.57
390.83	13.33	17.26	26.23	35.36
402.50	6.88	9.26	15.54	20.34
414.17 (top)	4.47	6.10	9.96	13.19

Table 4.6.4

STORAGE RACK PARAMETERS

Region 1	
Parameter	**Value**
Cell ID, in	8.8
Cell Wall thickness, in	0.075 ± 0.007
Cell Pitch, in	10.9
Boundary Sheathing Thickness, in	0.075
Inner Sheathing Thickness, in	0.035
Poison Thickness, in	0.106
Poison Width, in	7.25
Poison Gap, in	0.115
Flux Trap, in	1.65
B_4C content of Poison Plates, wt%	30.5 nom., 29.5 min.
Base Plate Extension, in	7/8
Region 2	
Parameter	**Value**
Cell ID, in	8.8
Cell Wall thickness, in	0.075 ± 0.007
Cell Pitch, in	9.028
Boundary Sheathing Thickness, in	0.075
Inner Sheathing Thickness, in	0.035
Poison Thickness, in	0.106
Poison Width, in	7.25
Poison Gap, in	0.118
B_4C content of Poison Plates, wt%	30.5 nom., 29.5 min.
Base Plate Extension, in	3/4

Table 4.8.1

SUMMARY OF THE CRITICALITY SAFETY ANALYSIS FOR REGION 1

Enrichment [wt% ^{235}U]		5.0
Uncertainties		
Bias Uncertainty (95%/95%)	± 0.0011	
Calculational Statistics (95%/95%, 2.0×σ)	± 0.0014	
Fuel Eccentricity	Negative	
Rack Tolerances	± 0.0070	
Fuel Tolerances	± 0.0033	
Statistical Combination of Uncertainties	± 0.0079	
Reference k_{eff} (MCNP4a)		0.9039
Biases		
Temperature Bias		0.0024
Calculational Bias		0.0009
Maximum k_{eff}		**0.9151**
Regulatory Limiting k_{eff}		**0.9500**

Table 4.8.2

REGION 1 ABNORMAL AND ACCIDENT CONDITIONS

Abnormal/Accident Condition	**Soluble Boron Requirement**
Abnormal Temperature	None
Dropped Assembly – Horizontal	Negligible
Dropped Assembly – Vertical Into Storage Cell	Negligible
Misloaded Assembly	N/A
Mislocated Assembly	276 ppm

Table 4.8.3

SUMMARY OF THE CRITICALITY SAFETY ANALYSIS FOR REGION 2

Enrichment [wt% ^{235}U]		5.0
Burnup [GWd/mtU]		49.55
Uncertainties		
Bias Uncertainty (95%/95%)	± 0.0011	
Calculational Statistics (95%/95%, 2.0×σ)	± 0.0012	
Fuel Eccentricity	Negative	
Rack Tolerances	± 0.0033	
Fuel Tolerances	± 0.0036	
Depletion Uncertainty	± 0.0159	
Statistical Combination of Uncertainties	± 0.0167	
Reference k_{eff} (MCNP4a)		0.9254
Biases		
Temperature Bias		0.0020
Calculational Bias		0.0009
Maximum k_{eff}		**0.9450**
Regulatory Limiting k_{eff}		**0.9500**

Table 4.8.4

REGION 2 BURNUP VERSUS ENRICHMENT CURVE

Enrichment (wt% U-235)	Minimum Burnup (GWd/mtU)
2	3.61
3	20.73
4	38.59
5	49.55

Table 4.8.5

REGION 2 ABNORMAL AND ACCIDENT CONDITIONS

Abnormal/Accident Condition	**Soluble Boron Requirement**
Abnormal Temperature	None
Dropped Assembly – Horizontal	Negligible
Dropped Assembly – Vertical Into Storage Cell	Negligible
Misloading Assembly	119 ppm
Mislocated Assembly	Bounded by Region 1

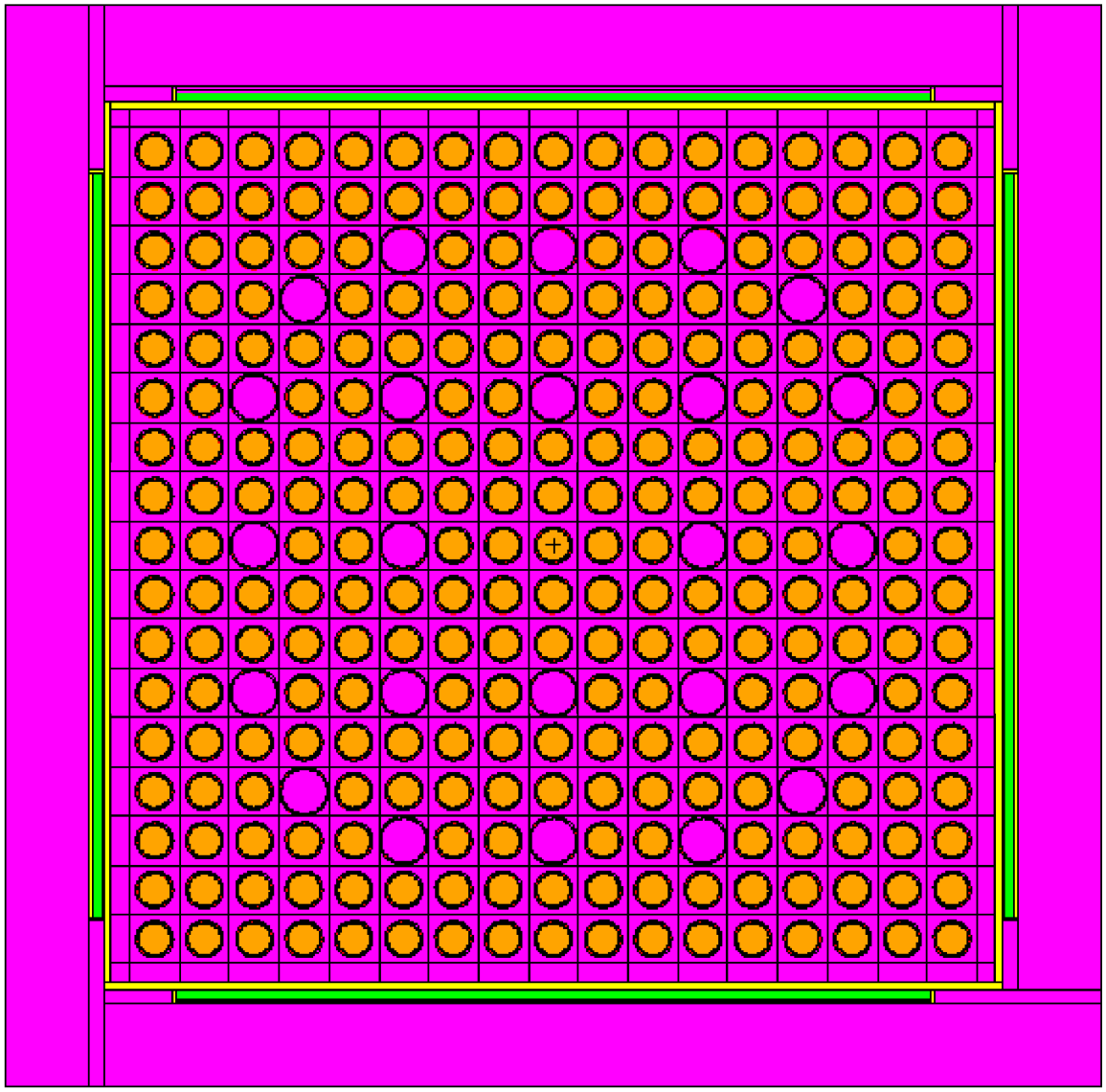

Figure 4.6.1 Region 1 Calculational Model (MCNP)

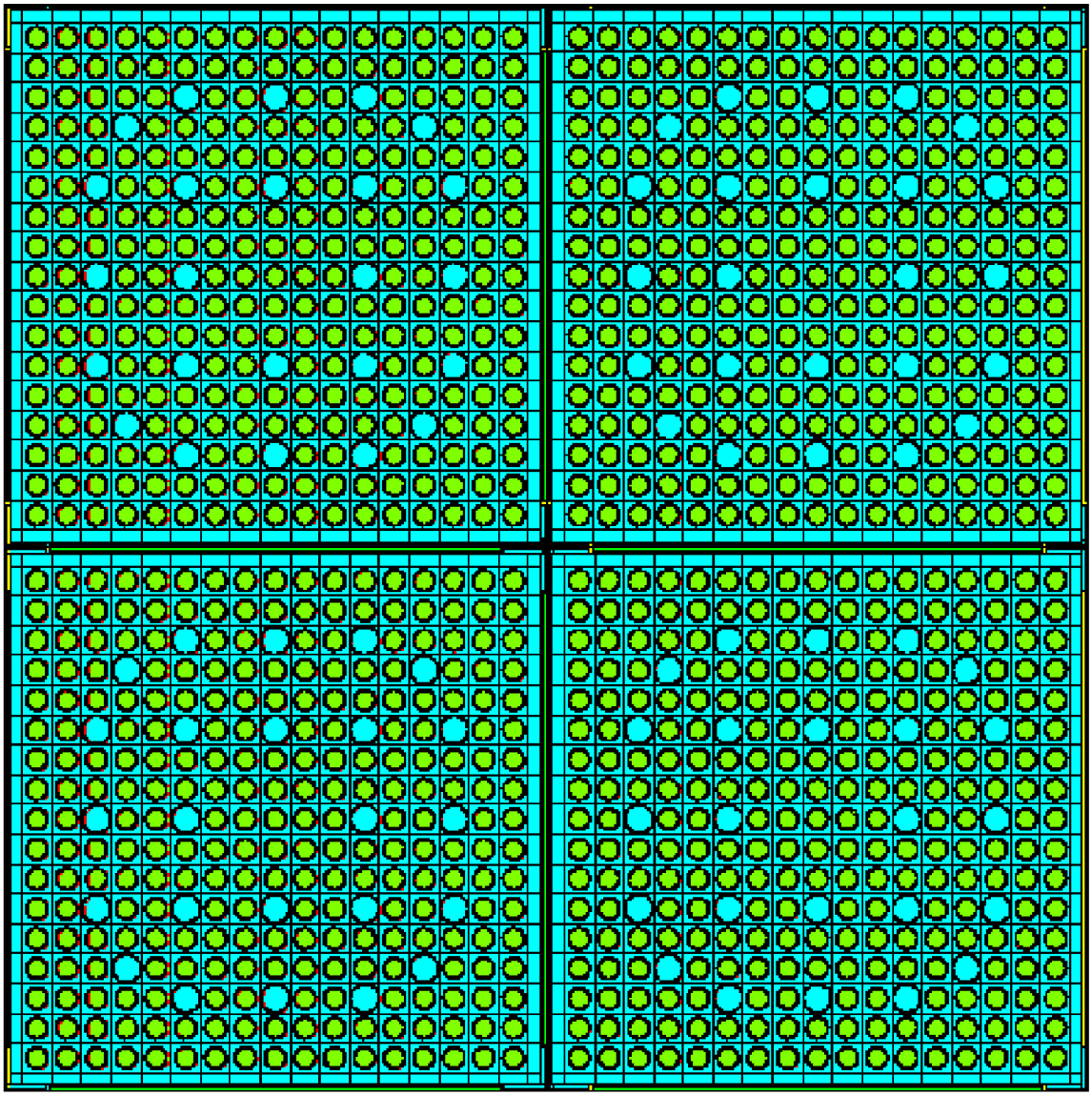

Figure 4.6.2 Region 2 Calculational Model (MCNP)

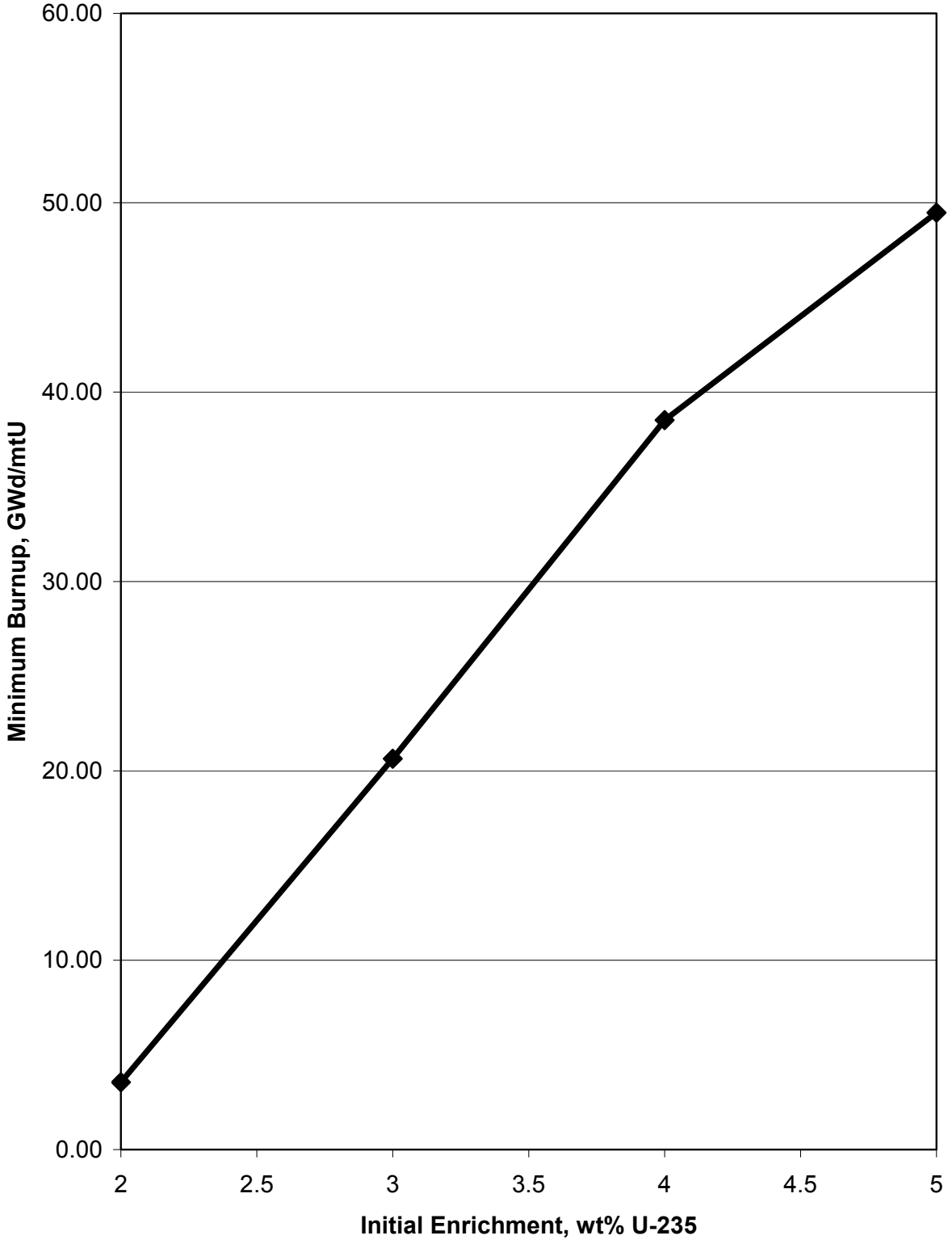

Figure 4.8.1 Loading Curve for Region 2 Racks

5.0 STRUCTURAL/SEISMIC CONSIDERATIONS

5.1 Introduction

This topical report provides information on the new and spent fuel storage racks to support a COLA for the Calvert Cliffs Nuclear Power Plant (CCNPP) Unit 3 U.S. EPR. This chapter, specifically, provides information on the required structural performance characteristics of the fuel storage racks.

5.2 Acceptance Criteria

To confirm the structural integrity of the racks, it is necessary to demonstrate compliance with the USNRC Standard Review Plan [5-1] and the OT Position Paper [5-2]. The rack structures are designed to meet the requirements of the ASME Code, Section III, Subsection NF for Class 3 linear-type supports. The relevant design criteria are discussed below, with additional details provided in the text associated with each analysis.

There are three principal design criteria, which must be satisfied by the rack modules:

a. Kinematic Criteria

According to Section 3.8.5 of Ref [5-1] and Ref [5-2], the minimum required safety margin under a Safe Shutdown Earthquake (SSE) event is 1.1. The margin of safety is defined here as the ratio of the rotation required to produce incipient tipping in either principal plane to the actual maximum rotation in that plane from the time history solution. The maximum rotations of the rack (about the two principal axes) are obtained from a post processing of the rack time history response output. All ratios from the SSE event should be greater than 1.1, to satisfy the regulatory acceptance criteria.

b. Stress Limit Criteria

The stress limits defined in ASME Code, Section III, Subsection NF must not be exceeded under the postulated load combinations. Load combinations are discussed in Section 5.3.

c. Fatigue Criteria

The cumulative damage factor, U, as defined in Section 5.6.9, must be shown to be less than or equal to 1.0.

5.3 Loads and Load Combinations

The applicable loads and their combinations that must be considered in the seismic analysis of rack modules are excerpted from Section 3.8.4 of Ref [5-1] and from Ref [5-2]. The load combinations considered are identified below (note that there is no Operating Basis Earthquake (OBE) event defined for CCNPP Unit 3; therefore, loading conditions associated with an OBE event are not considered):

Loading Combination	Service Level
$D + L$ $D + L + T_o$	Level A
$D + L + T_o + P_f$	Level B
$D + L + T_a + E'$	Level D
$D + L + F_d$	The functional capability of the fuel racks must be demonstrated.

where:

D are the dead weight-induced loads (including fuel assembly weight).

L is the live load (not applicable for fuel racks, since there are no moving objects in the rack load path).

P_f is the upward force on the racks caused by postulated stuck fuel assembly. This load is considered to be an accident condition. The evaluation of this load condition is discussed in Chapter 7.

F_d is the impact force from accidental drop of the heaviest load from the maximum possible height. This load is considered to be an accident condition. The evaluation of this load condition is discussed in Chapter 7.

E' are the loads from an SSE event.

T_o are differential temperature induced loads (normal operating or shutdown condition based on the most critical transient or steady state condition).

T_a are differential temperature induced loads (the highest temperature associated with the postulated abnormal design conditions).

T_a and T_o produce local thermal stresses. The worst thermal stress field in a fuel rack is obtained when an isolated storage location has a fuel assembly generating heat at maximum postulated rate and surrounding storage locations contain no fuel. Heated water makes unobstructed contact with the inside of the storage walls, thereby producing maximum possible temperature difference between adjacent cells. Secondary stresses produced are limited to the body of the rack; that is, support pedestals do not experience secondary (thermal) stresses. Thermal stresses are considered in Subsection 5.6.10.2.

5.4 Analysis Methods

The subsections in this section describe the analysis methods to be used in performing licensing-basis calculations to demonstrate that the structural performance requirements for the fuel storage racks are satisfied. Similar structural analyses have been used for previous fuel storage rack licensing at many nuclear plants worldwide (see Table 5.4.1 for a *partial* list).

5.4.1 Overview of Rack Structural Analysis Methodology

The response of a freestanding rack module to seismic inputs is highly nonlinear and involves a complex combination of motions (sliding, rocking, twisting, and turning), resulting in impacts and friction effects. Some of the unique attributes of the rack dynamic behavior include a large fraction of the total structural mass in a confined rattling motion, friction support of rack pedestals against lateral motion, and large fluid coupling effects due to deep submergence and independent motion of closely spaced adjacent structures.

Linear methods, such as modal analysis and response spectrum techniques, cannot accurately simulate the structural response of such a highly nonlinear structure to seismic excitation. An accurate simulation is obtained only by direct integration of the nonlinear equations of motion with the three pool slab acceleration time-histories applied as the forcing functions acting simultaneously.

Whole Pool Multi-Rack (WPMR) analysis is the vehicle required to simulate the dynamic behavior of the complex spent fuel storage rack configuration.

For the new fuel storage layouts, which feature racks of essentially the same design as that of spent fuel racks with the exception of rack sizes, can be analyzed using the 3-D single rack analysis approach. The new fuel storage vaults will not contain any water (i.e., new fuel assemblies will be stored in the racks in a dry condition). As such there will be no inter-rack fluid coupling forces during seismic events. Further, the new fuel rack modules are sufficiently separated from each other so that the seismic motion of one rack does not influence any adjacent racks. Therefore, it is technically appropriate to analyze the new fuel rack modules by the so-called “single rack seismic analysis” procedure. The single rack analysis method, and the analysis code used to perform the calculations, is identical to the WPMR analysis method except that the model includes a single rack as opposed to all racks in the pool. In fact, the “building block” for the WPMR analysis is a 3-D multi-degree of freedom model of each rack in the pool.

The following sections provide the basis for this section and discussion on the development of the methodology.

5.4.1.1 Background of Analysis Methodology

Reliable assessment of the stress field and kinematic behavior of the rack modules calls for a conservative dynamic model incorporating all *key attributes* of the actual structure. This means that the model must feature the ability to execute the concurrent motion forms compatible with the freestanding installation of the modules.

The model must possess the capability to effect momentum transfers which occur due to rattling of fuel assemblies inside storage cells and the capability to simulate lift-off and subsequent impact of support pedestals with the underlying bearing pads. The contribution of the water mass in the interstitial spaces around the rack modules and within the storage cells (not applicable to the dry new fuel storage racks) must be modeled in an accurate manner, since erring in quantification of fluid coupling on either side of the actual value is no guarantee of conservatism.

The Coulomb friction coefficient at the pedestal-to-bearing pad interface may lie in a rather wide range and a conservative value of friction cannot be prescribed *a priori*. In fact, a perusal of results of rack dynamic analyses in numerous dockets (Table 5.4.1) indicates that an upper bound value of the coefficient of friction often maximizes the computed rack displacements as well as the equivalent elastostatic stresses.

In short, there are a large number of parameters with potential influence on the rack kinematics. The comprehensive structural evaluation must deal with all of these without sacrificing conservatism.

The three-dimensional single rack dynamic model introduced by Holtec International in the Enrico Fermi Unit 2 rack project (ca. 1980) and used in some 50 rerack projects since that time (Table 5.4.1) addresses most of the above-mentioned array of parameters. The details of this methodology are also published in the permanent literature [5-3]. Despite the versatility of the 3-

D seismic model, the accuracy of the single rack simulations has been suspect due to one key element; namely, hydrodynamic participation of water around the racks (not applicable to the dry new fuel storage racks). During dynamic rack motion, hydraulic energy is either drawn from or added to the moving rack, modifying its submerged motion in a significant manner. Therefore, the dynamics of one rack affects the motion of all others in the pool.

A dynamic simulation, which treats only one rack, or a small grouping of racks, is intrinsically inadequate to predict the motion of rack modules submerged in water with any quantifiable level of accuracy. Three-dimensional Whole Pool Multi-Rack analyses carried out for many previous plants demonstrate that single rack simulations under-predict rack displacement during seismic responses in a water environment [5-4].

Briefly, the 3-D rack model dynamic simulation, involving one or more spent fuel racks, handles the array of variables as follows:

Interface Coefficient of Friction: Parametric runs are made with upper bound and lower bound values of the coefficient of friction. The limiting values are based on experimental data, which have been found to be bounded by the values 0.2 and 0.8. Simulations are also performed with the array of pedestals having randomly chosen coefficients of friction in a Gaussian distribution with a mean of 0.5 and lower and upper limits of 0.2 and 0.8, respectively. In the fuel rack simulations, the Coulomb friction interface between rack support pedestal and bearing pad is simulated by piecewise linear (friction) elements. These elements function only when the pedestal is physically in contact with the bearing pad.

Rack Beam Behavior: Rack elasticity, relative to the rack base, is included in the model by introducing linear springs to represent the elastic bending action, twisting, and extensions.

Impact Phenomena: Compression-only gap elements are used to provide for opening and closing of interfaces such as the pedestal-to-bearing pad interface, and the fuel assembly-to-cell wall interface. These interface gaps are modeled using nonlinear spring elements. The term "nonlinear

spring" is a generic term used to denote the mathematical representation of the condition where a restoring force is not linearly proportional to displacement.

Fluid Coupling: Holtec International extended Fritz's classical two-body fluid coupling model to multiple bodies and utilized it to perform the first two-dimensional multi-rack analysis (Diablo Canyon, ca. 1987). Subsequently, laboratory experiments were conducted to validate the multi-rack fluid coupling theory. This technology was incorporated in the Holtec-proprietary computer program DYNARACK [5-6], which handles simultaneous simulation of all racks in the pool as a Whole Pool Multi-Rack 3-D analysis. This development was first utilized in Chinshan, Oyster Creek, and Shearon Harris plants [5-3, 5-5] and, subsequently, in numerous other rack projects. The WPMR analyses have corroborated the accuracy of the single rack 3-D solutions in predicting the maximum structural stresses, and also serve to improve predictions of rack kinematics.

For closely spaced racks, demonstration of kinematic compliance is verified by including all modules in one comprehensive simulation using a WPMR model. In WPMR analysis, all rack modules are modeled simultaneously and the coupling effect due to this multi-body motion is included in the analysis. Due to the superiority of this technique in predicting the dynamic behavior of closely spaced submerged storage racks, the Whole Pool Multi-Rack analysis methodology is used to analyze the spent fuel storage rack configurations.

5.4.2 WPMR Methodology

Recognizing that the analysis work effort must deal both with stress and displacement criteria, the sequence of model development and analysis steps that must be undertaken are summarized in the following:

a. Prepare 3-D dynamic models suitable for a time-history analysis of the fuel storage racks. These models include the assemblage of all rack modules in the spent fuel pool. Include all fluid coupling interactions and mechanical coupling appropriate to performing an accurate non-linear simulation. This 3-D simulation is referred to as a Whole Pool Multi-Rack model.

b. Perform 3-D dynamic analyses on various physical conditions (such as coefficient of friction and extent of cells containing fuel assemblies). Archive appropriate displacement and load outputs from the dynamic model for post-processing.

c. Perform stress analysis of high stress areas for the limiting case of all the rack dynamic analyses. Demonstrate compliance with ASME Code Section III, Subsection NF limits on stress and displacement.

5.4.2.1 Model Details for Racks

The dynamic modeling of the rack structure must be prepared with special consideration of all nonlinearities and parametric variations. Particulars of modeling details and assumptions for the WPMR analysis of racks are given in the following:

a. The fuel rack structure motion is captured by modeling the rack as a 12 degree-of-freedom structure. Movement of the rack cross-section at any height is described by six degrees-of-freedom of the rack base and six degrees-of-freedom at the rack top. In this manner, the response of the module, relative to the baseplate, is captured in the dynamic analyses once suitable springs are introduced to couple the rack degrees-of-freedom and simulate rack stiffness.

b. Rattling fuel assemblies within the rack are modeled by five lumped masses located at H, 0.75H, 0.5H, 0.25H, and at the rack base (H is the rack height measured above the baseplate). Each lumped fuel mass has two horizontal degrees-of-freedom. Vertical motion of the fuel assembly mass is assumed equal to rack vertical motion at the baseplate level. The centroid of each fuel assembly mass can be located off-center, relative to the rack structure centroid at that level, to simulate a partially loaded rack.

c. Seismic motion of a fuel rack is characterized by random rattling of fuel assemblies in their individual storage locations. The out of phase motion of the individual fuel assemblies has been appropriately considered by modifying the mass of the individual lumped masses discussed above.

d. Fluid coupling between the rack and fuel assemblies, and between the rack and wall, is simulated by appropriate inertial coupling in the system kinetic energy. Inclusion of these effects uses the methods of [5-9, 5-10] for rack-to-fuel coupling and for rack-to-rack coupling.

e. Fluid damping and form drag are conservatively neglected.

f. Sloshing is found to be negligible at the top of the rack and is, therefore, neglected in the analysis of the racks.

g. Potential impacts between the cell walls of the racks and the contained fuel assemblies are accounted for by appropriate compression-only gap elements between masses involved. The possible incidence of rack-to-wall or rack-to-rack impact is simulated by gap elements at the top and bottom of the rack in two horizontal directions. Bottom gap elements are located at the baseplate elevation. The initial gaps reflect the presence of baseplate extensions, and the rack stiffnesses are chosen to simulate local structural detail.

h. The model for the rack is considered supported, at the base level, on four pedestals. Pedestals are modeled by non-linear compression gap elements in the vertical direction and as "rigid links" for transferring horizontal stress. Each pedestal support is linked to the bearing pad by two piecewise linear friction spring elements. These elements are properly located with respect to the centerline of the rack beam, and allow for arbitrary rocking and sliding motions. The spring rate for the friction springs includes any lateral elasticity of the stub pedestals. Local pedestal vertical spring stiffness accounts for floor elasticity and for local rack elasticity just above the pedestal.

i. Rattling of fuel assemblies inside the storage locations causes the gap between fuel assemblies and cell wall to change from a maximum of twice the nominal gap to a theoretical zero gap. Fluid coupling coefficients are based on the nominal gap in order to provide a conservative measure of fluid resistance to gap closure.

5.4.2.2 Element Details

Figure 5.1 shows a schematic of the dynamic model of a single rack. The schematic depicts many of the characteristics of the model including all of the degrees-of-freedom and most of the spring restraint elements.

Table 5.2 provides a complete listing of each of the 22 degrees-of-freedom for a rack model. Six translational and six rotational degrees-of-freedom (three of each type at top and bottom of rack) describe the motion of the rack structure. Rattling fuel mass motions (shown at nodes 1^*, 2^*, 3^*, 4^*, and 5^* in Figure 5.1) are described by ten horizontal translational degrees-of-freedom (two at each of the five fuel masses). The vertical fuel mass motion is assumed (and modeled) to be the same as that of the rack baseplate.

Figure 5.2 depicts the fuel to rack impact springs (used to develop potential impact loads between the fuel assembly mass and rack cell inner walls) in a schematic isometric. Only one of the five fuel masses is shown in this figure. Four compression-only springs, acting in the horizontal direction, are provided at each fuel mass.

Figure 5.3 provides a 2-D schematic elevation of the storage rack model, discussed in more detail in Section 5.4.2.4. This view shows the vertical location of the five storage masses and some of the support pedestal spring members.

Figure 5.4 shows the modeling technique and degrees-of-freedom associated with rack elasticity. In each bending plane a shear and bending spring simulate elastic effects [5-11]. Linear elastic springs coupling rack vertical and torsional degrees-of-freedom are also included in the model.

Figure 5.5 depicts the inter-rack impact springs (used to develop potential impact loads between racks or between rack and wall).

5.4.2.3 Multi-Body Fluid Coupling Phenomena

During the seismic event, all racks in the pool are subject to the input excitation simultaneously. The motion of each freestanding module would be autonomous and independent of others as long as they did not impact each other and no water were present in the pool. While the scenario of inter-rack impact is not a common occurrence and depends on rack spacing, the effect of water (the so-called fluid coupling effect) is a universal factor. As noted in Refs [5-10, 5-12], the fluid forces can reach rather large values in closely spaced rack geometries. It is, therefore, essential that the contribution of the fluid forces be included in a comprehensive manner for the spent fuel pool analyses. This is possible only if all racks in the pool are *allowed* to execute 3-D motion in the mathematical model. For this reason, single rack or even multi-rack models involving only a portion of the racks in the pool, are inherently inaccurate. The Whole Pool Multi-Rack model removes this intrinsic limitation of the rack dynamic models by simulating the 3-D motion of all modules simultaneously. The fluid coupling effect, therefore, encompasses interaction between *every* set of racks in the pool (i.e., the motion of one rack produces fluid

forces on all other racks and on the pool walls). Stated more formally, both near-field and far-field fluid coupling effects are included in the analysis.

The derivation of the fluid coupling matrix [5-12] relies on the classical inviscid fluid mechanics principles, namely the principle of continuity and Kelvin's recirculation theorem. While the derivation of the fluid coupling matrix is based on no artificial construct, it has been nevertheless verified by an extensive set of shake table experiments [5-12].

In its simplest form, the so-called "fluid coupling effect" [5-9, 5-10] can be explained by considering the proximate motion of two bodies under water. If one body (mass m_1) vibrates adjacent to a second body (mass m_2), and both bodies are submerged in frictionless fluid, then Newton's equations of motion for the two bodies are:

$$(m_1 + M_{11})\,\ddot{X}_1 + M_{12}\,\ddot{X}_2 = \text{applied forces on mass } m_1 + O\,(X_1^2)$$

$$M_{21}\,\ddot{X}_1 + (m_2 + M_{22})\,\ddot{X}_2 = \text{applied forces on mass } m_2 + O\,(X_2^2)$$

$\ddot{X}_1$, and $\ddot{X}_2$ denote absolute accelerations of masses m_1 and m_2, respectively, and the notation $O(X^2)$ denotes nonlinear terms.

M_{11}, M_{12}, M_{21}, and M_{22} are fluid coupling coefficients which depend on body shape, relative disposition, etc. Fritz [5-10] gives data for M_{ij} for various body shapes and arrangements. The fluid adds mass to the body (M_{11} to mass m_1), and an inertial force proportional to acceleration of the adjacent body (mass m_2). Thus, acceleration of one body affects the force field on another. This force field is a function of inter-body gap, reaching large values for small gaps. Lateral motion of a fuel assembly inside a storage location encounters this effect. For example, fluid coupling behavior will be experienced between nodes 2 and 2* in Figure 5.1. The rack analysis also contains inertial fluid coupling terms, which model the effect of fluid in the gaps between adjacent racks.

Terms modeling the effects of fluid flowing between adjacent racks in a single rack analysis suffer from the inaccuracies described earlier. These terms are usually computed assuming that all racks adjacent to the rack being analyzed are vibrating in-phase or 180° out of phase. The WPMR analyses do not require any assumptions with regard to phase.

Rack-to-rack gap elements have initial gaps set to 100% of the physical gap between the racks or between outermost racks and the adjacent pool walls.

5.4.2.4 Stiffness Element Details

Three element types are used in the rack models. Type 1 elements represent the linear elastic beam-like behavior of the integrated rack cell matrix. Type 2 elements are the piecewise linear friction springs used to develop the appropriate horizontal forces between the rack pedestals and the supporting bearing pads. Type 3 elements are non-linear gap elements, which model gap closures and subsequent impact loadings (i.e., between fuel assemblies and the storage cell inner walls, rack outer periphery spaces, and the vertical forces between the rack pedestals and the supporting bearing pads).

If the simulation model is restricted to two dimensions (one horizontal motion plus one vertical motion, for example), for the purposes of model clarification only, then Figure 5.3 describes the configuration. This simpler model is used to elaborate on the various stiffness modeling elements.

Type 3 gap elements modeling impacts between fuel assemblies and racks have local stiffness K_i in Figure 5.3. Support pedestal spring rates K_S are modeled by type 3 gap elements. Local compliance of the concrete floor is included in K_S. The type 2 friction elements are shown in Figure 5.3 as K_f. The spring elements depicted in Figure 5.4 represent type 1 elements.

Friction at the support/bearing pad interface is modeled by the piecewise linear friction springs with suitably large stiffness K_f up to the limiting lateral load μN, where N is the current compression load at the interface between support and liner. At every time-step during transient

analysis, the current value of N (either zero if the pedestal has lifted off the liner, or a compressive finite value) is computed.

The gap element K_S, modeling the effective compression stiffness of the structure in the vicinity of the support, includes stiffness of the pedestal, local stiffness of the underlying pool slab, and local stiffness of the rack cellular structure above the pedestal.

The previous discussion is limited to a 2-D model solely for simplicity. Actual analyses incorporate 3-D motions.

5.4.2.5 Coefficients of Friction

To eliminate the last significant element of uncertainty in rack dynamic analyses, multiple simulations must be performed to adjust the friction coefficient ascribed to the support pedestal/pool bearing pad interface. These friction coefficients are chosen consistent with the two bounding extremes from Rabinowicz's data [5-8]. Simulations are also performed by imposing intermediate value friction coefficients developed by a random number generator with Gaussian normal distribution characteristics. The assigned values are then held constant during the entire simulation in order to obtain reproducible results.[†] Thus, in this manner, the WPMR analysis results are brought closer to the realistic structural conditions.

The coefficient of friction (μ) between the pedestal supports and the pool floor is indeterminate. According to Rabinowicz [5-10], results of 199 tests performed on austenitic stainless steel plates submerged in water show a mean value of μ to be 0.503 with standard deviation of 0.125. Upper and lower bounds (based on twice standard deviation) are 0.753 and 0.253, respectively. Analyses are therefore performed for coefficient of friction values of 0.2 (lower limit) and for 0.8 (upper limit), and for random friction values clustered about a mean of 0.5. The bounding values

[†] It is noted that DYNARACK has the capability to change the coefficient of friction at any pedestal at each instant of contact based on a random reading of the computer clock cycle. However, exercising this option would yield results that could not be reproduced. Therefore, the random choice of coefficients is made only once per run.

of μ = 0.2 and 0.8 have been found to envelope the upper limit of module response in previous rerack projects.

5.4.2.6 Governing Equations of Motion

Using the structural model discussed in the foregoing, equations of motion corresponding to each degree-of-freedom are obtained using Lagrange's Formulation [5-11]. The system kinetic energy includes contributions from solid structures and from trapped and surrounding fluid. The final system of equations obtained has the matrix form:

$$[M]\left[\frac{d^2 q}{d t^2}\right] = [Q] + [G]$$

where:

[M] is the total mass matrix (including structural and fluid mass contributions). The size of this matrix will be 22n x22n for a WPMR analysis (n = number of racks in the model).

q is the nodal displacement vector relative to the pool slab displacement (the term with q indicates the second derivative with respect to time, i.e., acceleration)

[G] is a vector dependent on the given ground acceleration

[Q] is a vector dependent on the spring forces (linear and nonlinear) and the coupling between degrees-of-freedom

The above column vectors have length 22n. The equations can be rewritten as follows:

$$\left[\frac{d^2 q}{d t^2}\right] = [M]^{-1}[Q] + [M]^{-1}[G]$$

This equation set is mass uncoupled, displacement coupled at each instant in time. The numerical solution uses a central difference scheme built into the Holtec-proprietary computer program DYNARACK [5-6].

5.5 Preliminary Structural Evaluation of Racks

To provide a demonstration that the proposed rack layouts and rack designs (see Chapters 1 and 2) will appropriately satisfy the requirements discussed in the preceding sections of this chapter, a series of preliminary structural evaluations have been performed and are described in the remaining sections of this chapter. These preliminary evaluations are not intended as final qualifications, which will be performed in the future in accordance with the preceding sections of this chapter, but rather to give confidence that the proposed racks are suitably designed.

5.5.1 Description of Rack Layout

The analyzed new fuel storage racks and spent fuel storage rack configurations are depicted in Figures 1.1 and 1.2.

The various components for each of the rack styles are described in detail in Section 2.6. The models prepared for the DYNARACK simulations account for all of the pertinent features and characteristics of each rack type (i.e., Region 1 and Region 2). Rack material is defined in Table 5.4.3. Figure 1.2 shows the proposed layout of the spent fuel new high-density racks. In the WPMR model, the racks are numbered from 1 to 14 beginning in the northwest corner of the SFP (i.e., Rack 1 in Figure 1.2) and continuing West to East and North to South. Thus, rack number 14 is in the southeast corner of the SFP (i.e., Rack 14 in Figure 1.2)).

The cartesian coordinate system utilized within the dynamic models has the following orientation:

x = Horizontal axis along plant East (in an east-west direction)
y = Horizontal axis along plant North (in a north-south direction)
z = Vertical axis upward from the rack base

For the dynamic rack simulations, the dry fuel weight is conservatively taken to be 1,916 lbs to account for the maximum fuel weight and consideration of fuel inserts at every location.

5.5.2 Synthetic Time-Histories

Synthetic time-histories in three orthogonal directions (N-S, E-W, and vertical) were generated in accordance with the provisions of Section 3.7.1 of the SRP [5-1]. In order to prepare an acceptable set of acceleration time-histories, the Holtec-proprietary code GENEQ [5-7] was utilized. As required by the recent issues of the SRP [5-1], the code GENEQ was used to develop five sets of acceleration time histories for the design basis response spectra.

The following criteria required by SRP Section 3.7.1 have been satisfied:

1. Each time history set (2 horizontal and 1 vertical) must be statistically independent. This is demonstrated by calculating the cross correlation coefficient for each time history with each of the other two events. The absolute value of each of the three correlation coefficients must be less than 0.16.

2. For each of the time histories:

    - The time history shall have a sufficiently small time increment and sufficiently long duration. Records shall have a Nyquist frequency of at least 50 Hz, (e.g., a time increment of at most 0.010 seconds) and a total duration of at least 20 seconds.

    - Spectral acceleration at 5% damping shall be computed at a minimum of 100 points per frequency decade, uniformly spaced over the log frequency scale from 0.1 Hz to 50 Hz or the Nyquist frequency. The comparison of the response spectrum obtained from the artificial ground motion time history with the target response spectrum shall be made at each frequency computed in the frequency range of interest.

3. For each of the *average* response spectra:

- The computed 5% damped response spectrum of the accelerogram shall not fall more than 10% below the target response spectrum at any one frequency.

- The computed 5% damped response spectrum of the artificial ground motion time history shall not exceed the target response spectrum at any frequency by more than 30% (a factor of 1.3) in the frequency range of interest. If the response spectrum for the accelerogram exceeds the target response spectrum by more than 30% at any frequency range, the power spectrum density of the accelerogram needs to be computed and shown to not have significant gaps in energy at any frequency over this frequency range.

5.5.3 Stress Limit Evaluations

The stress limits presented below apply to the rack structure and are derived from the ASME Code, Section III, Subsection NF [5-13]. Parameters and terminology are in accordance with the ASME Code. Material properties are obtained from the ASME Code Section II, Part D [5-16], and are listed in Table 5.4.3.

(i) <u>Normal and Upset Conditions (Level A or Level B)</u>

a. Allowable stress in tension on a net section is:

$F_t = 0.6\ S_y$

where, S_y = yield stress at temperature, and F_t is equivalent to primary membrane stress.

b. Allowable stress in shear on a net section is:

$F_v = .4\ S_y$

c. Allowable stress in compression on a net section is:

$$F_a = S_y \left(.47 - \frac{k\ \ell}{444\ \mathrm{r}} \right)$$

where kl/r for the main rack body is based on the full height and cross section of the honeycomb region and does not exceed 120 for all sections.

l = unsupported length of component

k = length coefficient which gives influence of boundary conditions. The following values are appropriate for the described end conditions:

1 (simple support both ends)

2 (cantilever beam)

½ (clamped at both ends)

r = radius of gyration of component

d. Maximum allowable bending stress at the outermost fiber of a net section, due to flexure about one plane of symmetry is:

$F_b = 0.60\ S_y$ (equivalent to primary bending)

e. Combined bending and compression on a net section satisfies:

$$\frac{f_a}{F_a} + \frac{C_{mx}\ f_{bx}}{D_x\ F_{bx}} + \frac{C_{my}\ f_{by}}{D_y\ F_{by}} < 1$$

where:

f_a	=	Direct compressive stress in the section
f_{bx}	=	Maximum bending stress along x-axis
f_{by}	=	Maximum bending stress along y-axis
C_{mx}	=	0.85
C_{my}	=	0.85
D_x	=	$1 - (f_a/F'_{ex})$
D_y	=	$1 - (f_a/F'_{ey})$
$F'_{ex,ey}$	=	$(\pi^2 E)/(2.15\ (kl/r)^2_{x,y})$
E	=	Young's Modulus

and subscripts x,y reflect the particular bending plane.

f. Combined flexure and compression (or tension) on a net section:

$$\frac{f_a}{0.6\,S_y} + \frac{f_{bx}}{F_{bx}} + \frac{f_{by}}{F_{by}} < 1.0$$

The above requirements are to be met for both direct tension or compression.

g. Welds

Allowable maximum shear stress on the net section of a weld is given by:

$F_w = 0.3\ S_u$

where S_u is the weld material ultimate strength at temperature. For fillet weld legs in contact with base metal, the shear stress on the gross section is limited to $0.4S_y$, where S_y is the base material yield strength at temperature.

(ii) Level D Service Limits

Section F-1334 (ASME Section III, Appendix F) [5-14], states that the limits for the Level D condition are the minimum of 1.2 (S_y/F_t) or ($0.7S_u/F_t$) times the corresponding limits for the Level A condition. S_u is ultimate tensile stress at the specified rack design temperature. Examination of material properties for 304L stainless demonstrates that 1.2 times the yield strength is less than the 0.7 times the ultimate strength.

Exceptions to the above general multiplier are the following:

a) Stresses in shear shall not exceed the lesser of $0.72S_y$ or $0.42S_u$. In the case of the Austenitic Stainless material used here, $0.72S_y$ governs.

b) Axial Compression Loads shall be limited to 2/3 of the calculated buckling load.

c) Combined Axial Compression and Bending - The equations for Level A conditions shall apply except that:

F_a = 0.667 x Buckling Load/ Gross Section Area,

and the terms F'_{ex} and F'_{ey} may be increased by the factor 1.65.

d) For welds, the Level D allowable maximum weld stress is not specified in Appendix F of the ASME Code. An appropriate limit for weld throat stress is conservatively set here as:

$F_w = (0.3\ S_u)$ x factor

where:

factor = (Level D shear stress limit)/(Level A shear stress limit)

5.5.3.1 Dimensionless Stress Factors

For convenience, the stress results are presented in dimensionless form. Dimensionless stress factors are defined as the ratio of the actual developed stress to the specified limiting value. The limiting value of each stress factor is 1.0.

Stress factors reported are:

R_1 = Ratio of direct tensile or compressive stress on a net section to its allowable value (note pedestals only resist compression)

R_2 = Ratio of gross shear on a net section in the x-direction to its allowable value

R_3 = Ratio of maximum x-axis bending stress to its allowable value for the section

R_4 = Ratio of maximum y-axis bending stress to its allowable value for the section

R_5 = Combined flexure and compressive factor (as defined in the foregoing)

R_6 = Combined flexure and tension (or compression) factor (as defined in the foregoing)

R_7 = Ratio of gross shear on a net section in the y-direction to its allowable value.

5.5.4 Parametric Simulations

Comprehensive 3-D acceleration-time history analyses were performed for the SSE design basis event. The following rack configurations (cases) have been analyzed for Spent Fuel Racks and New Fuel Racks:

1) Whole Pool Multi Rack Configuration: This configuration is used for the spent fuel racks in the spent fuel pool. All the racks in the spent fuel pool are included in the seismic analysis with appropriate surrounding gaps.

2) Single Rack Configuration: This configuration considers only a single new fuel rack placed in the new fuel vault, free of water. Since a COF of 0.8 is shown to bound the WPMR analysis, the COF of 0.8 is used in single rack analysis. Since the new fuel vault will be dry, the single rack model neglects fluid coupling effect. Set 4 seismic event (i.e. run 6) produces the largest stresses in the rack modules, the single rack analysis is run with Set 4 seismic event as well for conservatism. All three new fuel racks are identical in design with the exception of rack to vault wall gaps. Since larger gaps tend to produce higher displacements the single rack model utilizes larger rack to rack gaps.

3) The following table presents a complete listing of the simulations discussed herein.

Consideration of the parameters described in Section 5.4.2 resulted in the following runs.

LIST OF SPENT FUEL RACK SIMULATIONS				
Run	Model	Load Case	COF	Event
1	WPMR	All Racks Fully Loaded	0.2	SSE, Set 1
2	WPMR	All Racks Fully Loaded	Random	SSE, Set 1
3	WPMR	All Racks Fully Loaded	0.8	SSE, Set 1
4	WPMR	All Racks Fully Loaded	0.8	SSE, Set 2
5	WPMR	All Racks Fully Loaded	0.8	SSE, Set 3
6	WPMR	All Racks Fully Loaded	0.8	SSE, Set 4
7	WPMR	All Racks Fully Loaded	0.8	SSE, Set 5
8[1]	WPMR	All Racks Fully Loaded	0.8	SSE, Set 4

LIST OF NEW FUEL RACK SIMULATIONS				
Run	Model	Load Case	COF	Event
9	Single Rack	New Fuel Rack	0.8	SSE, Set 4

where Random = Gaussian distribution with a mean of 0.5 coefficient of friction and upper and lower limits of 0.8 and 0.2.

5.6 Mechanical Evaluation of Racks

This section discusses the results of the structural analysis of the racks and the mechanical evaluation performed to show that the acceptance criteria, discussed in Section 5.2, are met. The evaluation of the racks to address their ability to withstand the postulated mechanical accidents is discussed in Chapter 7.

The results from the DYNARACK runs are provided in this section by extracting the worst case values from the parameters of interest; namely displacements, support pedestal forces, impact loads, and stress factors. This section also summarizes other analyses performed to develop and

1 Run 8 is identical to run 6 except that rack-to-rack spacing has been increased slightly to mitigate the rack-to-rack impact loads.

evaluate structural member stresses, which are not determined by the DYNARACK postprocessor.

5.6.1 Rack Displacements

The rack numbering scheme used to identify the racks in each simulation model, and the x and y coordinate axes used to identify displacement orientation are described in Subsection 5.4.3. The largest top of rack displacement for the spent fuel rack configurations considered is 3.12". Other simulations have smaller, but comparable, displacements in both x and y directions.

The largest top of rack displacement for the new fuel rack configurations considered is 4.50". The displacement of the new fuel rack is high because of the absence of any water in the new fuel vault. The displacement of the rack modules in air is always higher than those submerged in water because of the absence of any fluid coupling effect. Even with the higher rack displacement, by comparison of the maximum displacement with the width of the rack, it is obvious that rack overturning is of no concern.

5.6.2 Pedestal Vertical Forces

The highest vertical pedestal load from all spent fuel racks is 369,000 lbs, which bounds all other simulations. The highest vertical pedestal load for the new fuel rack is 268,000 lbs, which is bounded by the peak vertical load from the spent fuel racks.

5.6.3 Pedestal Friction Forces

The maximum friction load for the spent fuel racks is 189,000 lbs. This load has been used to evaluate the female pedestal-to-baseplate weld, as discussed in Section 5.6.7 (part b).

The maximum friction load for the new fuel racks is 110,000 lbs, which is bounded by the female pedestal-to-baseplate weld evaluation described above.

5.6.4 Rack Impact Loads

A freestanding rack, by definition, is a structure subject to potential impacts during a seismic event. Impacts arise from rattling of the fuel assemblies in the storage rack locations and, in some instances, from localized impacts between the racks, or between a peripheral rack and the pool wall. The following sections discuss the bounding values of these impact loads.

5.6.4.1 Rack Impacts

In order to protect the rack cell structure from impact during a seismic event and maintain the proper rack spacing, the rack baseplates extend beyond the perimeter envelope of the cell region. The racks are then installed in the pool with a very small separation between adjacent rack baseplates. Therefore, by design the racks are predisposed to impact each other at the baseplate level during a seismic event, rather than at the top of rack elevation. As a result, the 3/4 inch thick rack baseplates have been designed to accommodate the maximum in-plane contact forces.

The impact loads at the rack base are experienced on the perimeter edges of the baseplates and are insignificant compared to the plate capacity in compression. Local deformations will result in the impact load being spread across a substantial width of the entire baseplate. Therefore, the baseplates remain adequate. Rack to rack impacts do occur at the top of rack elevation between adjacent spent fuel racks at several locations in the spent fuel pool. The maximum rack to rack impact load at rack top is 157,900 lb observed between two racks. A buckling failure analysis of the impacted racks has been performed, and the safety factor against buckling failure is greater than 1.5.

No rack-to-wall impacts occur in any of the dynamic simulations. Thus, the freestanding racks do not transmit any forces to the SFP walls.

There are some impacts between the new fuel racks and between the racks and the new fuel storage vault walls. The maximum impact force being exerted on a new fuel rack is 322,500 lb, which is significant. In order to avoid plastic deformation of the cell walls, the new fuel racks will be equipped with "bumper bars" on all four corners of the rack at the top. The bumper bar is approximately 3/16" thick and 10" wide, which is welded to the rack. The bumper bars stiffen the rack cell structure, which prevents rack cell walls from buckling.

5.6.4.2 Fuel to Cell Wall Impact Loads

Even though limits on secondary stresses are not prescribed in the ASME Code for Class 3 NF structures, evaluations must be made to ensure that the localized impacts do not lead to plastic deformations in the storage cells which affect the sub-criticality of the stored fuel array. Local cell wall integrity is conservatively estimated from peak impact loads. Plastic analysis is used to obtain the limiting impact load, which would lead to gross permanent deformation.

A review of all simulations performed allows determination of the maximum instantaneous impact load between fuel assembly and fuel cell wall at any modeled impact site. For the spent fuel racks with a wall thickness of 0.075", the limiting side load is 3,210 lbs. The maximum fuel assembly impact load is 1,850 lbs. Therefore, the cell walls are structurally adequate.

5.6.5 Rack Stress Factors

The time history results from the DYNARACK solver provide the pedestal normal and lateral interface forces, which may be converted to the limiting bending moment and shear force at the bottom baseplate-pedestal interface. In particular, maximum values for the previously defined stress factors are determined for every pedestal in the array of racks. The net section maximum (in time) bending moments and shear forces can also be determined at the bottom baseplate-rack cellular structure interface for each spent fuel rack in the pool. Using these forces and moments, the maximum stress in the limiting rack cell (box) can be evaluated.

The stress factor results for male and female pedestals, and for the entire spent fuel rack cellular cross section just above the baseplate have been determined. These factors are reported for every rack in each simulation, and for each pedestal in every rack. These locations are the most heavily loaded net sections in the structure so that satisfaction of the stress factor criteria at these locations ensures that the overall structural criteria set forth in Section 5.4.5 are met.

For the spent fuel racks, the maximum stress factor for the DYNARACK simulations is 0.589, which occurs in the cellular region of the rack. This calculated value of stress factor is significantly less than the allowable of 1.0. The maximum stress factor computed for the rack supports is less than computed for the cellular region and obviously less than the allowable of 1.0.

For the new fuel racks, the maximum stress factor for the DYNARACK simulations is less than 0.5, which also occurs in the cellular region of the rack. This calculated value of stress factor is significantly less than the allowable of 1.0. The maximum stress factor computed for the rack supports is even less than computed for the cellular region and obviously less than the allowable of 1.0.

The stress factors, as defined in Subsection 5.4.5.1, for all of the simulations performed, leads to the conclusion that all stress factors are less than the mandated limit. Therefore, the requirements of Section 5.2 are satisfied for the load levels considered for every limiting location in the racks.

5.6.6 Pedestal Thread Shear Stress

For the Spent Fuel Racks and New Fuel Racks, the maximum average shear stress in the engagement region is 13,039 psi. These stresses are bounding for both the male and female pedestal threads. The allowable shear stress for Level D conditions is the lesser of: 0.72 S_y = 15,408 psi or 0.42 S_u = 27,762 psi (based on S_y and S_u for SA240-304L at 200°F).

5.6.7 Weld Stresses

Weld locations subjected to significant seismic loading are located at the bottom of the rack at the baseplate-to-cell connection, at the top of the pedestal support at the baseplate connection, and at cell-to-cell connections. Bounding values of resultant loads are used to qualify the connections.

a. Baseplate-to-Rack Cell Welds

Reference [5-13] (ASME Code Section III, Subsection NF) permits, for Level A or B conditions, an allowable weld stress τ = .3 * (66,100) = 19,830 psi. As stated in Subsection 5.4.5 (part ii) the allowable for Level D is 0.54 S_u, giving an allowable of 35,690 psi.

Weld stresses are determined through the use of a simple conversion (ratio) factor (based on area ratios) applied to the corresponding stress factor in the adjacent rack material. The conversion factor is developed from the differences in base material thickness and length versus weld throat dimension and length as follows:

$$\frac{0.075*(8.8+0.075)}{0.0625*0.7071*6.5}=2.317$$

where

0.075	is the cell wall thickness
8.8+0.075	is the mean box dimension
0.0625*0.7071	is the box-baseplate fillet weld throat size
6.5	is the length of the weld

The highest predicted cell to baseplate weld stress is calculated based on the highest R2, R6, and R7 values for the rack cell region (refer to Subsection 5.4.5.1 for definition of R2, R6, and R7 factors). It should be noted that the following calculation uses the worst-case stress factors from

both spent and new fuel racks to produce conservative results. These cell wall stress factors are converted into weld stress values as follows:

SSE

$$\{[R6 * (1.2)]^2 + [R2 * (0.72)]^2 + [R7 * (0.72)]^2\}^{1/2} * S_y * \text{Ratio}$$
$$= \{[0.589 * (1.2)]^2 + [0.095 * (0.72)]^2 + [0.083 * (0.72)]^2\}^{1/2} * (21{,}400) * 2.317$$
$$= 35{,}340 \text{ psi}$$

Since the calculated stress values are less than the corresponding allowable weld stresses, all welds between the baseplate and cell wall base are acceptable.

b. Baseplate-to-Pedestal Welds

The weld between baseplate and support pedestal is checked using finite element analysis to determine that the maximum stress is 34,850 psi for a ¼" fillet weld under a Level D event. This calculated stress value is below the Level D allowable of 35,690 psi.

c. Cell-to-Cell Welds

Cell-to-cell connections are by a series of connecting welds along the cell height. Stresses in storage cell to cell welds develop due to fuel assembly impacts with the cell wall. These weld stresses are conservatively considered by assuming that fuel assemblies in adjacent cells are moving out of phase with one another so that impact loads in two adjacent cells are in opposite directions and are applied simultaneously. This load application tends to separate the two cells from each other at the weld. In addition the cell-to-cell welds experience flexural shear loads due to bending of the rack cell structure. An evaluation of the SSE loads shows that the computed weld stress of 19,949 psi is less than the Level D allowable weld shear stress value of 35,690 psi. It is therefore concluded that the cell-to-cell welds and the adjacent materials are acceptable under all cases considered.

5.6.8 Level A Evaluation

The dead weight per pedestal for the heaviest loaded rack is 52,650 lbs, which is very low compared to an SSE load of 369,000 lbs. Since there are no primary shear loads on the pedestal and since the Level A loads are approximately 20% of the Level D loads, while the Level A limits are about 50% of the Level D limits, the SSE load condition bounds the dead load condition and no further evaluation is performed for dead load only.

5.6.9 Assessment of Rack Fatigue Margin

Alternating stresses in metals produce metal fatigue if the amplitude of the stress cycles is sufficiently large. In high-density racks designed for sites with moderate to high postulated seismic action, the stress intensity amplitudes frequently reach values above the material endurance limit, leading to expenditure of the fatigue "usage" reserve in the material.

Because the locations of maximum stress (viz., the pedestal/rack baseplate junction) and the close placement of racks, a post-earthquake inspection of the high stressed regions in the racks is not feasible. Therefore, the racks must be engineered to withstand multiple earthquakes without reliance of nondestructive inspections for post-earthquake integrity assessment. The fatigue life evaluation of racks is an integral aspect of a sound design. The time-history method of analysis, deployed in this report, provides the means to obtain a complete cycle history of the stress intensities in the highly stressed regions of the rack. Having determined the amplitude of the stress intensity cycles and their number, the cumulative damage factor, U, can be determined using the classical Miner's rule:

$$U = \Sigma \frac{n_i}{N_i}$$

where n_i is the number of stress intensity cycles of amplitude σ_i, and N_i is the permissible number of cycles corresponding to σ_i from the ASME fatigue curve for the material of construction. U must be less than or equal to 1.0.

Based on the time-history results, the peak stress intensity at the pedestals is determined to be 155,494 psi, and the corresponding number of stress intensity cycles is 40 for one SSE event

Following ASME Code guidelines the amplified alternating stress intensity after accounting for plasticity effects is obtained as 261,000 psi. The corresponding cumulative damage factor is determined as 0.418 due to one SSE event. This is well below the ASME Code limit of 1.0.

5.6.10 Local Stress Considerations

This section presents the results of evaluations for the possibility of cell wall buckling and the secondary stresses produced by temperature effects.

5.6.10.1 Cell Wall Buckling

The allowable local buckling stresses in the fuel cell walls is obtained by using classical plate buckling analysis as taken from Section 9.2 of Reference [5-15]. The resulting local buckling stress limit of 28,063 psi is not violated anywhere in the body of the rack modules, since the maximum compressive stress in the outermost cell is σ = (1.2)(21,300) * R6 (with R6 = 0.589 for SSE condition) = 15,130 psi.

5.6.10.2 Analysis of Welded Joints in Rack

Cell-to cell welded joints are examined under the loading conditions arising from thermal effects due to an isolated hot cell, in this subsection. This secondary stress condition is evaluated alone and not combined with primary stresses from other load conditions.

A thermal gradient between cells will develop when an isolated storage location contains a fuel assembly emitting maximum postulated heat, while the surrounding locations are empty. A conservative estimate of weld stresses along the length of an isolated hot cell can be obtained by considering a beam strip uniformly heated by 75°F, which is restrained from growth along one long edge. This thermal gradient is based on the results of the thermal-hydraulic analysis, which shows that the difference between the local cell maximum temperature and the bulk pool temperature is less than this value (actual temperature difference is 33ºF per Chapter 6 results).

Using shear beam theory and subjecting the strip to a uniform temperature rise ΔT = 75°F, one can calculate an estimate of the maximum value of the average shear stress in the strip. The strip is subjected to the following boundary conditions.

a. Displacement U_x (x,y) = 0 at x = 0, at y = H, all x.

b. Average force M_x, acting on the cross section Ht = 0 at x = l, all y.

The final result for wall shear stress, maximum at x = l, is found to be given as

$$\tau_{max} = \frac{E \alpha \Delta T}{0.931}$$

where E = 27.6 x 10^6 psi, α = 9.5 x 10^{-6} in/in °F and ΔT = 75°F.

Therefore, the maximum weld shear stress in an isolated hot cell, due to thermal gradient, is

$$\tau_{max} = 21{,}122 \text{ psi}$$

Since this is a secondary thermal stress that is outside the conditions covered by the ASME Code, we use the allowable shear stress criteria for faulted conditions ($0.42*S_u$=27,804 psi) as a guide to indicate that this maximum shear is acceptable. Therefore, the safety factor against cell wall shear failure due to secondary thermal stresses from cell wall growth under the worst case hot cell conditions is larger than 1.

5.7 Bearing Pad Analysis

To protect the pool slab from high localized dynamic loadings, bearing pads are placed between the pedestal base and the slab. Fuel rack pedestals impact on these bearing pads during a seismic event and pedestal loading is transferred to the liner. Bearing pad dimensions are set to ensure that the average pressure on the slab surface due to a static load plus a dynamic impact load does not exceed the bearing pressure provided in American Concrete Institute, ACI-349 [5-17].

All bearing pads are 2" thick and 11" x 11" made out of austenitic steel material. In order to determine the average bearing pressure on the concrete, the maximum vertical pedestal loads from the time-history solutions from all rack simulations have been surveyed. The maximum vertical load from all pedestals is applied against the available bearing area. The bearing pads will be located in the storage pools such that they are not located above the leak chases. The bearing pressure calculation below demonstrates that the bearing pad provides sufficient area to maintain the average pressure in the concrete underneath the bearing pads below the ACI-349 limit.

The bearing capacity of the concrete is based upon the ACI criteria,

$$V = 2 \times \phi \times 0.85 \times f_c \times A$$

where:

ϕ = strength reduction factor = 0.7

f_c = compressive strength of concrete = 6,000psi

A = total bearing area = 11in x 11in

Thus, the capacity is,

$$V = 863{,}900lb$$

By comparison the seismic force is 369,000 lbs, which yields a safety factor larger than 1.0. Therefore, the bearing pad design devised for the proposed racks is appropriate for the prescribed loadings.

5.8 Interface Loads on Spent Fuel Pool Structure

The Spent Fuel Pool (SFP) at CCNPP Unit 3 U.S. EPR is a Safety Related, Seismic Category I, reinforced concrete structure. In this section, the interface loads transmitted by the spent fuel racks to the SFP structure are identified so that they can be used to demonstrate the structural integrity of the SFP.

5.8.1 Description of Pool Structure

The Spent Fuel Pool is located inside the Fuel Building at elevation 19.50 m, south of the reactor drywell. The nominal inner dimensions of the pool are: 8.95 m (29’-4”) in the North-South direction, 11.95 m (39’-2”) in the East-West direction, and 14.40 m (47'-3") deep. The top of the 1.8 m (5’-11”) thick reinforced concrete slab is at elev. 5.10 m. The north and south SFP walls are 1.8 m (5’-11”) thick, the west wall is 1.25 m (4’-1”) thick, and the south wall is 1.30 m (4’-3”) thick.

5.8.2 Definition of Loads

Pool structural loading involves the following discrete components:

5.8.2.1 Static Loading (Dead Loads and Live Loads)

- Dead weight of reinforced concrete structure and steel liner (D).

- Maximum dead weight of rack modules and fuel assemblies stored in the modules (D). The buoyant weight of the racks when fully loaded with spent fuel shall be uniformly distributed on the total wetted area of the SFP slab. The maximum buoyant weight of the racks plus the stored fuel assemblies is 3,158,000 lbs.

- Hydrostatic pressure on walls and slab (F).

5.8.2.2 Seismic Induced Loads

- Vertical loads are transmitted by the rack support pedestals to the slab during a Safe Shutdown Earthquake (E'). Using the results from the Whole Pool Multi-Rack (WPMR) analyses, the total load from all rack pedestals less the dead weight load can be computed as a function of time. Identifying the instantaneous peak load and dividing by the wetted area of the slab defines the slab pressure that represents the seismically induced "pressure adder" from the rack dynamic motion. The total vertical force transmitted by the racks to the SFP slab during an SSE event is 5,286,200 lbs, which is roughly a 67% increase above the static dead load.

- Hydrodynamic inertia loads due to the contained water mass and sloshing loads (considered in accordance with [5-19]) which arise during a seismic event (E').

- Hydrodynamic pressures between racks and pool walls are caused by rack motion in the pool during a seismic event (E'). The lateral pressures on the pool walls below the top of the spent fuel racks are obtained from the WPMR analyses.

- Seismic inertia forces develop in the walls and slab during a seismic event (E').

5.8.2.3 Thermal Loading

Thermal loading is defined by the temperature existing at the faces of the pool concrete walls and slabs. Two thermal loading conditions must be considered: the normal operating temperature and the accident temperature. The maximum bulk pool temperatures are provided in Chapter 6 for various discharge scenarios.

5.8.3 Load Combinations

The various individual loads shall be combined in accordance with the requirements of NUREG-0800 Standard Review Plan [5-1] and ACI 349 [5-17] with the intent to obtain the most critical force and moment fields for the investigated reinforced concrete structure.

5.9 References

[5-1] USNRC NUREG-0800, Standard Review Plan, March 2007.

[5-2] (USNRC Office of Technology) "OT Position for Review and Acceptance of Spent Fuel Storage and Handling Applications", dated April 14, 1978, and January 18, 1979 amendment thereto.

[5-3] Soler, A.I. and Singh, K.P., "Seismic Responses of Free Standing Fuel Rack Constructions to 3-D Motions", Nuclear Engineering and Design, Vol. 80, pp. 315-329 (1984).

[5-4] Soler, A.I. and Singh, K.P., "Some Results from Simultaneous Seismic Simulations of All Racks in a Fuel Pool", INNM Spent Fuel Management Seminar X, January, 1993.

[5-5] Singh, K.P. and Soler, A.I., "Seismic Qualification of Free Standing Nuclear Fuel Storage Racks - the Chin Shan Experience, Nuclear Engineering International, UK (March 1991).

[5-6] Holtec Proprietary Report HI-961465 - WPMR Analysis User Manual for Pre&Post Processors & Solver, August 1997.

[5-7] Holtec Proprietary Report HI-89364 - Verification and User's Manual for Computer Code GENEQ, January 1990.

[5-8] Rabinowicz, E., "Friction Coefficients of Water Lubricated Stainless Steels for a Spent Fuel Rack Facility," MIT, a report for Boston Edison Company, 1976.

[5-9] Singh, K.P. and Soler, A.I., "Dynamic Coupling in a Closely Spaced Two-Body System Vibrating in Liquid Medium: The Case of Fuel Racks," 3rd International Conference on Nuclear Power Safety, Keswick, England, May 1982.

[5-10] Fritz, R.J., "The Effects of Liquids on the Dynamic Motions of Immersed Solids," Journal of Engineering for Industry, Trans. of the ASME, February 1972, pp 167-172.

[5-11] Levy, S. and Wilkinson, J.P.D., "The Component Element Method in Dynamics with Application to Earthquake and Vehicle Engineering," McGraw Hill, 1976.

[5-12] Paul, B., "Fluid Coupling in Fuel Racks: Correlation of Theory and Experiment", (Proprietary), NUSCO/Holtec Report HI-88243.

[5-13] ASME Boiler & Pressure Vessel Code, Section III, Subsection NF, 2004 Edition.

[5-14] ASME Boiler & Pressure Vessel Code, Section III, Appendices, 2004 Edition.

[5-15] Theory of Elastic Stability, Timoshenko and Gere, 2nd Edition, 1961, McGraw Hill.)

[5-16] ASME Boiler & Pressure Vessel Code, Section II, Part D, 2004 Edition.

[5-17] ACI 349-85, Code Requirements for Nuclear Safety Related Concrete Structures, American Concrete Institute, Detroit, Michigan, 1985.

[5-18] ACI 318-05, Building Code requirements for Structural Concrete," American Concrete Institute, Detroit, Michigan, 2005.

[5-19] "Nuclear Reactors and Earthquakes, U.S. Department of Commerce, National Bureau of Standards, National Technical Information Service, Springfield, Virginia (TID 7024).

Table 5.4.1 PARTIAL LISTING OF FUEL RACK APPLICATIONS USING DYNARACK		
PLANT	DOCKET NUMBER(s)	YEAR
Enrico Fermi Unit 2	USNRC 50-341	1980
Quad Cities 1 & 2	USNRC 50-254, 50-265	1981
Rancho Seco	USNRC 50-312	1982
Grand Gulf Unit 1	USNRC 50-416	1984
Oyster Creek	USNRC 50-219	1984
Pilgrim	USNRC 50-293	1985
V.C. Summer	USNRC 50-395	1984
Diablo Canyon Units 1 & 2	USNRC 50-275, 50-323	1986
Byron Units 1 & 2	USNRC 50-454, 50-455	1987
Braidwood Units 1 & 2	USNRC 50-456, 50-457	1987
Vogtle Unit 2	USNRC 50-425	1988
St. Lucie Unit 1	USNRC 50-335	1987
Millstone Point Unit 1	USNRC 50-245	1989
Chinshan	Taiwan Power	1988
D.C. Cook Units 1 & 2	USNRC 50-315, 50-316	1992
Indian Point Unit 2	USNRC 50-247	1990
Three Mile Island Unit 1	USNRC 50-289	1991
James A. FitzPatrick	USNRC 50-333	1990
Shearon Harris Unit 2	USNRC 50-401	1991
Hope Creek	USNRC 50-354	1990
Kuosheng Units 1 & 2	Taiwan Power Company	1990
Ulchin Unit 2	Korea Electric Power Co.	1990
Laguna Verde Units 1 & 2	Comision Federal de Electricidad	1991
Zion Station Units 1 & 2	USNRC 50-295, 50-304	1992
Sequoyah	USNRC 50-327, 50-328	1992
LaSalle Unit 1	USNRC 50-373	1992
Duane Arnold Energy Center	USNRC 50-331	1992
Fort Calhoun	USNRC 50-285	1992
Nine Mile Point Unit 1	USNRC 50-220	1993

Table 5.4.1 (continued) PARTIAL LISTING OF FUEL RACK APPLICATIONS USING DYNARACK		
PLANT	DOCKET NUMBER(s)	YEAR
Beaver Valley Unit 1	USNRC 50-334	1992
Salem Units 1 & 2	USNRC 50-272, 50-311	1993
Limerick	USNRC 50-352, 50-353	1994
Ulchin Unit 1	KINS	1995
Yonggwang Units 1 & 2	KINS	1996
Kori-4	KINS	1996
Connecticut Yankee	USNRC 50-213	1996
Angra Unit 1	Brazil	1996
Sizewell B	United Kingdom	1996
Waterford 3	USNRC 50-382	1997
J.A. Fitzpatrick	USNRC 50-333	1998
Callaway	USNRC 50-483	1998
Nine Mile Unit 1	USNRC 50-220	1998
Chin Shan	Taiwan Power Company	1998
Vermont Yankee	USNRC 50-271	1998
Millstone 3	USNRC 50-423	1998
Byron/Braidwood	USNRC 50-454, 50-455, 50-567, 50-457	1999
Wolf Creek	USNRC 50-482	1999
Plant Hatch Units 1 & 2	USNRC 50-321, 50-366	1999
Harris Pools C and D	USNRC 50-401	1999
Davis-Besse	USNRC 50-346	1999
Enrico Fermi Unit 2	USNRC 50-341	2000
Kewaunee	USNRC 50-305	2001
V.C. Summer	USNRC 50-395	2001
St. Lucie	USNRC 50-335, 50-389	2002
Turkey Point	USNRC 50-250, 251	2002

Table 5.4.2

DEGREES-OF-FREEDOM

LOCATION (Node)	DISPLACEMENT			ROTATION		
	U_x	U_y	U_z	θ_x	θ_y	θ_z
1	p_1	p_2	p_3	q_4	q_5	q_6
2	p_7	p_8	p_9	q_{10}	q_{11}	q_{12}
Node 1 is attached to the rack at the bottom most point. Node 2 is attached to the rack at the top most point. Refer to Figure 5.1 for node identification.						
2*	p_{13}	p_{14}				
3*	p_{15}	p_{16}				
4*	p_{17}	p_{18}				
5*	p_{19}	p_{20}				
1*	p_{21}	p_{22}				

where the relative displacement variables q_i are defined as:

$$
\begin{aligned}
p_i &= q_i(t) + U_x(t) && i = 1,7,13,15,17,19,21 \\
&= q_i(t) + U_y(t) && i = 2,8,14,16,18,20,22 \\
&= q_i(t) + U_z(t) && i = 3,9 \\
&= q_i(t) && i = 4,5,6,10,11,12
\end{aligned}
$$

p_i denotes absolute displacement (or rotation) with respect to inertial space

q_i denotes relative displacement (or rotation) with respect to the floor slab

* denotes fuel mass nodes

U(t) are the three known earthquake displacements

Table 5.4.3 RACK MATERIAL DATA (200°F) (ASME - Section II, Part D)			
Material	Young's Modulus E (psi)	Yield Strength S_y (psi)	Ultimate Strength Su (psi)
SA240; 304L S.S.	27.6×10^6	21,400	66,100
SUPPORT MATERIAL DATA (200°F)			
SA240, Type 304L (upper part of support feet)	27.6×10^6	21,400	66,100
SA-564-630 (lower part of support feet; age hardened at 1100°F)	28.5×10^6	106,400	140,000

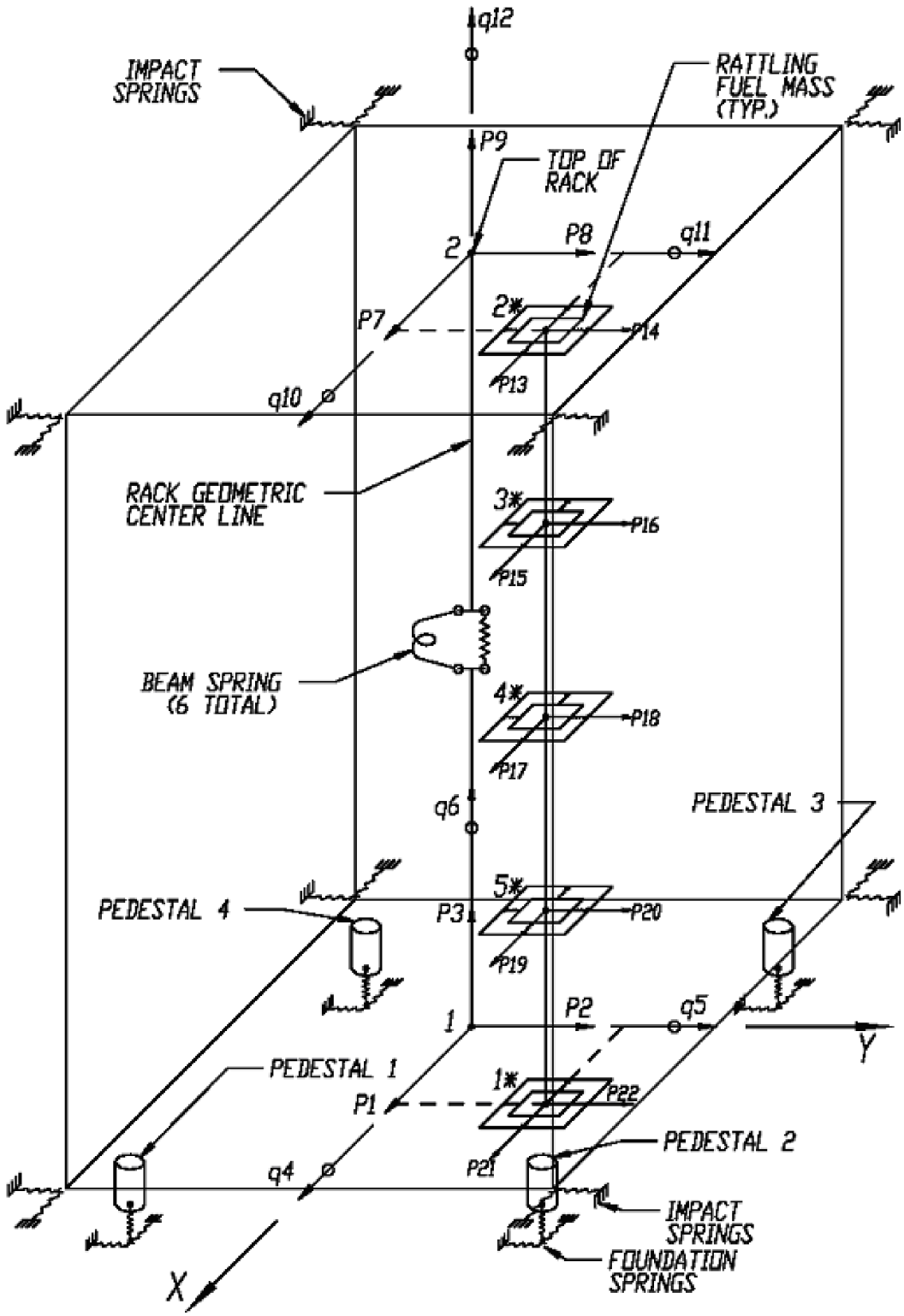

Figure 5.1: Single Rack Dynamic Model

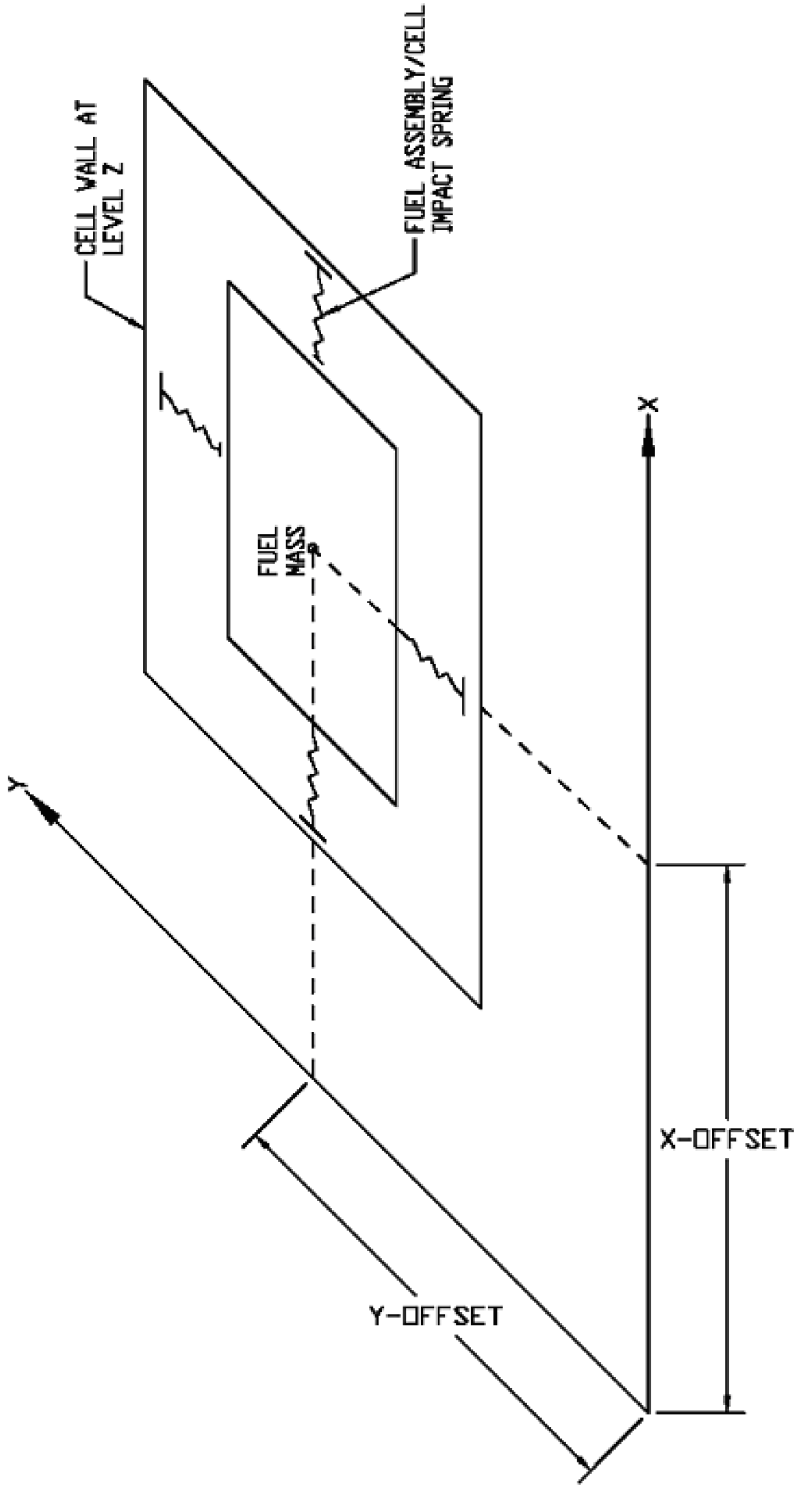

Figure 5.2: Fuel-to-Rack Impact Springs

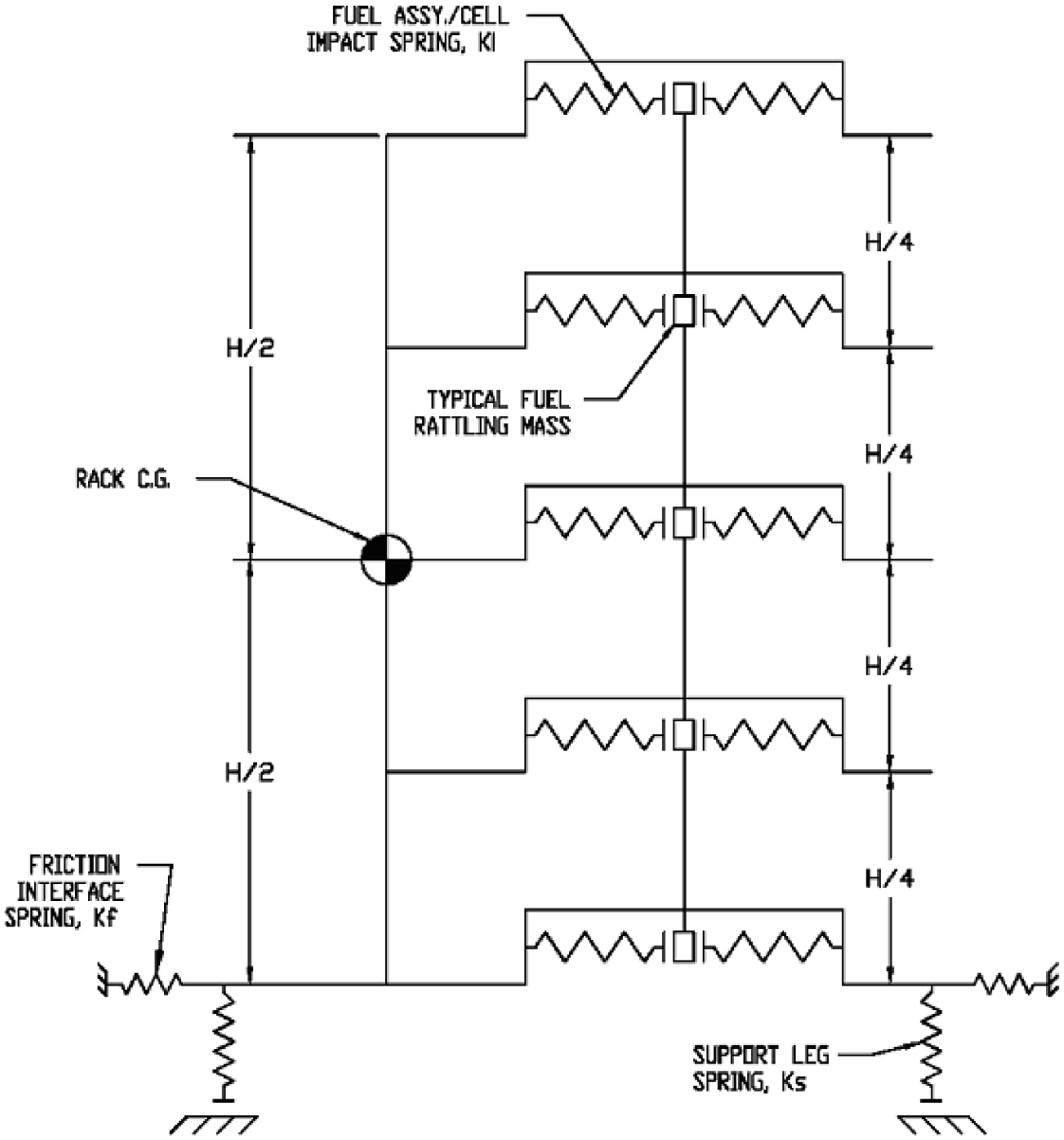

Figure 5.3: 2-D Schematic Elevation of the Storage Rack Model

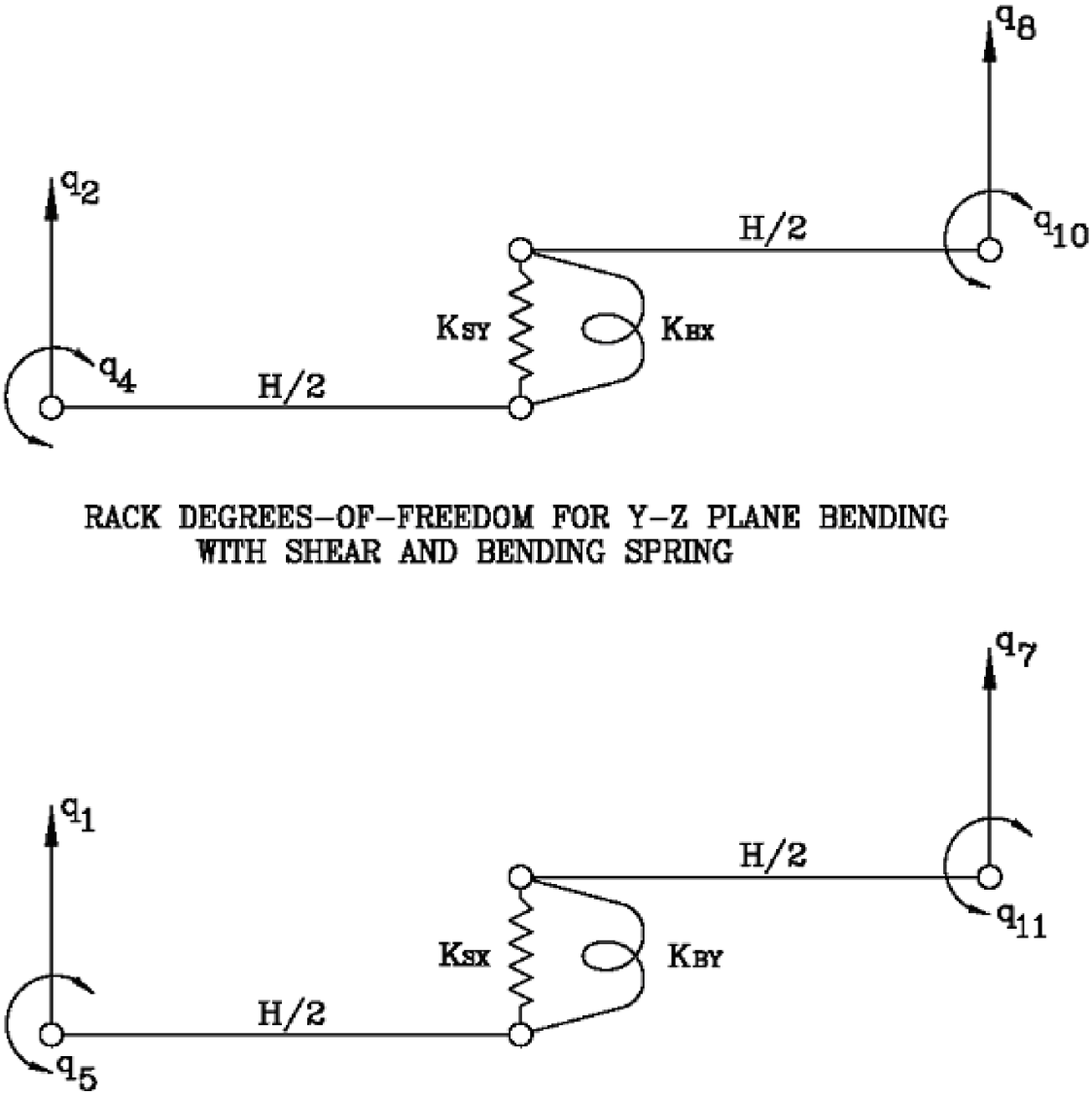

Figure 5.4: Rack Degrees of Freedom and Modeling Technique

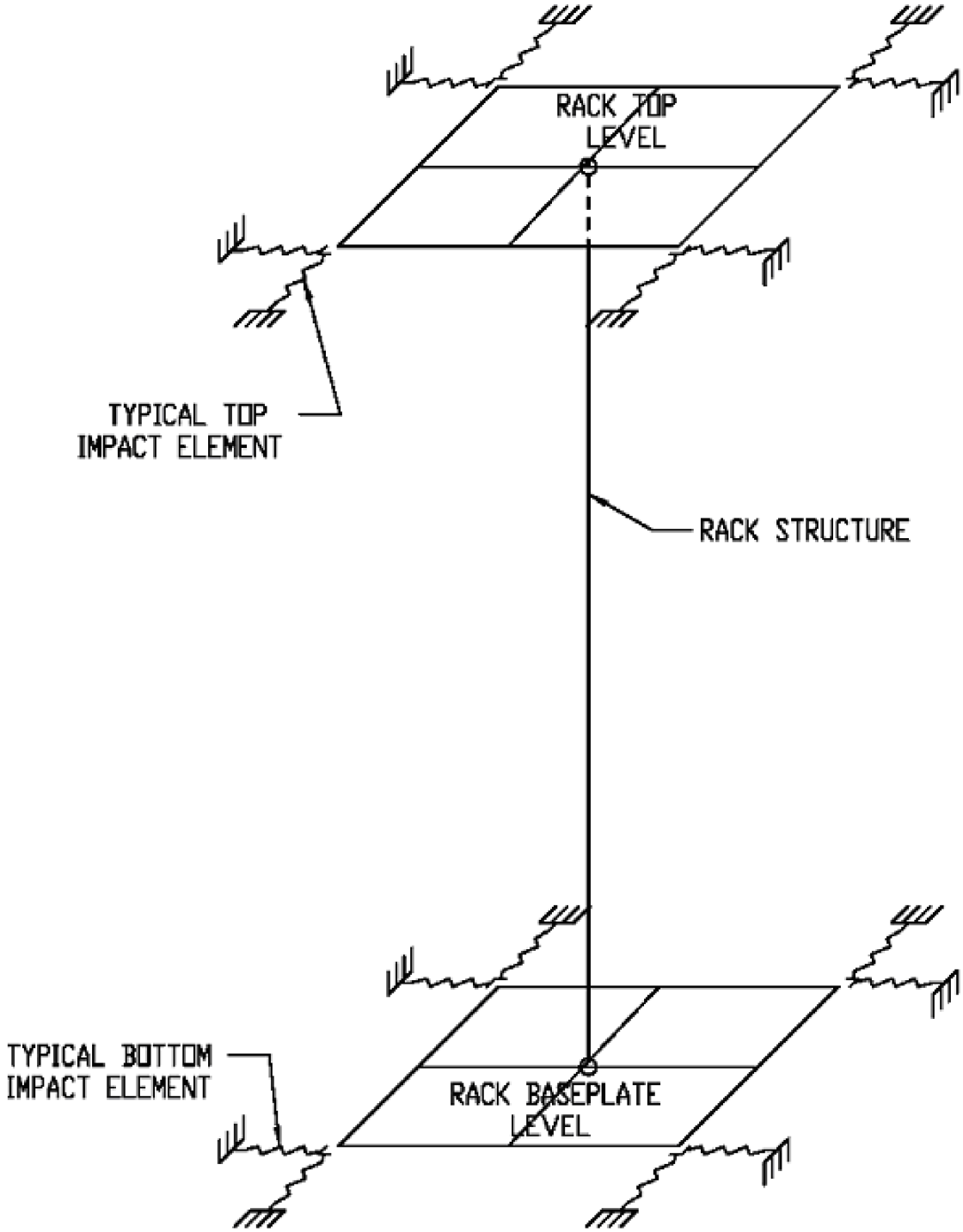

Figure 5.5: 2-D Inter-Rack Impact Springs

6.0 THERMAL-HYDRAULIC PERFORMANCE

This topical report provides information on the new and spent fuel storage racks to support a COLA for the Calvert Cliffs Nuclear Power Plant (CCNPP) Unit 3 U.S. EPR. This chapter, specifically, provides information on the required thermal-hydraulic performance characteristics of the fuel storage racks. As new (un-irradiated) fuel does not generate any heat, there are no thermal-hydraulic performance requirements for the new fuel storage racks. The remainder of this chapter, therefore, discusses the thermal-hydraulic performance requirements for the spent fuel storage racks.

6.1 Thermal-Hydraulic Design Conditions

In an NRC document entitled "OT Position Paper for Review and Acceptance of Spent Fuel Storage and Handling Applications" [1-5], guidance on the requirements for spent fuel storage facilities is provided. Based upon this guidance, a menu of thermal-hydraulic evaluations necessary to demonstrate adequate thermal-hydraulic performance of spent fuel storage equipment is developed as follows:

1. Calculation of the spent fuel decay heat. The decay heat contributions from both previously stored and recently discharged fuel assemblies must be considered.

2. Determination of the maximum SFP bulk water temperature. These determinations must consider realistic fuel offload scenarios and the potential for active component failures.

3. Calculation of the minimum time-to-boil during postulated loss of forced cooling events corresponding to the defined fuel offload scenarios.

4. A rigorous study to quantify the peak local water temperature in the fuel storage cells. While historically a number of calculation approaches have been used for these studies, recent licensing experience indicates that a Computational Fluid Dynamics (CFD) based methodology is required to obtain regulatory approval.

5. Determination of the maximum fuel clad temperature corresponding to the computed peak local water temperature.

For the CCNPP Unit 3 U.S. EPR, a number of fuel offload scenarios have been defined that encompass both partial core (i.e., in-reactor fuel shuffle) and full core offloads from the reactor to the SFP as well as the possible effects of active cooling system component failures. These defined scenarios are:

1. Partial Core Offload with Active Failure – 96 fuel assemblies discharged at the end of a normal operating cycle with the SFP cooled by one SFP cooling system train with two operating SFP cooling system pumps.

2. Full Core Offload with Active Failure – 241 fuel assemblies discharged at the end of a normal operating cycle with the SFP cooled by one SFP cooling system train with two operating SFP cooling system pumps.

3. Full Core Offload without Active Failure – 241 fuel assemblies discharged at the end of a normal operating cycle with the SFP cooled by two SFP cooling system trains each with two operating SFP cooling system pumps.

In the sections that follow, acceptance criteria that must be satisfied are prescribed, analysis methods are described, and the results of preliminary analyses are presented and discussed.

6.2 Acceptance Criteria

The design of the spent fuel storage racks must ensure that fuel assemblies are adequately cooled during all normal conditions and that sufficient time for remedial actions will exist during faulted conditions. For the CCNPP Unit 3 U.S. EPR, the following specific criteria are applied:

1. During a partial core offload with only one available SFP cooling system train, the SFP bulk temperature shall be limited to 140°F and local temperatures in the fuel storage rack cells shall be demonstrated to be below the local saturation temperature.

2. During a full core offload scenario with only one available SFP cooling system train, the SFP bulk temperature shall be limited to 140°F and local temperatures in the fuel storage rack cells shall be demonstrated to be below the local saturation temperature.

3. During a full core offload scenario with both SFP cooling system trains operating, the SFP bulk temperature shall be limited to 120°F and local temperatures in the fuel storage rack cells shall be demonstrated to be below the local saturation temperature.

4. During a loss of cooling event, sufficient time must be available to restore cooling water flow to the SFP before the SFP bulk temperature reaches the surface boiling temperature of 212°F.

5. The bounding maximum fuel cladding temperature in the SFP should be less than the local saturation temperature of water. If the fuel cladding temperature exceeds the local saturation temperature of water, it must be shown that departure from nucleate boiling (DNB) will not occur.

These criteria have been applied to the preliminary analyses presented later in this chapter.

6.3 Analysis Methods

The subsections in this section describe the analysis methods to be used in performing licensing-basis calculations to demonstrate that the thermal-hydraulic performance requirements for the spent fuel storage racks are satisfied. These are intended to be minimum requirements, and more sophisticated analysis models[1] may be used. Similar thermal-hydraulic analyses have been used for previous spent fuel storage rack licensing at many nuclear plants worldwide (see Table 6.3.1 for a *partial* list).

6.3.1 Decay Heat Computation

Calculations must be performed to determine the total decay heat load that exists in the SFP at the time it becomes full. This would correspond to the maximum fuel inventory in the SFP and, therefore, the maximum decay heat load. In the past, the most commonly used decay heat methodology was USNRC Branch Technical Position ASB 9-2 [6-1]. In the past decade, however, more accurate methodologies have become available, most notably the use of rigorous isotope depletion codes. The most commonly used such code is ORIGEN2 [6-2], developed at

1 Examples of more sophisticated analysis models would include transient bulk temperature analyses instead of steady-state analyses or considering the effects of both passive and active cooling mechanisms instead of active mechanisms only.

Oak Ridge National Laboratory in 1980. ORIGEN2 shall be used to perform the licensing-basis decay heat calculations.

6.3.2 Bulk Water Temperature Computation

The mathematical formulation for this analysis can be explained with reference to the simplified heat exchanger alignment shown in Figure 6.1. The governing differential equation for the bulk water temperature variation with time can be written by utilizing conservation of energy as:

$$C \times \frac{dT}{d\tau} = Q(\tau) - Q_{HE}(T) - Q_{EV}(T, T_A)$$

where:

C is the thermal capacity of water in the pool, Btu/°F

$dT/d\tau$ is the rate of change in the bulk temperature, °F/hr

$Q(\tau)$ is the time-varying heat generated by discharged fuel, Btu/hr

$Q_{HE}(T)$ is the SFP cooling system heat rejection, Btu/hr

$Q_{EV}(T, T_A)$ is the evaporative (passive) heat loss, Btu/hr

This differential equation can be reduced into an algebraic equation by conservatively neglecting transient effects (setting C to zero and using a pseudo-steady-state $Q(\tau)$). It can be further simplified by combining the heat generation terms and conservatively neglecting the passive heat loss terms, yielding:

$$Q_{GEN} = Q_{HE}(T)$$

where Q_{GEN} is the combined decay heat generation term and $Q_{HE}(T)$ is by the following governing equation:

$$Q_{HE}(T) = W_C \cdot c_C \cdot p \cdot (T - T_C)$$

where:

W_C is the component cooling water flow rate, lb/hr

c_C is the component cooling water specific heat rate, Btu/(lb×°F)

p is the SFP cooling system heat exchanger temperature effectiveness

T_C is the component cooling water inlet temperature, °F

To comport with this definition of $Q_{HE}(T)$, the SFP cooling system heat exchanger temperature must be defined as follows:

$$p = \frac{T_{C,o} - T_{C,i}}{T_{Pi} - T_{C,i}}$$

where:

$T_{C,o}$ is the component cooling water outlet temperature, °F

$T_{C,i}$ is the component cooling water inlet temperature, °F

T_{Pi} is the SFP water inlet temperature (to the exchanger), °F

Substituting the formula for p into that for $Q_{HE}(T)$ and substituting the result into the simplified heat balance equation yields a combined algebraic equation that can be solved for the maximum bulk temperature.

6.3.3 Time-to-Boil Computation

Starting with the same differential equation defined in Subsection 6.3.2, the SFP cooling system heat rejection term can be eliminated to obtain the governing equation for a loss-of-cooling event. Making the same decay heat simplifications as in Subsection 6.3.2 and again neglecting passive heat losses, the following governing equation is obtained:

$$C \times \frac{dT}{d\tau} = Q_{GEN}$$

This can be solved algebraically for the heat-up rate ($dT/d\tau$), which can then be multiplied by the difference between the maximum bulk temperature with cooling and the bulk boiling temperature (212°F) to obtain the minimum time-to-boil.

6.3.4 Local Water Temperature Computation

Adequate cooling of hot recently discharged fuel assemblies in the SFP is demonstrated by performing a rigorous evaluation of the velocity and temperature fields in the pool created by the interaction of buoyancy driven flows, spent fuel decay heat and cooling water injection/suction. To obtain an accurate representation of the couple flow and temperature fields, a three-dimensional Computational Fluid Dynamics (CFD) analysis is necessary.

There are several significant geometric and thermal-hydraulic features of the SFP that need to be considered for a rigorous CFD analysis. From a fluid flow-modeling standpoint, there are two regions to be considered. One region is the bulk pool region . The other region is the heat-generating zone of spent fuel storage racks loaded with fuel assemblies, located near the SFP bottom. In this zone, water flow is directed vertically upwards by the buoyancy forces through relatively small flow channels formed by the fuel assembly rod arrays in each rack cell. This situation is modeled as in which Darcy's Law [6-3] governs the pressure drop. The distributed heat sources in the spent fuel pool racks are modeled by identifying distinct heat generation zones considering full-core discharge, peaking effects, and the presence of background decay heat from previous fuel discharges.

While many CFD codes are available, Holtec has QA validated and benchmarked the FLUENT [6-4] fluid flow and heat transfer modeling program and has used it extensively for modeling spent fuel storage equipment. The FLUENT code enables buoyancy flow and turbulence effects to be included in the CFD analysis. Turbulence effects are modeled by relating time-varying "Reynolds' Stresses" to the mean bulk flow quantities using

6.3.5 Fuel Cladding Temperature Computation

The maximum specific decay power of a single fuel assembly among a recently discharged batch of assemblies (Q_A) can be determined as:

$$Q_A = Q_{average} \times f_r$$

where:

$Q_{average}$ is the average fuel assembly decay power, Btu/hr

f_r is the radial peaking factor

A fuel rod can produce f_z times the average heat emission rate over a small length, where f_z is the axial peaking factor. The axial heat distribution in a fuel rod is a maximum in the central region, and tapers off at its two extremities. Thus, peak cladding heat flux per unit heat transfer area of fuel assembly is given by the equation:

$$q_{peak} = \frac{Q_A \times f_z}{A_{rod}}$$

where A_{rod} is the total cladding external heat transfer area in the active fuel length region of a single fuel assembly (ft^2).

Within each fuel assembly sub-channel (the area between four adjacent fuel rods forming the corners of a square), water is continuously heated by the cladding as it moves axially upwards from bottom to top under laminar flow conditions. Rohsenow and Hartnett [6-5] report a Nusselt number (Nu) for heat transfer in a laminar flow situation through a heated channel. Nu is defined as follows:

$$Nu = \frac{h_c}{k_{water}} \times D_h = 4.364$$

where:

h_c is the laminar flow convective heat transfer coefficient, Btu/(hr×ft^2×°F)
k_{water} is the water thermal conductivity, Btu/(hr×ft×°F)
D_h is the sub-channel hydraulic diameter, ft

This equation can be rearranged to obtain a formula for h_c as:

$$h_c = 4.364 \times \frac{k_{water}}{D_h}$$

In order to ensure that the solution bounds irradiated fuel, it is necessary to assume that the fuel cladding has a crud deposit thermal resistance (R_{crud}) that covers the entire surface. The overall heat transfer coefficient (U) including the crud deposit resistance is defined by:

$$U = \frac{1}{\left(\frac{1}{h_c} + R_{crud}\right)}$$

The temperature difference between the outer surface of the fuel cladding and the water flowing up through the assembly at the peak cladding flux location can then be computed as:

$$\Delta T_c = \frac{q_{peak}}{U}$$

This temperature difference is added to the maximum local water temperature to obtain a bounding maximum fuel cladding temperature.

6.4 Preliminary Analyses

Using the analysis methods described in Section 6.3, preliminary analyses have been performed for the CCNPP Unit 3 U.S. EPR. Brief summaries of these analyses are presented in this section.

6.4.1 Decay Heat Computation

These preliminary computations were performed using the methodology described in Subsection 6.3.1. The key input data used are presented in the following table:

INPUT PARAMETER	INPUT VALUE
Number of Fuel Storage Cells	1360
Reactor Thermal Power	4612 MW
Reactor Core Size	241 assemblies
Maximum Batch Size Cycle 1 Cycle 2+	 120 96
Fuel Assembly Burnup	62,000 MWd/MTU
Fuel Assembly Initial Enrichment	5 wt%
Fuel Assembly Uranium Weight	535.9 kg
In-Core Hold Time	90 hr
Fuel Transfer Time	40 hr

Total SFP decay heat loads for both partial core and full core offloads that fill the SFP are computed and reported in the following table.

OFFLOAD SCENARIO	TOTAL DECAY HEAT
Partial Core Offload	29,033,110 Btu/hr
Full Core Offload	64,211,300 Btu/hr

No acceptance criteria are applied to these results.

6.4.2 Bulk Water Temperature Computation

These preliminary computations were performed using the methodology described in Subsection 6.3.2. The additional key input data used are presented in the following table:

INPUT PARAMETER	INPUT VALUE
Component Cooling Water Inlet Temperature	100.4°F
Component Cooling Water Outlet Temperature	113.2°F
Component Cooling Water Flow Rate per HX	2645000 lb/hr
SFP Water Inlet Temperature to HX	120°F

Maximum bulk water temperatures are computed for all scenarios defined in Section 6.1 and reported in the following table.

OFFLOAD SCENARIO	MAXIMUM BULK TEMPERATURE
Partial Core Offload with Active Failure	117°F
Full Core Offload with Active Failure	138°F
Full Core Offload without Active Failure	119°F

All of the computed maximum bulk water temperatures are below the applicable acceptance criteria stipulated in Section 6.2, indicating preliminary acceptability of the proposed spent fuel storage racks.

6.4.3 Time-to-Boil Computation

These preliminary computations were performed using the methodology described in Subsection 6.3.3. The additional key input data used are presented in the following table:

INPUT PARAMETER	INPUT VALUE
SFP Length	~39 ft
SFP Width	~29 ft
SFP Water Depth	~46 ft
Total Weight of Spent Fuel Storage Racks	310,000 lb
Maximum Weight of Fuel Assembly	807 kg

Minimum time-to-boil values are computed for all scenarios defined in Section 6.1, with initial temperatures set equal to the maximum bulk temperature values computed as described in Subsection 6.4.2. Results are reported in the following table.

OFFLOAD SCENARIO	MINIMUM TIME-TO-BOIL
Partial Core Offload with Active Failure	8.8 hr
Full Core Offload with Active Failure	3.1 hr
Full Core Offload without Active Failure	3.9 hr

While there are no specific time-to-boil acceptance times that must be met, all of the computed minimum time-to-boil values are in excess of three hours. This should provide adequate time for remedial actions, satisfying the applicable acceptance criterion stipulated in Section 6.2 and indicating preliminary acceptability of the proposed spent fuel storage racks.

6.4.4 Local Water Temperature Computation

These preliminary computations were performed using the methodology described in Subsection 6.3.4. The additional key input data used are presented in the following table:

INPUT PARAMETER	INPUT VALUE
Rack-to-Wall Gaps	
North Wall	11 in
South Wall	60 in
East Wall	4 1/4 in
West Wall	4 1/4 in
Rack Bottom Plenum Height	
Rack Baseplate + Cell Height	197 3/4”
Active Fuel Length	4200 mm
Fuel Assembly Array Size	17x17
Region 1 Rack Cell Pitch	10.9 in
Region 2 Rack Cell Pitch	9.03 in
Minimum Rack Cell Nominal ID	8.8 in
Number of Side Holes per Cell	4
Pedestal Cell Side Hole Diameter	1 ½”

Examining the scenarios defined in Section 6.1, it is readily apparent that the full core offload with a single active failure will have the highest decay heat and the highest bulk temperature. The peak local water temperature is computed for this most bounding scenario as 145°F (a temperature contour plot is presented in Figure 6.2). This is less than the local saturation temperature at the top of the heated length (~245°F), satisfying the applicable acceptance criterion stipulated in Section 6.2 and indicating preliminary acceptability of the proposed spent fuel storage racks.

6.4.5 Fuel Cladding Temperature Computation

These preliminary computations were performed using the methodology described in Subsection 6.3.4. The additional key input data used are presented in the following table:

INPUT PARAMETER	INPUT VALUE
Fuel Crud Layer Thermal Resistance	0.0005 (hr×ft^2×°F)/Btu
Fuel Rod Outer Diameter	9.50 mm
Fuel Rod Pitch	0.496 in
Axial Peaking Factor	1.65

As described in the previous subsection, the full core offload with a single active failure scenario will have the highest decay heat and the highest bulk temperature and, therefore, the highest local water temperature. It will also have, for the same reasons, the highest clad temperature. The bounding fuel cladding temperature is computed for this most bounding scenario, and reported in the following table.

RESULTS PARAMETER	COMPUTED VALUE
Fuel Cladding Superheat	26°F
Bounding Fuel Clad Temperature	171°F

This is less than the local saturation temperature at the top of the heated length (~245°F), satisfying the applicable acceptance criterion stipulated in Section 6.2 and indicating preliminary acceptability of the proposed spent fuel storage racks.

6.5 References

[6-1] USNRC Branch Technical Position ASB 9-2, "Residual Decay Energy for Light Water Reactors for Long Term Cooling," Rev. 2, 7/81.

[6-2] A.G. Croff, "ORIGEN2 - A Revised and Updated Version of the Oak Ridge Isotope Generation and Depletion Code," ORNL-5621, Oak Ridge National Laboratory, 1980.

[6-3] "Flow of Fluids Through Valves, Fittings, and Pipe," Crane Technical Paper No. 410, Crane Valve Company, Twenty-Second Printing, 1985.

[6-4] FLUENT Computational Fluid Dynamics Software, Fluent Inc., Centerra Resource Park, 10 Cavendish Court, Lebanon, NH 03766.

[6-5] Rohsenow, W.M. and J.P. Hartnett, "Handbook of Heat Transfer," McGraw Hill Book Company, NY, 1973.

Table 6.3.1 PARTIAL LISTING OF RERACK APPLICATIONS USING SIMILAR METHODS OF THERMAL-HYDRAULIC ANALYSIS	
PLANT	DOCKET NO.
Enrico Fermi Unit 2	USNRC 50-341
Quad Cities 1 and 2	USNRC 50-254, 50-265
Rancho Seco	USNRC 50-312
Grand Gulf Unit 1	USNRC 50-416
Oyster Creek	USNRC 50-219
Pilgrim	USNRC 50-293
V.C. Summer	USNRC 50-395
Diablo Canyon Units 1 and 2	USNRC 50-275, 50-455
Byron Units 1 and 2	USNRC 50-454, 50-455
Braidwood Units 1 and 2	USNRC 50-456, 50-457
Vogtle Unit 2	USNRC 50-425
St. Lucie Unit 1	USNRC 50-425
Millstone Point Unit 1	USNRC 50-245
D.C. Cook Units 1 and 2	USNRC 50-315, 50-316
Indian Point Unit 2	USNRC 50-247
Three Mile Island Unit 1	USNRC 50-289
J.A. FitzPatrick	USNRC 50-333
Shearon Harris Unit 2	USNRC 50-401
Hope Creek	USNRC 50-354
Kuosheng Units 1 and 2	Taiwan Power Company

Table 6.1.1 (continued) PARTIAL LISTING OF RERACK APPLICATIONS USING SIMILAR METHODS OF THERMAL-HYDRAULIC ANALYSIS	
Ulchin Unit 2	Korea Electric Power Corporation
Laguna Verde Units 1 and 2	Comision Federal de Electricidad
Zion Station Units 1 and 2	USNRC 50-295, 50-304
Sequoyah	USNRC 50-327, 50-328
La Salle Unit One	USNRC 50-373
Duane Arnold	USNRC 50-331
Chin Shan Units 1 and 2	Taiwan Power Company
Fort Calhoun	USNRC 50-285
Nine Mile Point Unit One	USNRC 50-220
Beaver Valley Unit One	USNRC 50-334
Limerick Unit 2	USNRC 50-353
Ulchin Unit 1	Korea Electric Power orporation
J.A. Fitzpatrick	USNRC 50-333
Callaway	USNRC 50-483
Byron/Braidwood	USNRC 50-454, 50-455, 50-567, 50-457
Wolf Creek	USNRC 50-482
Plant Hatch Units 1 & 2	USNRC 50-321, 50-366
Harris Pools C and D	USNRC 50-401
Waterford 3	USNRC 50-382

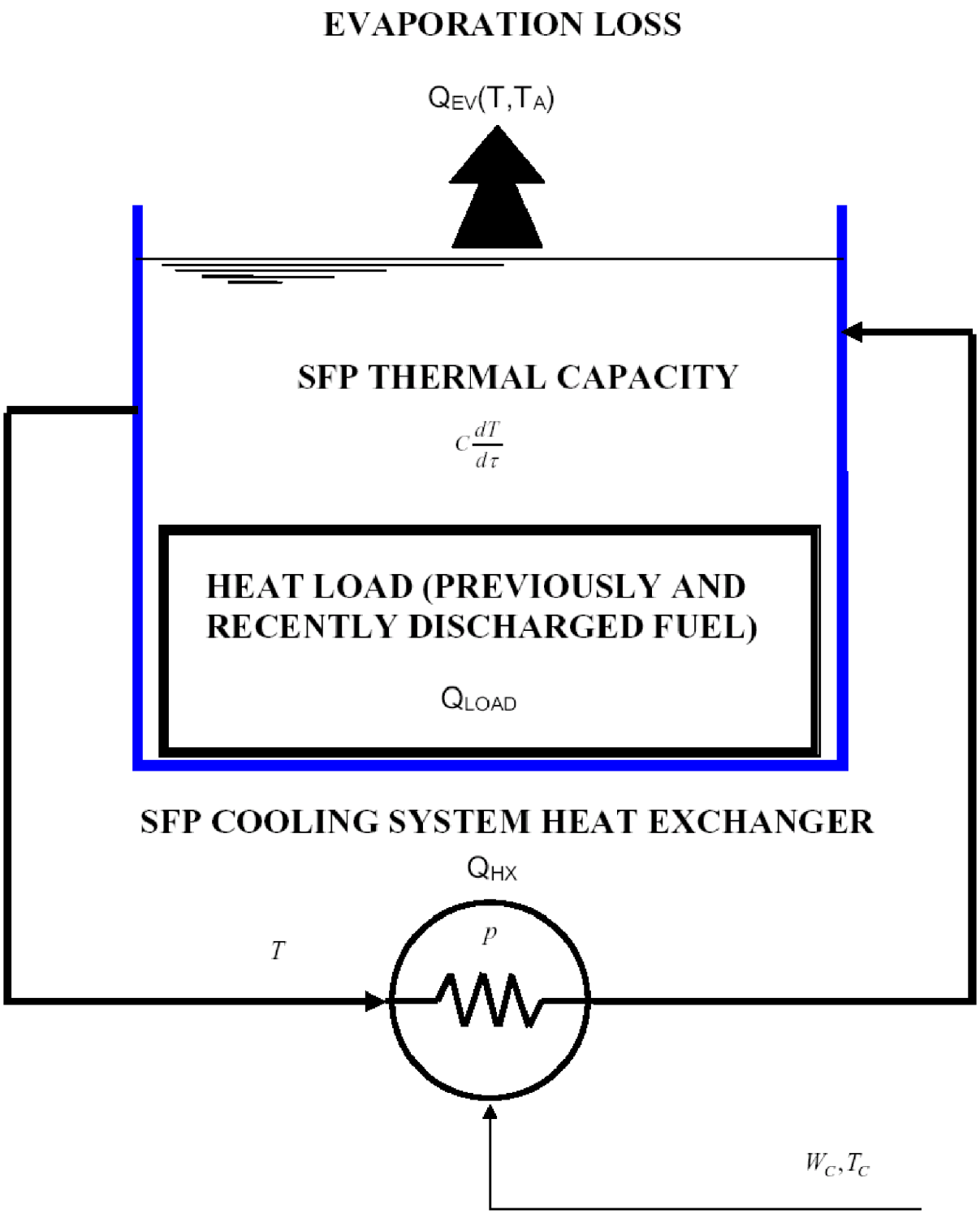

Figure 6.1: Simplified Heat Exchanger Alignment

PROPRIETARY FIGURE REDACTED

Figure 6.2: Contours of Static Temperature in a Vertical Plane through the Center of the SFP

7.0 MECHANICAL ACCIDENTS

7.1 Introduction

This topical report provides information on the new and spent fuel storage racks to support a COLA for the Calvert Cliffs Nuclear Power Plant (CCNPP) Unit 3 U.S. EPR. This chapter, specifically, provides information on the required mechanical accident performance characteristics of the fuel storage racks.

7.2 Description of Mechanical Accidents and Acceptance Criteria

The USNRC OT position paper [7-1] specifies that the design of the racks must ensure the functional integrity of the spent fuel racks under all credible fuel assembly drop events. Four categories of mechanical accidents are considered. Each of these four categories is described in the following paragraphs.

In the so-called "straight shallow drop" event (Figure 7.1), an impactor (i.e., a fuel assembly plus its handling tool) is assumed to drop vertically and hit the top of the rack. Inasmuch as the racks are of honeycomb construction, the deformation produced by the impact is expected to be confined to the cell walls that are directly impacted. However, the "depth" of damage to the affected cell walls must be demonstrated to remain limited to the portion of the cell above the top of the "active fuel region", which is essentially the elevation of the top of the neutron absorber. Stated in quantitative terms, this criterion implies that the permanent deformation of the rack cell walls should not extend more than 22 inches (downwards) from the top. To conservatively estimate the damage to the cell wall, the rack is assumed to absorb the maximum kinetic energy generated by the impactor.

The so-called "straight deep drop" event postulates that the impactor falls through an empty storage cell impacting the rack baseplate.

The deep drop event can be classified into two scenarios (i.e., the second and the third types of accidents), namely, drop in an interior cell away from the support legs (Figure 7.2), and drop through the cell located above a support leg (Figure 7.3).

In deep drop scenario 1 (Figure 7.2), the impactor strikes the rack baseplate away from the support leg, where it is more flexible. If the baseplate is pierced by the fuel assembly or deforms sufficiently, the liner may be damaged leading to an uncontrollable loss of water. An additional consideration is that the baseplate deformation may lead to an abnormal condition, where the fuel assembly active zone is outside the neutron absorber-equipped space of the fuel rack. This condition must be considered in the criticality evaluations and must be limited to ensure criticality control. Severing and large deflection of the baseplate leading to a secondary impact with the pool liner are unacceptable results.

In deep drop scenario 2 (Figure 7.3), the rack baseplate is buttressed by the support legs and presents a hardened impact surface, resulting in a high impact load. The principal design objective is to ensure that the support leg does not tear the liner that overlays the reinforced concrete pool slab.

In addition to the preceding drop accidents, a fourth "stuck fuel" accident is analyzed to determine the damage to the rack due to a 5,000 lbf uplift force applied to the rack by a stuck fuel assembly. Similar to the shallow drop accident, the damage to the cell wall shall be limited to the portion of the rack structure above the neutron absorber.

7.3 Analysis Methods

The subsections in this section describe the analysis methods to be used in performing licensing-basis calculations to demonstrate that the mechanical accident performance requirements for the fuel storage racks are satisfied. These are intended to be minimum requirements, and more sophisticated analysis models may be used. Similar mechanical accident analyses have been used for previous fuel storage rack licensing at many nuclear plants worldwide.

7.3.1 Calculation of Incident Impact Velocity

The previously discussed drop events fall into two broad categories of underwater motion, which may be denoted as "geometry unconstrained" (GU) and "geometry constrained" (GC). The impactor in the shallow drops and in the early stages of the deep drops is accelerated by the gravitational force with the sole opposing force arising from the form drag effect of the unconfined body of water. In this case the Newtonian equation of motion has the form:

$$(m + m_H)\ddot{x} = mg - \frac{C_D A \rho \dot{x}^2}{2}$$

where:

m is the mass of the impactor
m_H is the hydrodynamic (virtual) mass (due to submergence)
x is the displacement variable
g is the acceleration due to gravity
C_D is the form drag coefficient
A is the area subject to drag forces
ρ is the density of water
• (dot) is the derivative with respect to time
τ is the time coordinate

For a drop from a given height, the initial conditions are:

$$\tau = 0, \dot{x} = 0, x = 0$$

The above nonlinear second order differential equation is readily solved to obtain the incident impact velocity.

The geometry constrained (GC) drop scenario corresponds to the downward movement of the impactor through a storage cell.

The constrained geometry equation of motion is also a nonlinear second order differential equation, which can be numerically integrated to determine the incident velocity of the impactor at the instant of its collision with the baseplate.

7.4 Preliminary Analyses

The postulated drop accidents involve two types of racks (i.e., Region 1 and Region 2 racks) that are fabricated with same material type and thickness. Preliminary drop analyses were conservatively performed based on the bounding impact energy and rack configuration.

For a shallow drop event, because of the same drop height and mass, the initial impact velocity and hence initial impact energy due to fuel assembly drop are identical for both Region 1 and 2 racks. Based on a review of rack configurations, the impact location for the shallow drop analysis is chosen to be at the top of a Region 2 rack periphery panel, which has the weakest weld connection with the adjoining cell walls.

The initial impact velocities for both shallow and deep drop scenarios are summarized in Table 7.4.1.

The following bounding drop cases were analyzed.

1. Shallow drop of a fuel assembly onto the top of a Region 2 rack
2. Deep drop (scenario 1) of a fuel assembly involving a Region 1 rack
3. Deep drop (scenario 2) of a fuel assembly involving a Region 1 rack

While the impactor was conservatively modeled as a rigid solid with no energy absorption capacity, detailed configurations of the impact target (i.e., the rack cells or baseplate) were modeled in all analyzed events.

For the "stuck fuel" accident, the analysis is based on classical formulations of the strength of materials.

7.4.1 Straight Shallow Drop Event

For the shallow drop event, the analysis shows that the maximum depth of plastic deformation due to the drop accident was limited to less than 8.45 inches, which is below the design limit of 22 inches. This ensures that configuration analyzed in the criticality evaluation remains valid.

7.4.2 Straight Deep Drop Events

The deep drop through an interior cell produced some deformation of the baseplate, but the baseplate was not pierced. The fuel assembly support surface is lowered by a maximum of 2.79 inches, which is less than the distance of 5.5 inches from the baseplate to the liner. Therefore, the pool liner will not be contacted by the deformed baseplate.

In the deep drop event where the impact region is located above the support leg it was found that the structural integrity of the support leg is not compromised by the impact, since the maximum stress of 1,527 psi (impact force of 24,279 lbf) is well below the 106.4 ksi yield stress of the material. Also, the magnitude of the impact force is significantly less than the peak support leg load of 369,000 lbs from rack seismic analysis as described in Chapter 5 of this report. Therefore, this accident case is bounded by the rack seismic analysis of the racks.

7.4.3 Stuck Fuel Event

Results of the analysis show that the maximum stress in the rack cell due to a stuck fuel assembly is only 3,500 psi, which is well below the material yield strength. Therefore, the fuel racks are adequate to withstand a 5,000 lbf uplift force due to a stuck fuel assembly.

7.5 Conclusion

Several preliminary mechanical accidents were analyzed and found to produce localized damage well within the design limits for the racks. The straight shallow drop event was found to produce some localized plastic deformation in the top of the storage cell, but the region of permanent strain is limited to the portion of the rack structure above the top of the active fuel region. The analysis of the straight deep drop event at cell locations selected to maximize baseplate deformation indicated that the baseplate will not experience puncture and the downward displacement of the baseplate will not lead to a secondary impact of the fuel assembly with the pool liner. Finally, the stuck fuel accident analysis indicated that any damage to the cell wall would occur well above the “poison zone” of the rack. It is therefore preliminarily concluded that the fuel storage racks possess acceptable margins of safety under the postulated mechanical accidents.

7.6 References

[7-1] (USNRC Office of Technology) "OT Position for Review and Acceptance of Spent Fuel Storage and Handling Applications", dated April 14, 1978, and January 18, 1979 amendment thereto.

Table 7.4.1 IMPACT EVENT DATA				
Case	Impactor Weight (lb)	Impactor Type	Drop Height (in)	Impact Velocity (in/sec)
1. Shallow drop event	2083.4	Fuel assembly plus handling tool	47-1/16 above top-of-rack	172.1
2. Deep drop event (away from support leg)	2083.4	Fuel assembly plus handling tool	244-1/16 above baseplate	258.1
3. Deep drop event (above support leg)	2083.4	Fuel assembly plus handling tool	244-1/16 above baseplate	107.5

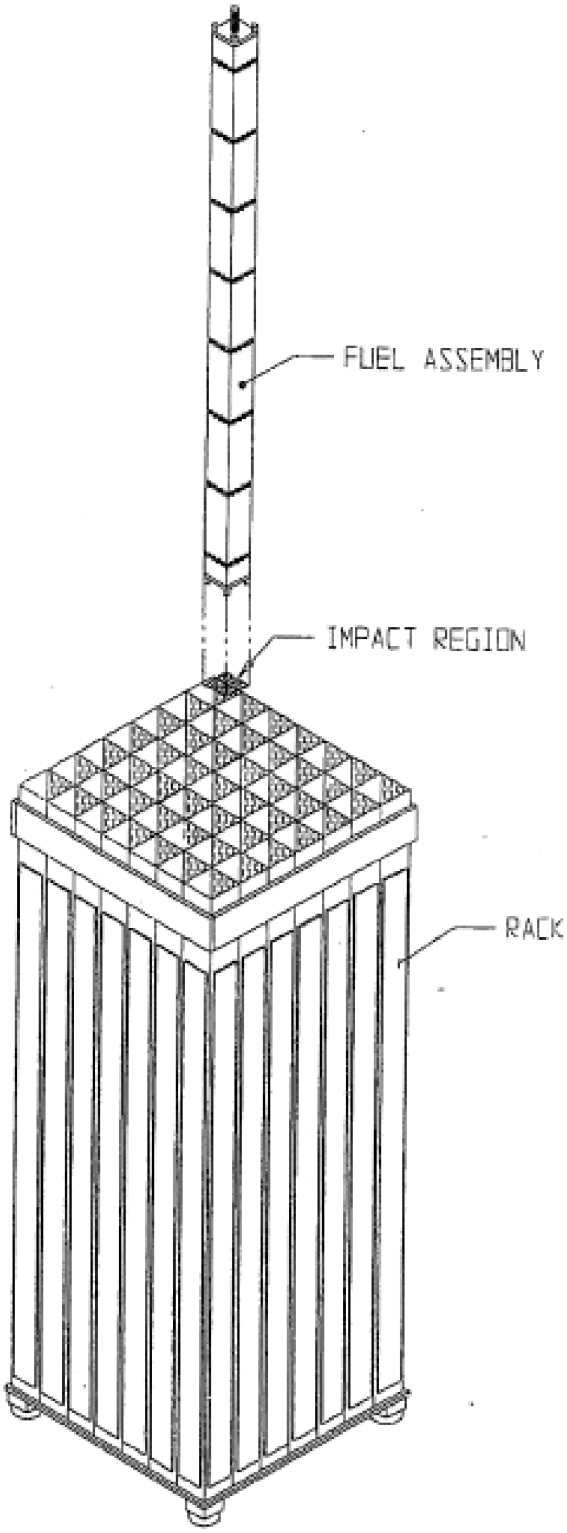

Figure 7.1: Schematic of the Straight Shallow Drop on a Rack Cell

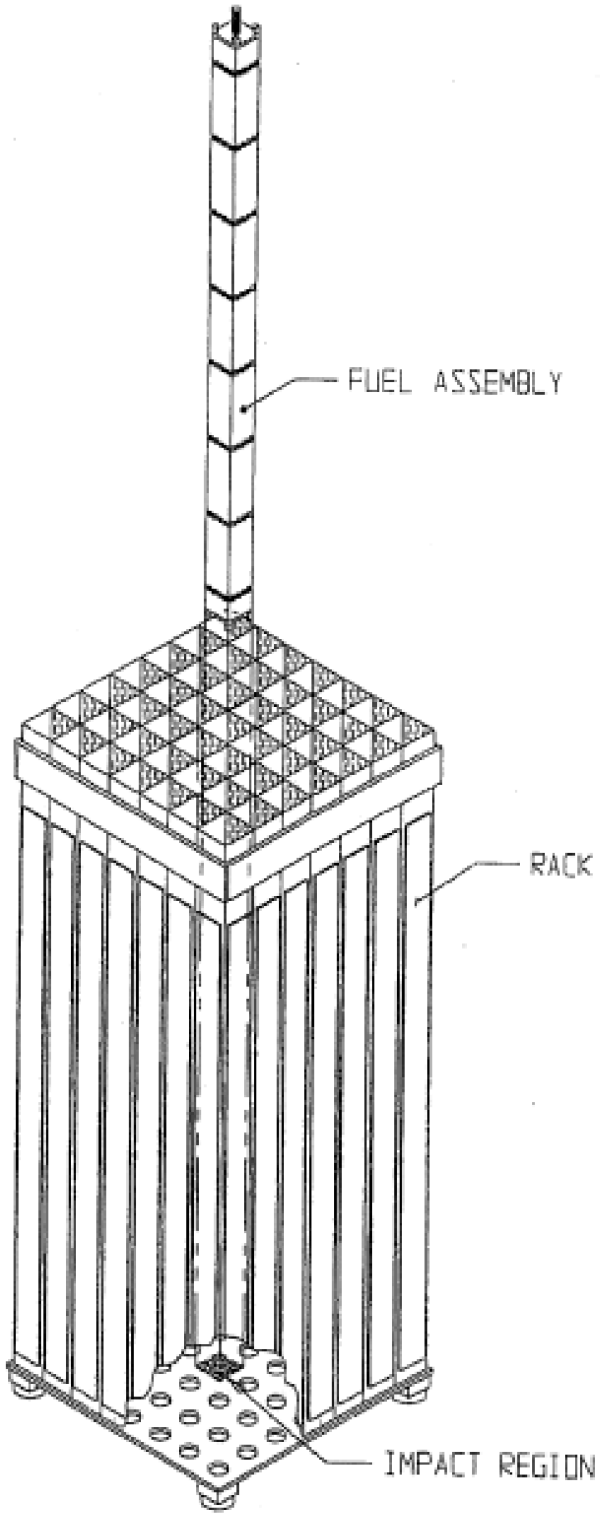

Figure 7.2: Schematic of the Deep Drop Scenario 1 on a Center Cell Location

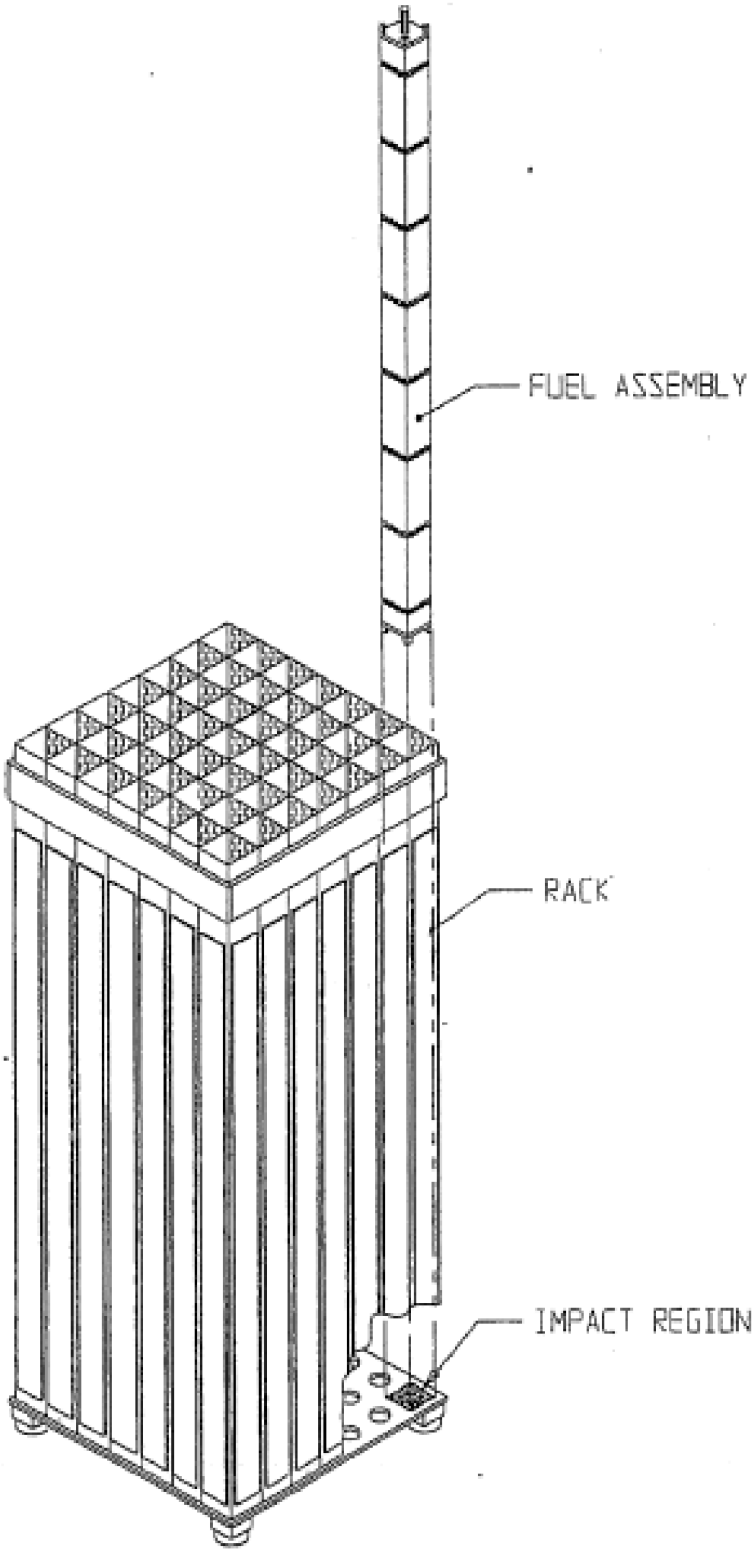

Figure 7.3 Schematic of the Deep Drop Scenario 2 on a Support Leg Location

8.0 RADIOLOGICAL PERFORMANCE

This topical report provides information on the new and spent fuel storage racks to support a COLA for the Calvert Cliffs Nuclear Power Plant Unit 3 U.S. EPR. This chapter, specifically, provides information on the required radiological performance assessments of the fuel storage racks. As new (un-irradiated) fuel does not generate any radiation, no radiological performance assessments are required for the new fuel storage racks. The remainder of this chapter, therefore, discusses the radiological performance assessments to be performed for the spent fuel storage racks.

8.1 Introduction

There are two performance areas that must be assessed for the spent fuel storage racks. First, it is necessary to evaluate the gamma dose rate at the surface of the SFP water. Second, the radiological consequences of a fuel handling accident must be determined.

8.2 Acceptance Criteria

There are no explicit regulatory radiation dose rates to be applied as acceptance criteria for these assessments. The gamma dose rate at the surface of the SFP water will be used to define requirements for personnel operating spent fuel handling equipment or performing other activities over the SFP. The results of the fuel handling accident will be used to evaluate the post-accident building environmental conditions and, possibly, offsite doses.

8.3 Assumptions and Input Data

Certain basic parameter values, all of which are consistent with values specified in the licensing basis for the plant, will be applied in the radiological evaluations. These basic parameter values are given in the following table.

INPUT PARAMETER	INPUT VALUE
Reactor Thermal Power	4612 MW
Fuel Assembly Initial Enrichment	5 wt%
Fuel Assembly Exposure	62,000 MWd/MTU
Minimum Fuel Cooling Time	34 hr

8.4 Dose Rate at the Surface of the SFP

The calculated gamma dose rate at the surface of the SFP is the sum of the dose rate from radionuclides in the SFP water, the dose rate from a fuel assembly in transit, and the dose rate from the fuel stored in the spent fuel storage racks.

8.4.1 Dose Due to Radionuclides in the Water

Normally, the sources of radionuclides in the SFP water are crud and some fission products plated on the fuel surfaces, and small amounts of primary system water carried over into the SFP during refueling operations. These sources result in an increase in the contamination level of the SFP during refueling and are soon reduced to normal levels after refueling is completed. Aged fuel typically will not contribute significantly to the radionuclide burden in the SFP water.

8.4.2 Dose Due to Spent Fuel

The SFP surface dose rate attributable to stored spent fuel is dominated by the fuel being unloaded from the core during a refueling. The dose at the SFP surface from an assembly in transit from the core during refueling is dependant upon the operating specific power in the core and the time after shutdown when the spent fuel is moved. Aged fuel assemblies that accumulate in the SFP from previous refuelings have decayed such that their contribution to the SFP surface dose rate will be negligible compared to the assembly in transit.

8.5 Fuel Handling Accident

For dose calculations, the highest specific inventory of each contributing radionuclide will be used. The fuel handling accident will be assumed to result in the release of the gaseous fission products contained in the fuel/cladding gaps of all fuel rods in a peak-power fuel assembly plus any ruptured rods in an impacted assembly. Gap inventories of fission products available for release will be estimated using the release fractions identified in Regulatory Guide 1.183 [8-1].

The gaseous fission products that have significant impacts on the off-site doses following short fuel cooling periods are the short-lived nuclides, which reach saturation inventories during in-core operation. These inventories depend primarily on the fuel specific power over the few months immediately preceding reactor shutdown. In the highest power assemblies the specific power, and hence the inventory of iodine and xenon, will be proportional to the peaking factor. All of the gap activity in any damaged rods is assumed to be instantaneously released following the fuel handling accident. Radionuclides that are considered include xenons, kryptons, halogens, cesiums and rubidiums.

The offsite doses are to be analyzed by only crediting the scrubbing of iodine by the refueling water. Hence, fuel handling accidents inside containment and the auxiliary building are treated in the same manner. Cesium iodide, which accounts for about 95 percent of the gap iodine, is nonvolatile and does not readily become airborne after dissolving. This species is assumed to completely dissociate and re-evolve as elemental iodine immediately after damage to the fuel assembly. The dose activity released will presume:

- Core thermal power – 4612 MWt
- Decay time after shutdown – 34 hr
- Activity release period – 2 hr
- One of 241 fuel assemblies in the core is completely damaged
- Maximum rod radial peaking factor – 1.7

- Iodine and noble gas fission product gap fractions - Regulatory Guide 1.183, regulatory position C.3.2
- Iodine chemical form – Regulatory Guide 1.183, regulatory position C.3.5
- Pool decontamination for iodine – Regulatory Guide 1.183, Appendix B
- Filtration – none

The Exclusion Area Boundary (EAB) and Low Population Zone (LPZ) doses will be determined and shown to be well below the 25 rem TEDE guidelines in 10 CFR 50.34.

8.6 References

[8-1] Regulatory Guide 1.183, "Alternative Radiological Source Terms for Evaluating Design Basis Accidents at Nuclear Power Reactors," Revision 0, July 2000.

[8-2] C. E. Beyer, et al., "Assessment of the Use of Extended Burnup Fuel in Light Water Power Reactors," NUREG/CR-5009, Pacific Northwest Laboratory, February 1988.